RADC-TR-81-242
Final Technical Report
September 1981

ACOSS EIGHT (ACTIVE CONTROL OF SPACE STRUCTURES), PHASE II

TRW

Sponsored by
Defense Advanced Research Projects Agency (DOD)
ARPA Order No. 3654

ROME AIR DEVELOPMENT CENTER
Air Force Systems Command
Griffiss Air Force Base, New York 13441

This report has been reviewed by the RADC Public Affairs Office (PA) and is releasable to the National Technical Information Service (NTIS). At NTIS it will be releasable to the general public, including foreign nations.

RADC-TR-81-242 has been reviewed and is approved for publication.

APPROVED: Richard W. Carman

RICHARD W. CARMAN
Project Engineer

APPROVED: Mylan A. Haugen

MYLAN A. HAUGEN, Colonel, USAF
Chief, Surveillance Division

FOR THE COMMANDER: John P. Huss

JOHN P. HUSS
Acting Chief, Plans Office

If your address has changed or if you wish to be removed from the RADC mailing list, or if the addressee is no longer employed by your organization, please notify RADC (OCSE) Griffiss AFB NY 13441. This will assist us in maintaining a current mailing list.

Do not return copies of this report unless contractual obligations or notices on a specific document requires that it be returned.

ACOSS EIGHT (ACTIVE CONTROL OF SPACE STRUCTURES), PHASE II

Ralph P. Iwens
Robert J. Benhabib
Frank C. Tung

Contractor: TRW
Contract Number: F30602-80-C-0198
Effective Date of Contract: 21 May 1980
Contract Expiration Date: 1 May 1981
Short Title of Work: Acoss Eight
Program Code Number: OE20
Period of Work Covered: May 80 - Apr 81

Principal Investigator: Ralph P. Iwens
Phone: 213 536-1871

Project Engineer: Richard W. Carman
Phone: 315 330-3148

This research was supported by the Defense Advanced Research Projects Agency of the Department of Defense and was monitored by Richard W. Carman (RADC/OCSE), Griffiss AFB NY 13441 under Contract F30602-80-C-0198.

UNCLASSIFIED

SECURITY CLASSIFICATION OF THIS PAGE (When Data Entered)

REPORT DOCUMENTATION PAGE		READ INSTRUCTIONS BEFORE COMPLETING FORM
1. REPORT NUMBER RADC-TR-81-242	2. GOVT ACCESSION NO. AD-A108 629	3. RECIPIENT'S CATALOG NUMBER
4. TITLE (and Subtitle) ACOSS EIGHT (ACTIVE CONTROL OF SPACE STRUCTURES), PHASE II		5. TYPE OF REPORT & PERIOD COVERED Final Technical Report May 80 - Apr 81
		6. PERFORMING ORG. REPORT NUMBER 36296-6001-UT-00
7. AUTHOR(s) Ralph P. Iwens Robert J. Benhabib Frank C. Tung		8. CONTRACT OR GRANT NUMBER(s) F30602-80-C-0198
9. PERFORMING ORGANIZATION NAME AND ADDRESS TRW One Space Park Redondo Beach CA 90278		10. PROGRAM ELEMENT, PROJECT, TASK AREA & WORK UNIT NUMBERS 62301E C6540108
11. CONTROLLING OFFICE NAME AND ADDRESS Defense Advanced Research Projects Agency 1400 Wilson Blvd. Arlington VA 22209		12. REPORT DATE September 1981
		13. NUMBER OF PAGES 192
14. MONITORING AGENCY NAME & ADDRESS(if different from Controlling Office) Rome Air Development Center (OCSE) Griffiss AFB NY 13441		15. SECURITY CLASS. (of this report) UNCLASSIFIED
		15a. DECLASSIFICATION/DOWNGRADING SCHEDULE N/A

16. DISTRIBUTION STATEMENT (of this Report)

Approved for public release; distribution unlimited.

17. DISTRIBUTION STATEMENT (of the abstract entered in Block 20, if different from Report)

Same

18. SUPPLEMENTARY NOTES

P DC Project Engineer: Richard Carman (OCSE)

19. KEY WORDS (Continue on reverse side if necessary and identify by block number)

Control Theory
Large Space Structures
Structural Dynamics
Flexible Vehicles
Stability Augmentation
Mirror Vibration
Suppression

20. ABSTRACT (Continue on reverse side if necessary and identify by block number)

This effort addresses three areas of active structure control/vibration control: (1) Stability ensuring designs in the presence of modal truncation/inaccurate structural models using a method based on the positivity of operators; (2) On-orbit parameter identification using the maximum likelihood method; (3) Trade-offs between model reference adaptive control and fixed gain control with and without on-orbit parameter identification and system tuning.

DD FORM 1473, 1 JAN 73 EDITION OF 1 NOV 65 IS OBSOLETE

UNCLASSIFIED

SECURITY CLASSIFICATION OF THIS PAGE (When Data Entered)

Developed a stability ensuring design methodology which does not rely on modal truncation, has only low sensitivity to the exact knowledge of the structures model and, with some modifications, can be extended to non-linear systems. The method yields good performance, but is not necessarily optimal. ~~Studied~~ the maximum likelihood method of parameter identification. Parameter data collected on-orbit could be used to update the control model and improve performance. An alternative to explicit parameter identification and subsequent system tuning is direct adaptive control. Trade-offs between parameter identification and tuning versus adaptive controls were coordinated and the results are presented.

was studied

ACKNOWLEDGEMENT

This work was performed by TRW Defense and Space Systems Group under Contract No. F30602-80-C-0198 for the U. S. Government. The research was sponsored by the Defense Advanced Research Projects Agency (DARPA) of the Department of Defense, and was monitored by the Rome Air Development Center (RADC), Air Force Systems Command. This final technical report covers the period from May 1980 through February 1981. The technical monitors of this program were Lt. Col. A. Herzberg (DARPA) and Mr. R. Carman (RADC).

The program manager at TRW was Dr. Ralph P. Iwens. This study was performed within the Control and Sensor Systems Laboratory of TRW's Space Systems Division. The Control and Sensor Systems Laboratory is managed by Dr. I. J. Williams.

The contributors to this report are:

Section 1: Dr. Ralph P. Iwens

Section 2: Mr. Robert J. Benhabib

Section 3: Dr. Frank C. Tung

Section 4: Mr. Robert J. Benhabib

TABLE OF CONTENTS

TABLE OF CONTENTS (Continued)

TABLE OF CONTENTS (Continued)

LIST OF FIGURES

LIST OF FIGURES (Continued)

LIST OF FIGURES (Continued)

LIST OF FIGURES (Continued)

LIST OF TABLES

1.0 INTRODUCTION AND SUMMARY

1.1 BACKGROUND

Future DOD large space system concepts such as High Altitude Large Optics (HALO), High Energy Laser Optics (HELO) and Millimeter (MM) Wave applications have stringent line-of-sight (LOS) pointing and jitter performance requirements which cannot readily be met with existing technology. Under the Active Control of Space Structures (ACOSS) Program, the Defense Advanced Research Projects Agency (DARPA) has sponsored a number of studies for the development of a unified structural dynamics and control technology base to support the future development of large space systems missions. Major emphasis in these studies has been placed on generic control law development for active vibration suppression.

This document reports the results of one of these studies, namely ACOSS-8, conducted by TRW Defense and Space Systems Group for DARPA from May 1980 through April 1981. The study addressed three areas of active structure control/vibration control:

- Stability ensuring designs in the presence of modal truncation/inaccurate structural models using a method based on the positivity of operators.
- On-orbit parameter identification using the maximum likelihood method.
- Tradeoffs between model reference adaptive control and fixed gain control with and without on-orbit parameter identification and system tuning.

1.2 SUMMARY

One of the challenges in the active control of large space structures (LSS) is to assure stability of control system designs based on inaccurate structural models. The two main errors in the dynamic model of a structure

arise from modal truncation and inaccurate knowledge of the modal frequencies and mode shapes obtained by finite element methods. Additional errors are introduced by poor knowledge of structural damping and the effects of structural nonlinearities.

What is needed, therefore, is a stability ensuring design methodology that does not rely on modal truncation, has only low sensitivity to the exact knowledge of the structural model (robust), and, with some modifications, can be extended to nonlinear systems. We are presenting such a method here, based on the positivity of operators. This method yields good performance, but it is not necessarily optimal when significant model uncertainties are present, because robustness with respect to knowledge of the modal data tends to occur at the expense of a more conservative design.

A major result of this study is a design philosophy for active control of LSS that can provide robust stability and also meet stringent performance requirements. In order to assure robust stability the positivity method is applied to design the active structural controllers. Once the entire system is on-orbit, tests will be conducted to identify critical model parameters (e.g. modal data and structural damping). Parameter identification methods which appear most suitable for this are the maximum likelihood method and some of the frequency response methods. In the present study we concentrated on the maximum likelihood method. Data from the on-orbit identification tests are transmitted to ground where the identification algorithm is applied and the a priori knowledge of model paramaters updated. The improved model parameters are then used to recompute, on the ground, new control parameters in order to tune the system to achieve the desired performance. Figure 1-1 illustrates the concept.

An alternative to explicit parameter identification and subsequent system tuning is direct adaptive control. Model reference adaptive control (MRAC) is particularly attractive, since it allows specification of the desired performance through a reference model. Figure 1-2 shows a basic model reference adaptive configuration. Among the advantages of MRAC are (1) autonomy, (2) automatic on-line controller adjustments for component failures, and (3) automatic on-line controller adjustments in response to

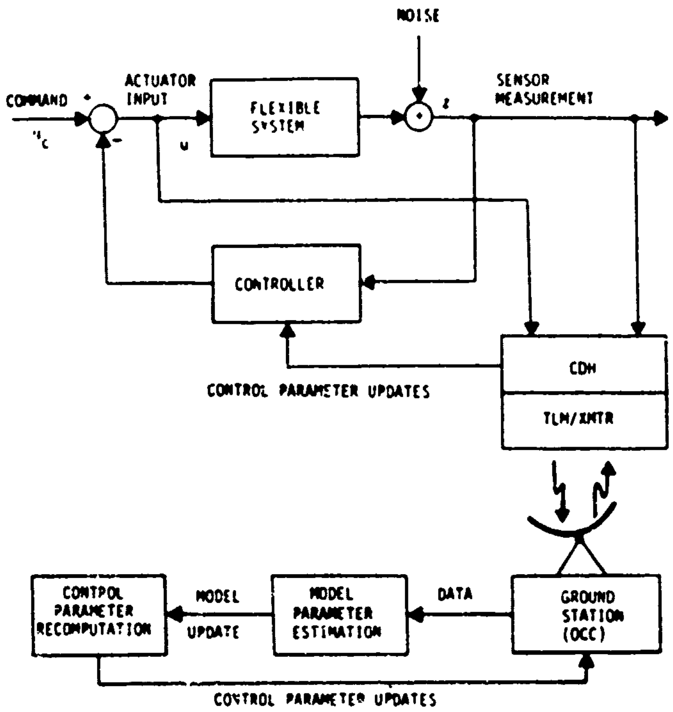

Figure 1-1. On-Orbit Model Identification and System Tuning

changing conditions, e.g. changes in the thermal environment or reorientation of large, articulated sub-structures. On-line implementation of MRAC is, however, more complex than parameter identification and subsequent system tuning. Tradeoffs between these control approaches have been conducted in this study.

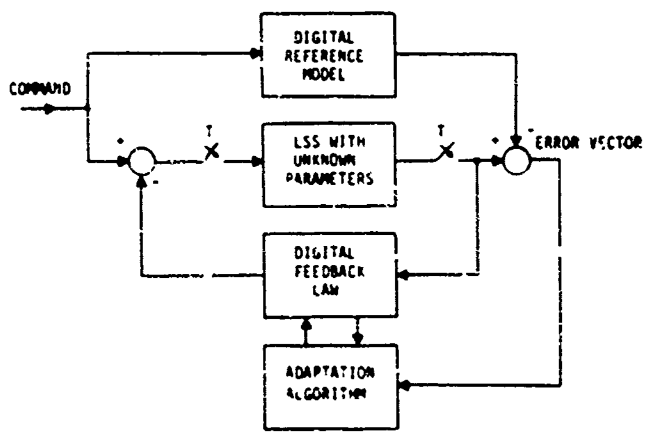

Figure 1-2. Digital Model Reference Adaptive Control

1.3 STUDY CONCLUSIONS

The positivity approach has been shown to work well for the design of LSS control Systems. It has been successfully applied to the design of the attitude control and active structural damping systems for the Draper Model #2 whose payload LOS was inertially stabilized. The resulting control system performed well and was robust with respect to model parameter variations. To achieve optimal performance as specified, the system had to be subsequently tuned, assuming improved knowledge of the system model (mode shapes, frequencies and structural damping). In the positivity approach the improved model knowledge allows then the use of more elaborate "embedding operators" (related to the classical Popov multipliers and absolute stability sectors) which leads to less conservative stability results, e.g. higher gain/bandwidth, and therefore better performance. If the system can justifiably be assumed linear, the tuning process can directly apply the multivariable frequency domain design techniques of MacFarlane and others, using frequency domain shaping of the open loop characteristic gains of the system.

As the study results have clearly shown, there exist tradeoffs between the robustness of a design and its performance: one is obtained at the expense of the other. Model uncertainty may be large, but to generate a robust design, the accuracy of the LSS model must be known within some specifiable limits. If the model uncertainty is small, robustness may be traded for performance.

Model uncertainty is reduced through on-orbit parameter identification. Using the maximum likelihood method, excellent estimates of physical and modal LSS parameters were obtained. Structural damping is the most difficult parameter to estimate because it is generally very small so that the measurement data exhibits only a low sensitivity to the parameter and longer data lengths are required. Furthermore, the mathematical parameterization of structural damping is usually not accurate, i.e., not truly representative of the physical phenomenon. The estimation of physical LSS parameters, such as mass distribution, cross-section of members, dimensions, polar moments, spring constants, etc., instead of modal parameters has

significant advantages, since it drastically reduces the number of parameters that must be estimated.

Model reference adaptive control (MR) is an alternative to explicit on-orbit parameter identification and control system tuning. In this study MRAC was applied to control a perturbed model of the Draper tetrahedron structure (Draper Model #1) and very good results were achieved. MRAC was shown to be a viable approach to LSS control and it works well. However, the study showed that model parameter identification followed by a controller tune-up results in still better performance, because the human designer can use his more global knowledge of the system in the design. For example, poor observability of critical modes in the sensor measurements can be accounted for (to a certain degree) by a designer, while a model reference adaptive controller is completely oblivious to the situation. This was the case in the tetrahedral structure, where the modes which are critically affecting the motion of the apex, are only poorly observable/controllable from the supporting bi-peds of the tetrahedron where the sensors and actuators are located.

The conclusion is that explicit on-orbit model parameter identification and subsequent controller tuning via ground command is the preferred approach. Model reference adaptive control should only be used in cases where spacecraft autonomy is absolutely essential and/or where unexpected, non-preprogrammable changes in the system are likely to occur. Otherwise, the increased on-board software complexity of model reference adaptive control cannot be justified.

Finally, we conclude that the proposed three-step design approach for LSS control systems appears to be the correct approach in the sense that it minimizes risk with the potential for maximizing performance.

1) It assures stability with robustness via the positivity design method.

2) It identifies model parameters through on-orbit tests.

3) It tunes the controller to maximize performance.

1.4 RECOMMENDATIONS FOR FURTHER STUDY

Further studies in the positivity design approach should address example designs with non-collocated actuators and sensors, nonlinearities in the controller, and further work on the development of an easy-to-follow, computer-aided design methodology.

In on-orbit parameter identification, non-zero initial dynamic conditions of the spacecraft should be addressed. Frequency domain identification techniques should be studied in more depth and compared with the maximum likelihood method.

Finally, for realistic design applications, controller implementation issues must be addressed. Foremost among these are actuator and sensor development, modelling, and laboratory test.

1.5 ORGANIZATION OF REPORT

Section 2 addresses the positivity design approach and Section 3 on-orbit parameter identification. Model reference adaptive control and performance comparisons with fixed gain controllers are presented in Section 4. Quoted references are listed following Section 4. Appendix A contains a description of the Draper Model #2.

2.0 THE STABILITY ENSURING DESIGN APPROACH VIA POSITIVITY

The stability ensuring design methodology makes use of positivity/energy dissipation theory to ensure the stability of the LSS. The key results are:

- The negative feedback connection of a positive system with a strictly positive system is stable

- An LSS with collocated, ideal (by ideal we mean infinite bandwith), actuators and rate sensors is a positive system

- Embedding operations permit the treatment of non-positive systems, e.g., systems with realistic, bandwidth-limited actuators and sensors.

The usefulness of the theory becomes apparent as one realizes that no assumptions are made about the dimensionality or linearity of the systems involved. It is for this reason that the theory permits the treatment of modal truncation, stability robustness and nonlinearities. The price one pays for the generality is that designs tend to be conservative. It has therefore been proposed to use positivity in conjunction with on-orbit identification and control "tune-up". Positivity will be used in the pre-flight design where there is parameter uncertainty; then as information is gathered on-orbit, multivariable frequency domain techniques combined with positivity (to treat non-linearities) can be used to tune the design for high performance.

It is clear that as system knowledge increases, the need for a conservative pre-flight design diminishes. In cases where good pre-flight information is available over approximately twice the control band, the positivity/multivariable frequency domain approach may be applied directly without on-orbit identification.

The positivity method has been successfully applied in this study to various examples: a flat plate (Section 2.2) the Draper tetrahedron (Section 4.2.2) and the Draper Model #2 (Section 2.3). In each case, the positivity

approach led to a very simple* and stability robust design with good performance. Subsequent controller tuning based on assumed improved plant modelling (obtained via on-orbit parameter identification, as in Section 3) then permitted all designs to meet all the desired performance specifications.

2.1 The Positivity Design Methodology

2.1.1 General Background On Positivity

The positivity method is a direct outgrowth of V. M. Popov's work on absolute and hyperstability. The basic underlying theory is general, makes extensive use of functional analysis, and is not restricted to linear time-invariant plants. In fact, the method has in the past been associated with the stability of nonlinear systems (Lur'e problem) where both the nonlinear and linear parts of the system must meet certain positivity conditions. These conditions are only sufficient conditions for stability and therefore tend to be conservative at times. Since well-known necessary and sufficient conditions exist to establish the stability of linear systems, it is apparent why positivity techniques have in the past generally not been applied to linear systems.

The stability problem in the control of large space structures (LSS) differs from more conventional linear systems, because the plant to be controlled is theoretically of infinite order (and practically of very high order), while the controller/estimator must, of necessity, be of relatively low order. It appears, therefore, desirable to use tests which do not require explicit evaluation of the closed loop system, but which impose conditions individually on the plant and the controller, assuring stability when the loop is closed by negative feedback. The stability theory based on the positivity of operators is a powerful method having just this characteristic.

---

* Typical frequency domain compensation consisted of second or fourth order lead-lag filtering.

Positivity Theorem: The system S (in Figure 2.1)* is asymptotically stable if at least one of the loop transfer matrices G and H is strictly positive real and the other is positive real.

The main advantage of this result is that conditions are imposed individually on the plant G(s) and the controller H(s), ensuring stability when the loop is closed by negative feedback.

For ease of understanding, and because they are presently of main interest, we have considered here only the linear stability result. However, the proof of the Theorem given in Reference [1], treats the controller and the plant as general operators, not necessarily linear, defined on a Hilbert function space. This extension of the theory to nonlinear systems will be summarized and used in Section 4.

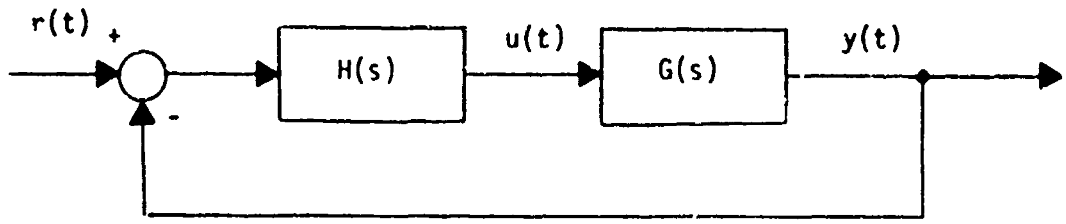

VECTOR VALUED SYSTEM "S"

Figure 2.1 System Considered By The Positivity Theorem

2.1.2 Definition And Meaning Of Positive Real

Positive real means exactly what it says. The real part of a transfer function as function of frequency is always greater-than-or-equal-to zero. Strict positive real means the real part is always greater than zero.

For single-input-single-output (SISO) transfer functions $g(j\omega)$, (strict) positive realness means therefore that

$$\mathrm{Re}\left\{ g(j\omega)\right\} \geq (>)\ 0, \text{ for all } -\infty < \omega < \infty$$

For multiple-input-multiple-output (MIMO) systems, the

* The theorem is also true when H is in the feedback path.

definition needs to be more precise as one is now dealing with a transfer matrix. Here, a square MIMO transfer matrix $G(j\omega)$ is (strictly) positive real if

$$\left\{G(j\omega) + G^*(j\omega)\right\} \text{ is non-negative (positive) definite for all } -\infty<\omega<\infty$$

It is interesting to note that positive realness is related to passivity. Otto Brune proved in the 1930's that if a filter (electrical network) was to be realizable by passive circuit components (only resistors, inductors and capacitors), then its driving point impedance had to be strictly positive real. The resulting filter is a passive network, is energy dissipating, and therefore always stable.

2.1.3 Testing For Positivity

In order to apply the positivity theorem to establish the stability of actively controlled LSS, we need a method to test when a square transfer matrix is (strictly) positive real. A time domain and frequency domain test have been found for this purpose.

Time Domain Positivity Test [2]. Results obtained by B.D.O. Anderson yield a relatively simple positivity test in the time domain. This is described next.

Let $G(s)$ be a square matrix of rational transfer functions such that $G(j\infty)$ is finite and G has poles which lie in $Re[s] < 0$ or are simple on $Re[s] = 0$. Let $\left\{A, B, C, G(\infty)\right\}$ be a minimal realization of G, i.e., define

$$G(s) = C(sI-A)^{-1} B + G(\infty)$$

where

$$\dot{x} = Ax+Bu \tag{1}$$

$$y = Cx+G(\infty)$$

and A is of least possible dimension. Then $G(s)$ is positive real if and only if there exists a symmetric positive definite matrix P and matrices

W_o and L such that

$$\text{(i)} \quad PA + A^T P = -LL^T$$

$$\text{(ii)} \quad W_o^T W_o = G(\infty) + G^T(\infty)$$

$$\text{(iii)} \quad C^T = PB + LW_o$$

The fact that this test allows only simple (non-repeated) poles on the $j\omega$-axis need not worry us, since any real structure has some damping, no matter how small, so that repeated modal frequencies are removed from the $j\omega$-axis by this limiting argument. Furthermore, examination of Anderson's proof reveals that it would allow completely undamped modal frequencies of multiplicity greater than one because the normal coordinate formulation of the structure allows strict diagonalization even with repeated eigenvalues. The direct sum method of modal subspaces applies then to each mode, regardless whether the modal frequency is repeated or not.

G(s) is <u>strictly</u> positive real if for a sufficiently small real $\sigma > 0$, $\hat{G}(s) \triangleq G(s-\sigma)$ is positive real.

Note that this statement is equivalent to modifying condition (i) of the test to

$$PA + A^T P = -Q$$

where $Q = LL^T$ must be positive definite.

<u>Frequency Domain Positivity Test [Appendix of Reference 1]</u>. A frequency test results when one directly applies the definition of positive real. To this end, define the <u>positivity index</u> $\delta(\omega)$ of a square transfer matrix G(s) by

$$\delta(\omega) = \lambda_{\min} \left\{ \frac{1}{2}[G(j\omega) + G^*(j\omega)] \right\} \tag{2}$$

where $\lambda_{min}\{\cdot\}$ denotes "minimum eigenvalue of"

Then

$\delta(\omega) > 0$ for all ω implies G(s) is strictly positive real

$\delta(\omega) \geq 0$ for all ω implies G(s) positive real

$\delta(\omega) \leq 0$ for some ω implies G(s) is not positive

A very important advantage of this frequency domain positivity test over the time domain test is that frequency response data may be obtained experimentally through ground and/or on-orbit testing. This significantly reduces the importance of detailed analytical modelling of a structure by finite element methods. Experimental frequency data, by necessity, also includes actuator and sensor dynamics. Finally, it reduces the importance of how to model damping in a structure as the effects of damping are directly contained in the frequency response data.

Positivity Tests As Applied To LSS In Normal Coordinates [1,3]

Consider the use of normal modal coordinates in describing a linear structure. The description for G(s) in (1) results then in state equations with the system matrix ("A-matrix") in block diagonal form,* i.e.,

$$A = \begin{bmatrix} A_1 & & & O \\ & A_2 & & \\ & & \ddots & \\ O & & & A_\ell \end{bmatrix} \quad \text{with} \quad A_j = \begin{bmatrix} 0 & 1 \\ -\omega_j^2 & -2\alpha_j \end{bmatrix}$$

where $\ell \to \infty$ (arbitrarily large), ω_j is the frequency of the j^{th} mode, $\alpha = \zeta_j\, \omega_j$, and ζ_j is the damping ratio of the j^{th} mode.

Anderson's positivity test can in this case be solved by hand for arbitarily large ℓ because of the block-diagonal form. An example solution satisfying Anderson's positivity test is

$$C^T = B$$

* Assuming judicious ordering of the states.

This means that the transfer matrix of a structure is positive real if ideal collocated actuators and rate sensors are used. (But other solutions exist also). Note that this result is completely independent of numerical modal data or the number of modes in the model. Note also that application of the positivity stability theorem to this case demands that the controller transfer matrix H(s) be strictly positive real.

The inclusion of actuator and sensor dynamics with the LSS destroys the convenient block diagonal form of the modal state equations and the time domain positivity test (Anderson) becomes too difficult to apply. The frequency domain test is, in this case, a more attractive method to test the positivity of the infinite-dimensional plant (LSS). This is mainly because a relatively simple closed form expression for the transfer matrix $G_o(s)$ for the structure can be found, thereby avoiding the requirement for repeated matrix inversions in the evaluation of the positivity index $\delta(\omega)$. The terms appearing in the closed form expression for G (s) are given by

$$G(s) = G_s(s)\ G_o(s)\ G_a(s) \quad \text{and} \quad G_o(s) = \sum_{j=1}^{\infty} \frac{1}{\Delta_j(s)}\, C_j \tilde{B}_j$$

where G(s) models the total dynamics, $G_s(s)$ models the sensor dynamics, $G_o(s)$ models the structure, and $G_a(s)$ models the actuators. $G_o(s)$ is further defined by:

$$\Delta_j(s) = s^2 + 2\alpha_j s + \omega_j^2 \qquad \tilde{B}_j = \begin{bmatrix} \phi_j(z_{a1}) & \cdots\cdots & \phi_j(z_{am}) \\ s\phi_j(z_{a1}) & \cdots\cdots & s\phi_j(z_{am}) \end{bmatrix} \qquad C_j = \begin{bmatrix} 0 & \phi_j(z_{s1}) \\ \vdots & \vdots \\ 0 & \phi_j(z_{sm}) \end{bmatrix}$$

where $\phi(z_{am})$ is the j^{th} mode shape at the m^{th} actuator location (z_s = sensor location).

Note that with actuator and sensor dynamics included, the positivity index $\delta(\omega)$ will now have negative peaks at some modal frequencies. This indicates that the system is no longer positive and that the positivity theorem must be augmented with operator embedding. This will be the subject of Section 2.1.6.

2.1.4 Control System Design Using Positivity

There are two basic steps involved when one uses positivity theory for control system design. One is to assure that the plant (LSS) is positive.* The other is to design a controller that is strictly positive. For the purposes of this section, assume that ideal collocated actuators and rate sensors are used. This means, from the arguments used in Section 2.1.3, that the LSS is already positive. Hence, what remains is the design of the strictly positive controller.

Time Domain Controller Design. Consider the linear quadratic Gaussian (LQG) controller topology shown in Figure 2.2. It consists of a state estimator followed by a state feedback gain. The state equations for the controller (without the B_c-loop) are given by

$$\dot{\hat{x}}_c = (A_c - G_c C_c)\, \hat{x}_c + G_c y$$

$$v = K_c\, \hat{x}_c$$

If this controller acknowledges only the existence of the controlled modes and no special precautions are taken, the system will surely suffer from the effects of observation and control spillover. The application of the positivity design approach, however, will assure stability.

The basic approach is to design the estimator gain matrix G_c first, and then apply Anderson's positivity criterion so that the transfer matrix H(s) of the controller is strictly positive, where H(s) is given by

* Although this section will presently assume the ideal situation where the LSS is positive, Section 2.1.6 will show that the statement: "the plant is positive", may be replaced by the statement: "the embedded plant is positive". This generalization will permit the treatment of non-positive LSS with the methods of this section.

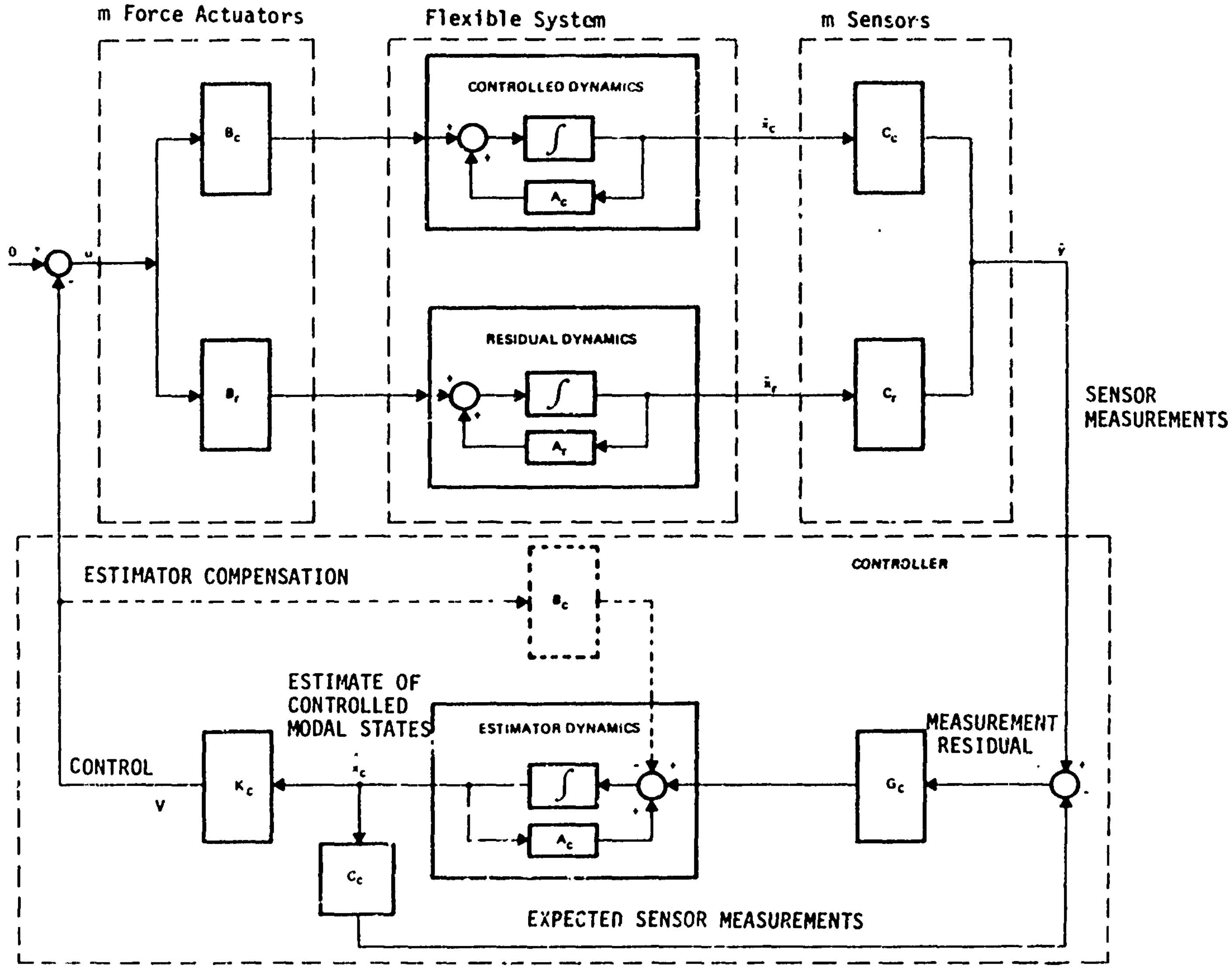

Figure 2.2. LQG CONTROLLER TOPOLOGY

$$H(s) = K_c (sI-\Gamma)^{-1} G_c \quad \text{with } \Gamma = A_c - G_c C_c$$

The estimator gain matrix G_c is, for example, determined as the steady state Kalman filter gain solution, or it is based on pole assignment, (i.e. a Luenberger observer), or it is based on any other method that appears desirable. The feedback gain matrix K_c is now observed to be the output matrix of the filter. So, from the Anderson test, if one solves the Lyapunov equation

$$P\Gamma + \Gamma^T P = -LL^T \triangleq -Q$$

for P, where Q is any positive definite symmetric matrix, K_c obtained from

$$K_c^T = P G_c$$

assures that H(s) is strictly positive real.

Note here that the choice of the matrix Q provides the needed design freedom to adjust performance.

The B_c compensation loop in the state estimator is dashed, because it cannot be explicitly present when K_c is directly determined via positivity. This is because the B_c loop makes K_c also a part of the system matrix of the filter, rather than K_c being only an output matrix. But when the state estimator gain matrix G_c is chosen to be equal to the plant input matrix B_c associated with the controlled modes, i.e., $G_c = B_c$, then the dashed loop may be added after K_c has been determined without violating the positivity of the controller.

2.1.5 Relationship Of The Time Domain Positivity Design To The General LQG Design

With the B_c-loop included in Figure 2-2, the topology of the LQG controller and time domain positivity designed controller are the same. The two design approaches can result in the same controller for special cases, although they are generally different.

In either the LQG or positivity case the designer must start by selecting certain positive definite matrices Q and R and then, respectively,

solve Ricatti and Liapunov equations. If the LSS is assumed to be described in normal modal coordinates and collocated actuators and rate sensors are used, Table 2.1 shows a set of conditions on the various Q's and R's that result in the same controller for either design approach.*

The subscript "F" in Table 2.1 is associated with the Kalman filter in the controller, and the subscript "OR" is associated with the optimal regulator solution for K_c. We define also the notation

$$\tilde{Q}_F = \text{diag}\begin{bmatrix}\tilde{Q}_{Fj}\end{bmatrix} \quad \text{with} \quad \tilde{Q}_{Fj} = \begin{bmatrix} 0 & 0 \\ 0 & 4\alpha_j\sigma_F^2 \end{bmatrix} \quad j = 1,2,\ldots \ell_c = \#\text{controlled modes}$$

where $\alpha_j = \zeta_j\omega_j$ = damping and σ_F^2 any positive number (in effect being variance of the observation noise). Finally, $\tilde{Q}$ is defined as

$$\tilde{Q} = \text{diag}\begin{bmatrix}\tilde{Q}_j\end{bmatrix} \quad \text{with} \quad \tilde{Q}_j = \begin{bmatrix} 0 & 0 \\ 0 & 4\,\alpha_j \end{bmatrix}$$

Table 2.1 One Set Of Conditions For Which The LQG Solution Equals The Time Domain Positivity Design.

	K-FILTER/REDUCED STATE ESTIMATOR	DETERMINATION OF FEEDBACK GAIN MATRIX
LQG	$R_F = \sigma_F^2 I$ $Q_F = \tilde{Q}_F + \sigma_F^2 B_C B_C^T$	$R_{OR} = \sigma_{OR}^2 I$ $Q_{OR} = \sigma_{OR}^2 (\tilde{Q} + B_C B_C^T)$
POSITIVITY	SAME AS FOR LQG	$Q = \tilde{Q} + 2B_C B_C^T$

* This set is not unique, but is one possible solution.

<u>Relationship Of The Time Domain Positivity Design To Other LSS Design Approaches</u>. Model error sensitivity suppression (MESS) [4] is a specialized case of LQG design. MESS is therefore related to the time domain positivity design in a manner similar to what was just discussed previously.

MESS with sensor throughput [4] (shown in Figure 2.3a) is related to the positivity design since it attempts to make the controller more positive. That is,

$$\underset{\substack{\uparrow\\ \text{MESS WITH}\\ \text{SENSOR THROUGH-}\\ \text{PUT}}}{\tilde{H}(s)} = \underset{\substack{\uparrow\\ \text{MESS}}}{H(s)} + \underset{\substack{\uparrow\\ \text{SENSOR}\\ \text{THROUGH-}\\ \text{PUT}}}{DI} \quad , \quad D > 0$$

makes $\tilde{H}(s)$ more positive.

The direct "innovations feedthrough" used by BALAS [5] (shown in Figure 2.3b) is a similar LQG type concept and also results in a more positive controller. If either MESS with sensor throughput or LQG with innovations feedthrough techniques are used with collocated actuators and sensors, as various researchers have done, a positive controller has in effect been generated.

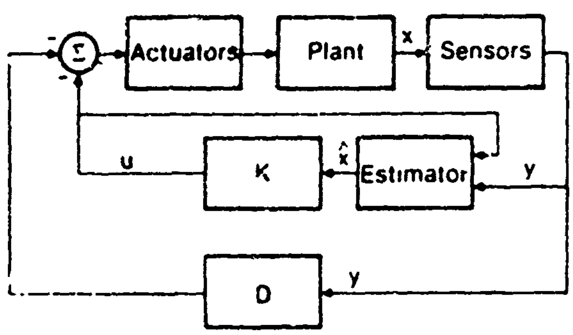

Figure 2.3a SENSOR THROUGH-PUT

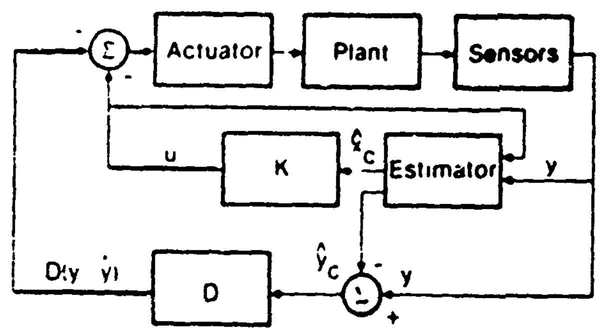

Figure 2.3b INNOVATIONS FEEDTHROUGH

Figure 2.3 LQG Variations Resulting In A More Positive Controller

2.1.6 Operator Embedding

Motivation For Using Embedding. The motivation for using operator embedding is that strict positivity is too restrictive a requirement to place on the physical plant. Using Anderson's results for establishing positivity, the transfer matrix representing a structure was shown to be always positive if ideal collocated actuators and rate sensors are used. However, when the effects of finite bandwidth in the actuators and sensors are included in the dynamic model of the structure, its transfer function ceases to be positive because of the additional phase shift introduced by these components. The use of pure position measurement and/or non-collocated actuators and sensors similarly destroy positivity by de-coordinating the spatial and time phase relationships existing between actuators and sensors.

Strict positivity also limits controller design. This is because the difference between the number of poles and zeros in a positive transfer function cannot differ by more than one. The closed loop input-output control transmission roll-off of a design is therefore constrained to be 10, or 20 dB/decade for a feedback or cascade controller, respectively. The net effect is that in feedback compensation, noise rejection is limited, while in cascade compensation, "Bode" sensitivity suffers.

Definition, Types, and Implications Of Embedding. In order to make the positivity theorem less restrictive and therefore more useful, operator embedding is used. Embedding essentially is a block diagram transformation of the original system into a stability equivalent system*; one then requires positivity of this new system.

Two types of embedding transformations have been considered in this study. "F" embedding, Figure below, refers to the cascade transformation, directly related to the Popov multipliers (simplest form is $1+jq\omega$).

---

* It is important to note that stability equivalent or invariance does not mean input-output transmission invariance.

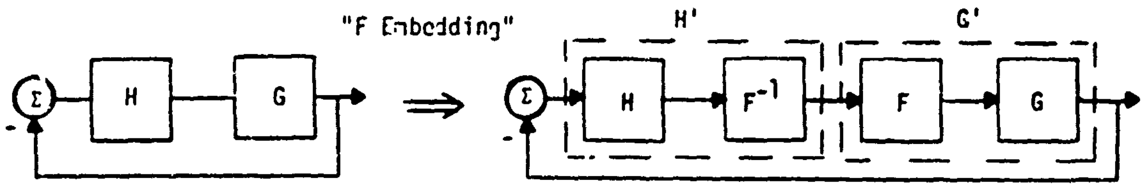

"D" embedding, Figure below, refers to the parallel transformation directly related to the Popov absolute stability sector gain (simplest form is 1/K).

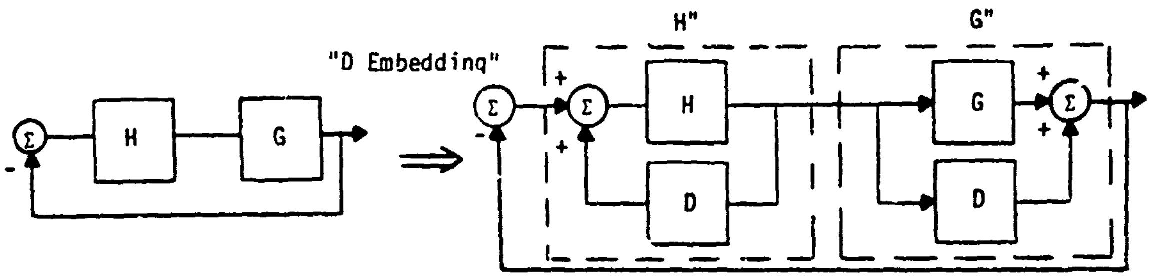

"F" and "D" embedding can obviously be combined to transform the G and H system into

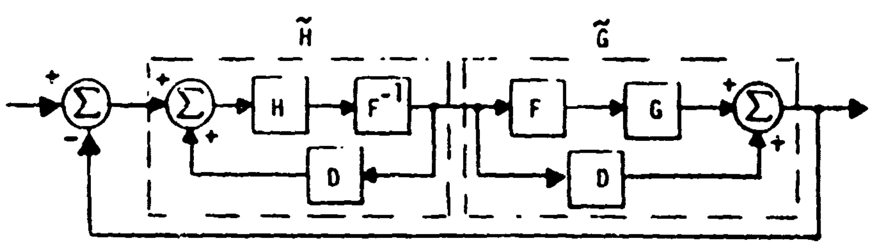

This block diagram transformation sequence results in the corresponding new transfer matrices given by

$$\tilde{H} = (I - F^{-1}HD) \quad F^{-1}H$$

and

$$\tilde{G} = GF + D$$

where F and D are any well-behaved transfer matrices (well-behaved operators), including constant matrices.

The judicious selection of F and D in the embedding process will make it possible to establish positivity of $\tilde{G}$ even though the plant G is not a positive operator. The controller H, however, must "pay" for this, since it must be very stable and positive to start with in order that the new $\tilde{H}$ will remain positive. To see this, set F = I and let D be a constant, diagonal positive definite matrix. This clearly helps to improve the positivity of $\tilde{G}$ (think of the trace of a matrix) but it wraps a positive feedback loop around H, so that H had to be very stable for $\tilde{H}$ to be (strictly) positive real.

It is important to note that the embedding transformation is only mathematical and is not physically implemented. The embedding may, however, impose conditions on the controller which must be physically implemented..

Generally, embedding requires some knowledge of the plant to be controlled. For example, constant "D" embedding will require that one has estimated (albeit, crudely) the norm of the mode shapes and damping ratio of the high frequency modes. If one has additional knowledge of the plant, more complex embedding can be used to yield less conservative stability conditions. In a gross manner, embedding permits one to quantify stability conditions as a function of system knowledge.

Selection and Effects of "D" Embedding. When the plant G(s) is not positive, "D" embedding may be used to establish positivity. This is done by finding an operator D such that G(s) + D is positive. The next question to be answered is how D should be chosen to assure that G" = G + D is positive. One suspects that one must first determine how negative G really is. For this purpose a positivity/negativity index of G must be determined.

The positivity index for $G(j\omega)$ was defined in Equation (2) as

$$\delta_G(\omega) = \lambda_{min} \left\{ 1/2[G(j\omega) + G^* (j\omega)] \right\}, \ \omega\epsilon[0, \infty)$$

where G(j) includes the structure plus actuators and sensors.

The operator D must then be determined so that

$$\delta_{G+D}(\omega) = \lambda_{min}\left\{\frac{1}{2}\ [(G+D) + (G+D)^*]\right\} > 0, \quad \omega \varepsilon [0,\infty)$$

This last task is considerably simplified if $[D(j\omega) + D^*(j\omega)]$ is chosen to have the same eigenvectors as $[G(j\omega) + G^*(j\omega)]$. That is, the same eigenvector matrix Q and its conjugate transpose Q^* ($x+x^*$ is Hermitian).

$$Q^*(j\omega)[G(j\omega) + G^*(j\omega)]\ Q(j\omega) = \Lambda_G$$

$$Q^*(j\omega)[D(j\omega) + D^*(j\omega)]\ Q(j\omega) = \Lambda_D$$

where $\Lambda_{(.)}$ denotes "The matrix containing the eigenvalues of $(\cdot)$". For this case, if $\delta_D(\omega)$ is chosen so that

$$\delta_D(\omega) + \delta_G(\omega) > 0, \ \forall\ \omega\varepsilon\ [0, \infty)$$

then

$$Q^*[D + D^*]\ Q + Q^*[G + G^*]\ Q > 0$$

$$Q^*[(D + G) + (D + G)^*]\ Q > 0$$

$$\delta_{D+G}(\omega) \qquad > 0\ , \quad \forall \omega \varepsilon [0,\infty)$$

Further simplifications exist if $D(j\omega) = d(j\omega)\cdot I$. For this case, $D(j\omega)$ always has the correct eigenvector structure, i.e.,

$$D(j\omega) = d(j\omega) \cdot I = d(j\omega) \cdot Q^*Q$$

so if the real part of $d(j\omega)$ is chosen as

$$\text{Re}\ [d(j\omega)] > -\delta_G(\omega)\ , \quad \forall \omega\varepsilon\ [0, \infty)$$

then

$$\delta_{D+G}(\omega) > 0, \quad \forall \omega \varepsilon \; [o, \infty)$$

The effect of "D" embedding is to cut the gain of the controller. To see this, consider "D" embedding in Figure 2.1 and let $H(s) = K > 0$, then $H" = (I - KD)^{-1} > 0$ implies $(I - KD)$ is positive.

Hence

$$tr[I - KD] = tr\,[I] - tr\,[KD] > 0 = \quad m > tr\,[KD]$$

Where m is the number of inputs to the system. For the case $m = 1$, $m > tr\,[KD] \nRightarrow \; k < 1/D$. Hence the gain is limited by 1/D. This has the obvious implications that "D" embedding gain stabilizes the system. It therefore places a limit on the achievable damping and disturbance rejection at high frequencies that can be achieved in a design*.

<u>"D" Embedding Design Via The Anderson Test</u>. The previously described time domain design using the Anderson Test (Page 2-4) may be used even with a non-positive plant. The key difference when the plant is non-positive is that the minimum of the positivity index

$$\delta_{min} = \min_{\omega} \left| \lambda_{min} \left\{ \frac{1}{2} \left[G(j\omega) + G^*\,(j\omega) \right] \right\} \right|, \; \omega \varepsilon [o, \infty)$$

must be computed. Then define a $\delta_o > -\delta_{min} > 0$ and wrap a $-\delta_o I$ feedback around the selected positive controller. This pre-feedback is implemented and it creates a new controller that is positive even after the "D" embedding wraps a $+\delta_o I$ feedback around it, see Figure 2.4.

---

* It should be noted that these limitations can be mitigated through pre-compensation of the plant or through "F" embedding. This will be shown later.

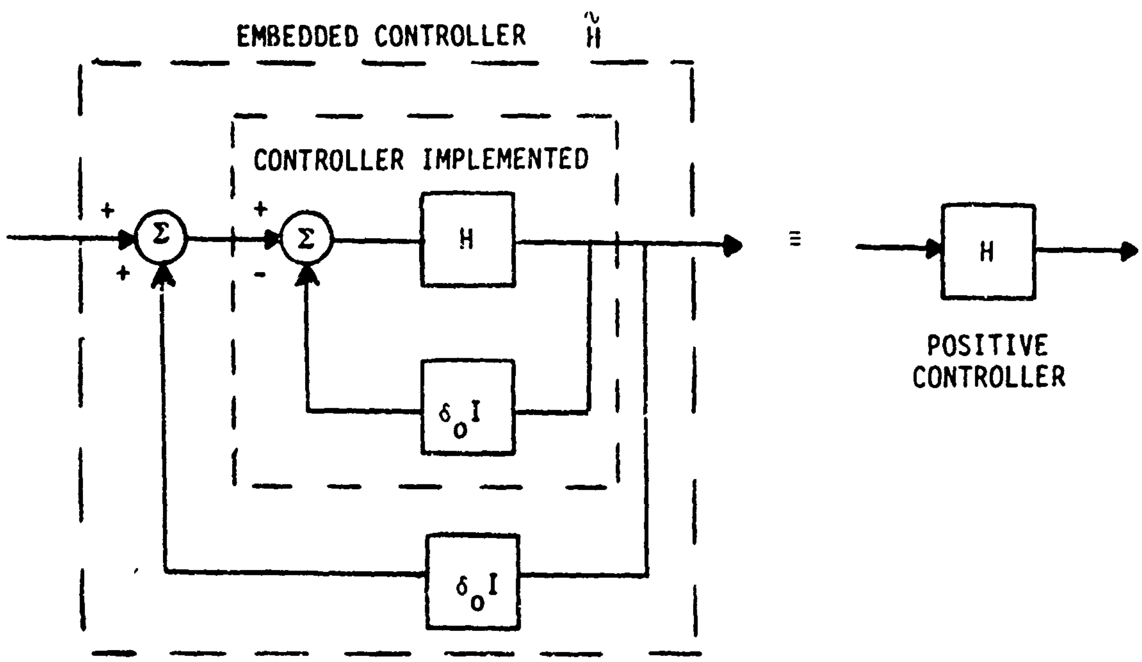

Figure 2.4 Embedded Controller $\tilde{H}$ = H After Pre-Feedback Compensation

The design steps using this approach are summarized as follows:

1) Determine the minimum of the positivity index, δ_{min}, of the plant and actuators + sensors. Choose a δ_o >- δ_{min}.

2) Design a state estimator for the truncated plant, e.g., steady state Kalman filter or Luenberger observer.

3) Solve the Lyapunov equation on page 2-4 to obtain the controller gains. This step will ensure that the controller, H, is positive

4) Wrap negative feedback $D = \delta_o I$ around H and implement this new controller so that it remains positive even after embedding.

The above steps will ensure that the closed loop system is stable by the positivity theorem, and will result in the controller topology shown in Figure 2.5.

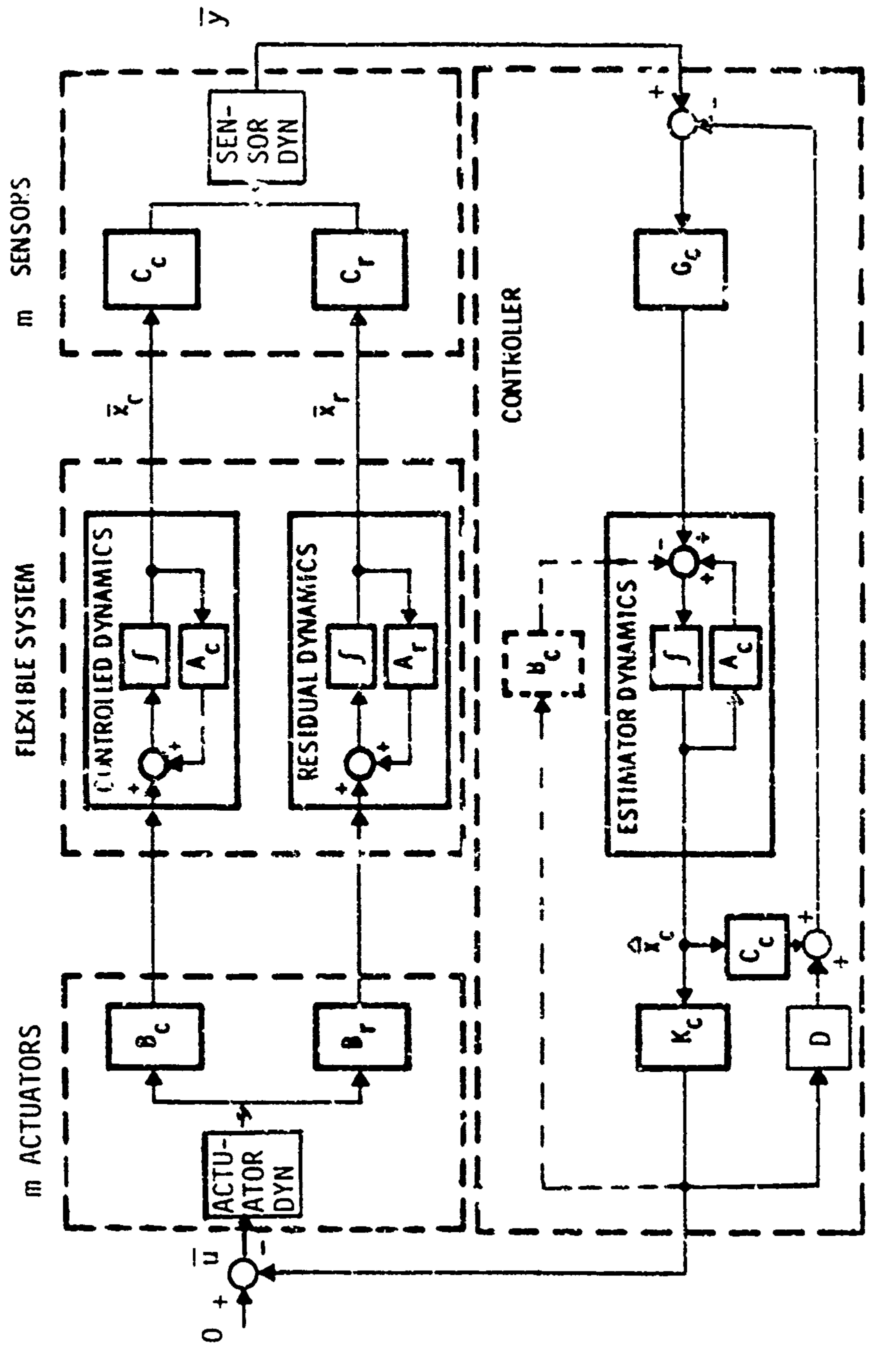

Figure 2.5 Pre-Feedback Compensated Time Domain Design

"D" Embedding Design Using The Positivity (P)-Plot. "D" embedding may be performed in a more direct manner in the frequency domain. Just as for the method using the Anderson Test, one needs to first determine the positivity index $\delta(\omega)$ of the plant and then determine $\delta_0 >- \delta_{min}$. However, steps two through four are combined by predesigning a controller H(s) to withstand the "D" embedding, i.e., such that

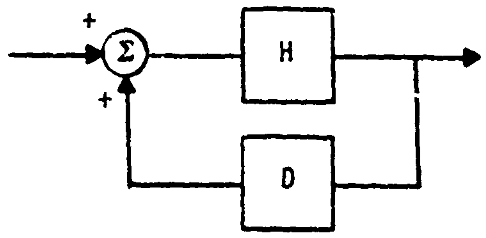

is positive

To do this, one uses a conformal map, called the positivity (P)-Plot. See Figure 2.6. P-Plot describes the closed-loop gain and phase of a positive feedback system as a function of its open-loop values. Hence, all one has to do is make sure that the controller H(s) with loop gain δ_0, lies within the $\pm$ 90° closed-loop phase region of the P-Plot (shaded region).

"D" Embedding Design Combined With Frequency Domain Precompensation. In practice, precompensation of the plant may be needed in order to meet stability and performance objectives. One can combine "M" precompensation and "D" embedding by first carrying out a full multivariable frequency domain type design (summarized next). This results in the determination of a cascade precompensator M(s). The net effect is a cascade pre-compensated system within which the controller, M(s), has already been designed for performance (low sensitivity, noise rejection and damping) and desired high frequency roll-off. The latter is important since the maximization of the roll-off minimizes uncertainties in the "D" embedding required. Once the performance design is completed, one can determine the "D" embedding operator that makes the precompensated plant positive. This is typically done by determining the positivity index $\delta(\omega)$ of the precompensated plant, finding its most negative peak δ_{min}, and choosing $D = \delta_0 I$, $\delta_0 >- \delta_{min} > 0$. The "H" part of the controller consists then merely of gains which must be set to less than or equal to $1/\delta_0$. The actually implemented controller satisfying the positivity design is, as shown in Figure 2.7, then given by $(1/\delta_0)M(s)$.

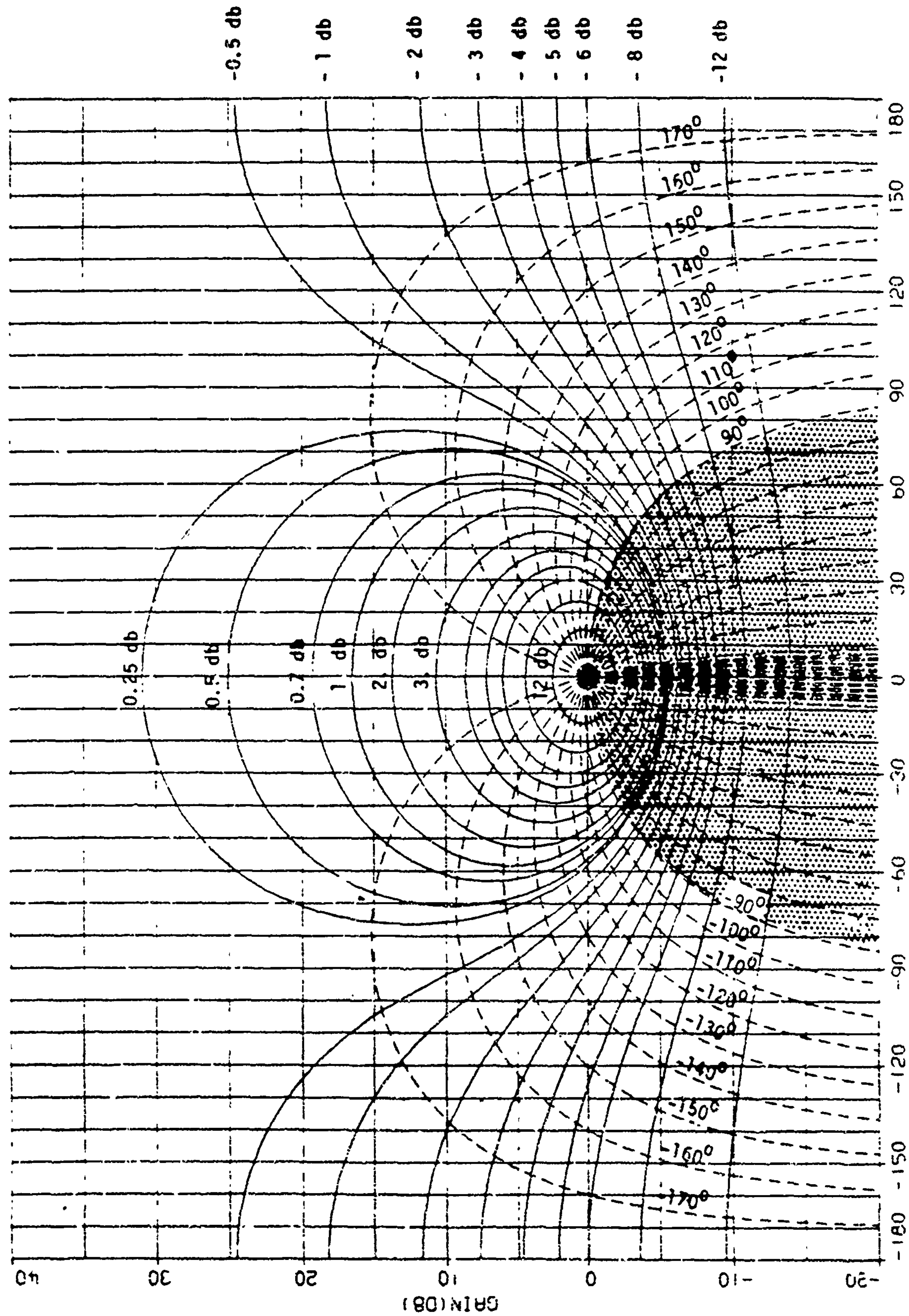

FIGURE 2.6 Positivity (P) - Plot

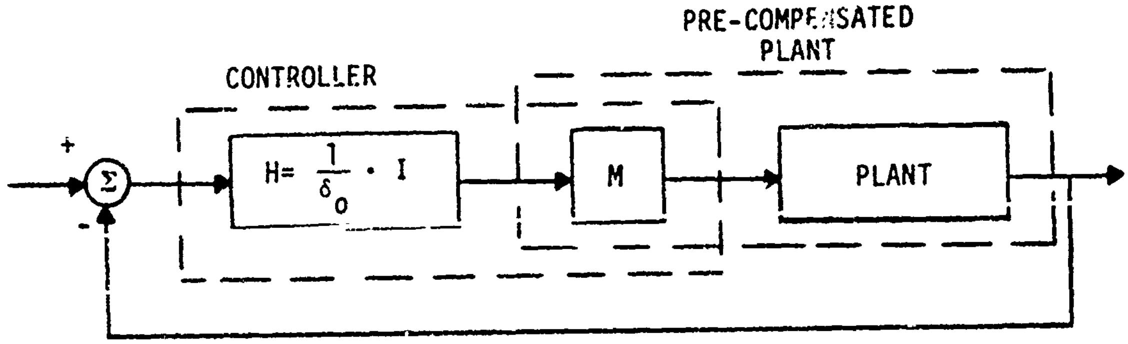

Figure 2.7. "D" Embedding A Precompensated Plant.

The key to the extension of the classical Nyquist/Bode approach to the multivariable case [6] are the characteristic gains of the transfer matrix, G(s), describing the open-loop plant. The characteristic gains λ (s) are defined as the solutions to the equation

$$\mathrm{DET}\,[\lambda(s) \cdot I - G(s)] = 0 \;; \quad s \in [oj, \infty j)$$

The importance of the characteristic gains stem from the fact that the characteristic gains of a unity feedback system are related to the open-loop values in a manner analogous to single-input-single-output systems. i.e.,

$$\text{closed-loop gain} = \frac{\text{open-loop gain}}{1 + \text{open-loop gain}}$$

The main results using this technique are:

1) Closed-loop stability occurs if and only if the net sum of counter-clockwise encirclements of the (-1,0.) point by the characteristic gains is equal to the number of open-loop unstable poles.

2) To achieve low control interaction in a frequency band, it is sufficient that all the characteristic gains have a large magnitude over that frequency band.

3) In frequency bands of low interaction, the notions of gain margin and phase margin may be applied as a qualitative assessment of performance.

4) There is a relationship between tracking accuracy and the magnitude of the characteristic gains. Under the appropriate assumptions the relationship is analogous to the single-input-single-output case.

2.1.7 General Formats For Computer Aided Design

The functions to be evaluated in the positivity design are lengthy and virtually impossible to do by hand. A computer aided design approach is therefore required. Figures 2.8a and 2.8b respectively show the general software formats for computer-aided time domain design and frequency domain design. Enclosed by the parenthesis are listed TRW programs/sub-programs which implement and perform the required computations. The key elements required to make the package useful are a fast computer, highly accurate linear algebra/eigenvalue subroutines, and a highly interactive man-machine iterative loop with graphics. The current TRW package employes this approach and makes extensive use of state-of-the-art subprograms and graphics from the IMSLIB, EISPAK and TGSLIB Libraries.

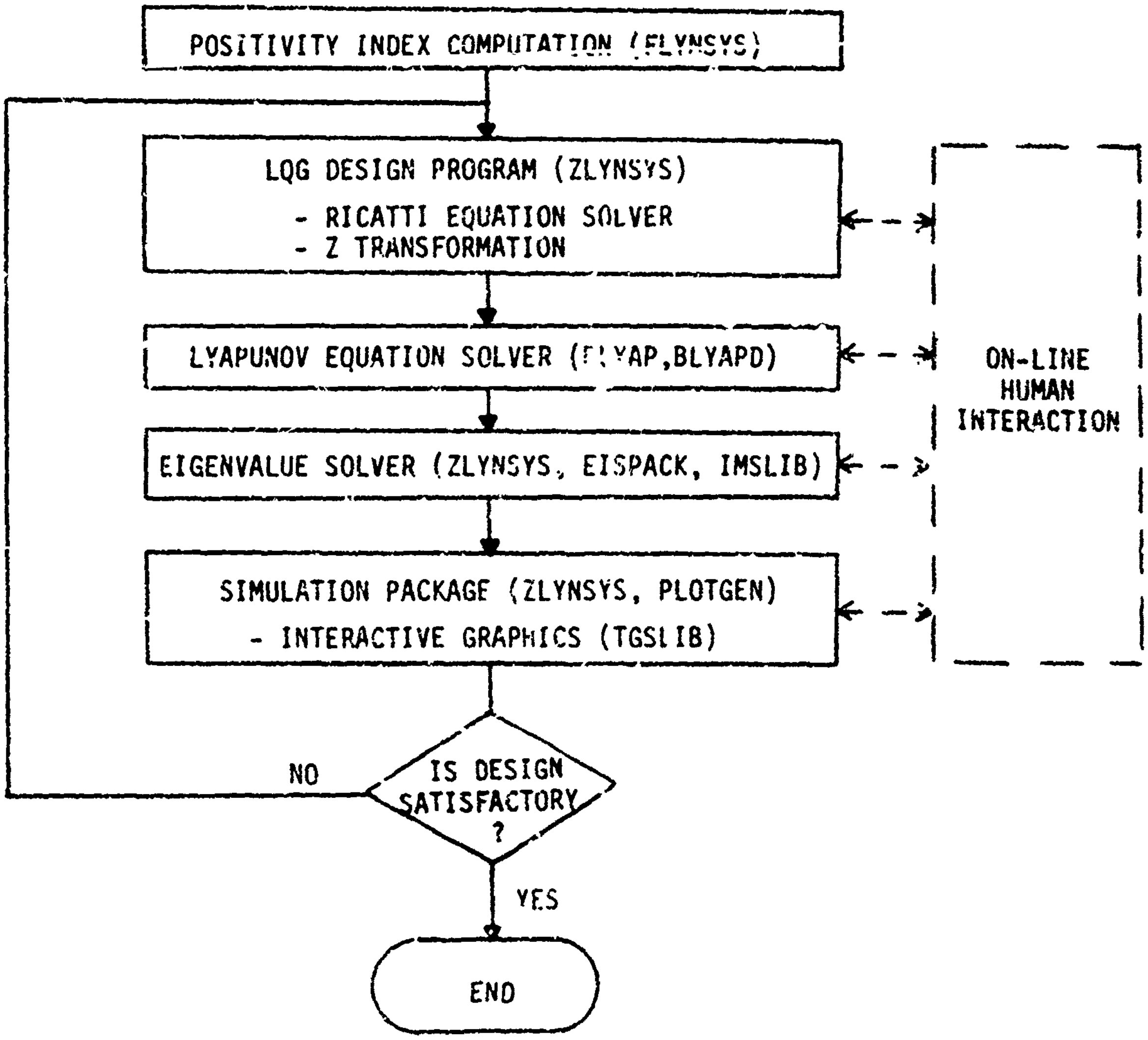

Figure 2.8a Computer Programs Required For Time-Domain Design

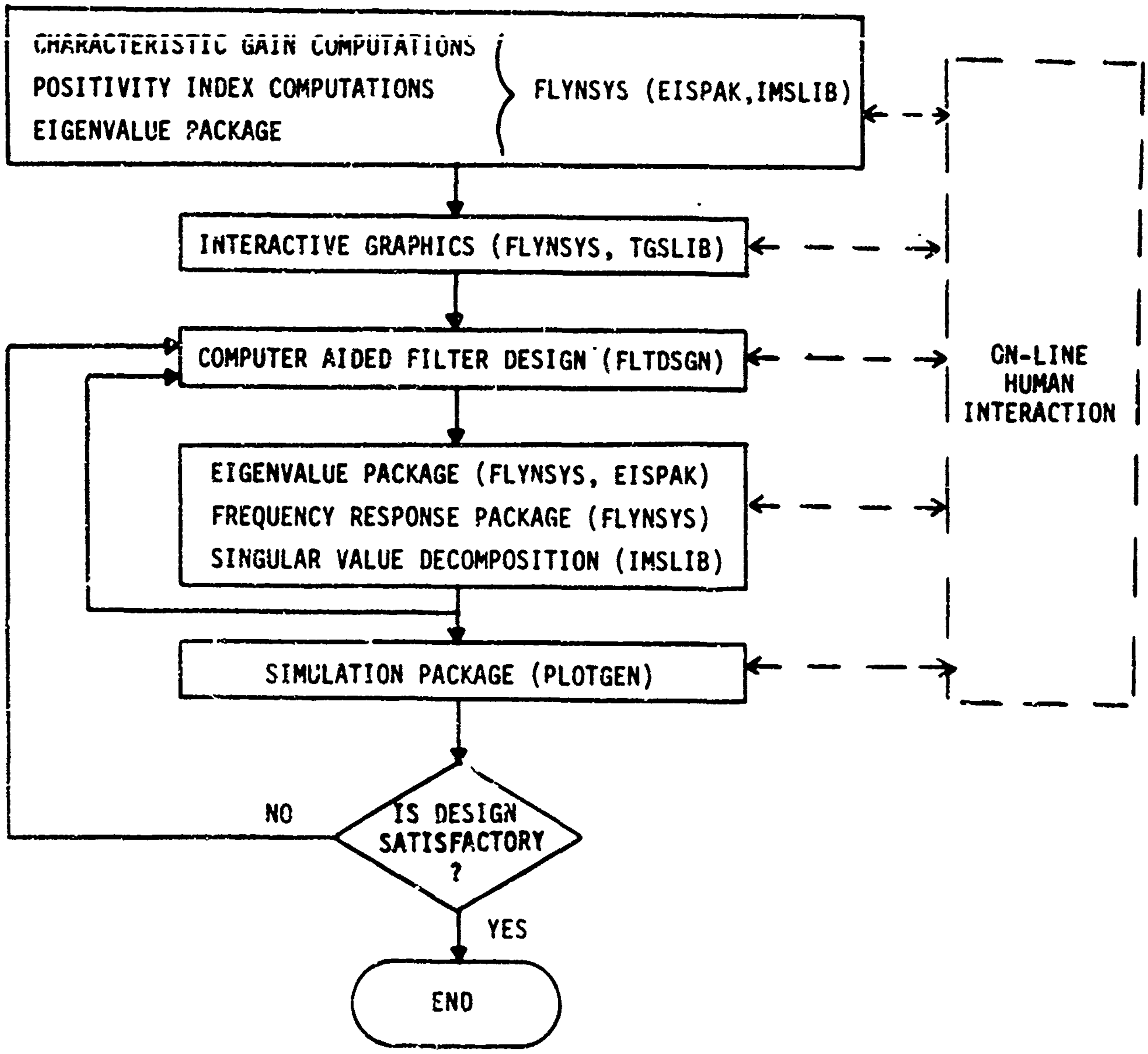

Figure 2.8b Computer Programs Required For Frequency Domain Design

2.2 FLAT PLATE E' ?LES

As an example consider a simply supported (pivoted, 4 sides), 1.5 x 1.5 m aluminum plate that is 1.5mm thick, shown in Figure 2.9. The first 10 modal frequencies* and a closed form expression for the mode shapes are given in the Table 2.2. Assume the objective is to actively control the first three modes. Since repeated modal frequencies are present, one requires at least two sensor/actuator pairs to ensure observability/ controllability. Two point-force actuators and two rate sensors collocated have therefore been chosen as shown in the Figure.

2.2.1 Idealized Time Domain Design Example

In the design assume we have ideal collocated actuators and ra.' sensors. The plate transfer matrix will therefore be positive real regardless of the exact values of the modal frequencies and modal truncation. The basic time-domain approach is then to design a strictly positive real controller transfer matrix H(s) by applying Anderson's positivity criterion.

Referring to Figure 2.2, first, since three modes are to be controlled, a sixth order state estimator is designed by solving for the steady-state Kalman filter gain, G_c, of the truncated model (3 controlled modes). Then one notes that K_c is the output matrix of the controller, i.e.,

$$H(s) = K_c\ (sI-\Gamma)^{-1}\ G_c \quad \text{with} \quad \Gamma = A_c - G_c\ C_c$$

So, from Anderson's test, one can solve a Lyapunov equation for the state feedback gain K_c which will ensure that the controller is positive. $LL^T=Q=$ Diagonal (100), here, was found to yield good performance. Since the plate is positive and the controller is designed to be strictly positive, the design is guaranteed to be stable even when an arbitrary number of residual modes are retained.

---

* Damping is .4%

Table 2-2 Modal Parameters For Plate Example

Mode Number j	Mode Shape Integers k	ℓ	Modal Frequency Hz
1	1	1	3.24
2	1	2	8.10
3	2	1	8.10
4	2	2	12.96
5	3	1	16.20
6	1	3	16.20
7	2	3	21.00
8	3	2	21.00
9	4	1	27.5
10	1	4	27.5

The mode shapes are obtained from the equation:

$$\phi_j(x, y) = .449 \sin\left(\frac{k\pi x}{1.5}\right) \sin\left(\frac{\ell\pi y}{1.5}\right)$$

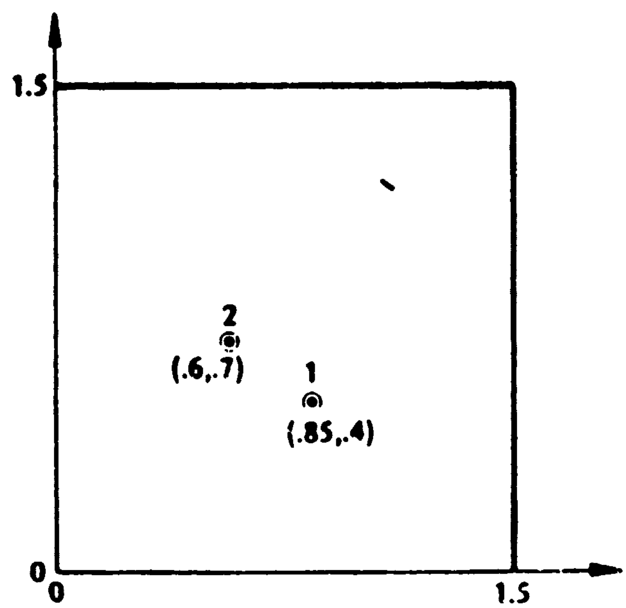

Figure 2.9 Flat Plate With Collocated Actuators/Sensors

Figures 2.10a-d show closed-loop simulation results for a plate model retaining the first 10 modes. Figure 2.10a and b show the plate deflection transient response and control effort at the control stations. Figures 2.10c and d show that the transient response of the controlled modes is good and the residual modes are stable.

2.2.2 Time Domain Design Example With "D" Embedding

Using the same flat plate model, the "D" embedding design method using the Anderson test will be used to demonstrate the positivity time-domain technique with finite bandwidth actuators and sensors. The actuators and sensors have been modelled as first order lags with a bandwidth of 30 Hz.

Following the design steps on page 2-17 one first computes the positivity index $\delta_G(\omega)$. This is plotted in Figure 2.11. Here, one notes that because of the collocated actuators and sensors $\delta_G(\omega)$ is positive except for some negativity at the modal frequencies. This effect is due to the phase shift in the actuators and sensors.

Next, as in the first example, one computes the Kalman gains G_c for the 3-controlled-mode, truncated plate model and computes the state feedback gain K_c according to the Lyapunov equation. This guarantees that H(s) is positive.

Finally, one compensates H(s) so that one can embed the system and have $\delta_{D+G}(\omega) > 0$ for all ω. The simplest way to do this is, as described earlier, to choose D equal to $\delta_0 \cdot I$, where $\delta_0 > -\delta_{min} > 0$ and δ_{min} is the most negative value of $\delta_G(\omega)$. $\delta_0 = 0.15$ is a good choice here.

The implemented controller

$$H_I = (I + HD)^{-1} H$$

will therefore permit a fictitious "D" embedding with $D = 0.15 \cdot I$ and still remain positive. This leaves the closed-loop system looking like that shown in Figure 2.5 and it is stable by positivity theory.

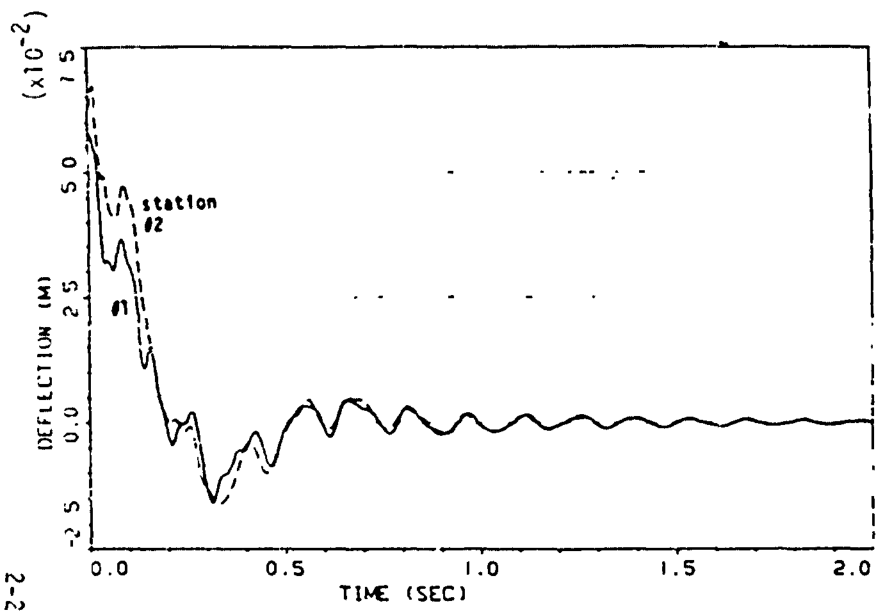

Figure 2.10a PLATE DEFLECTION AT STATIONS

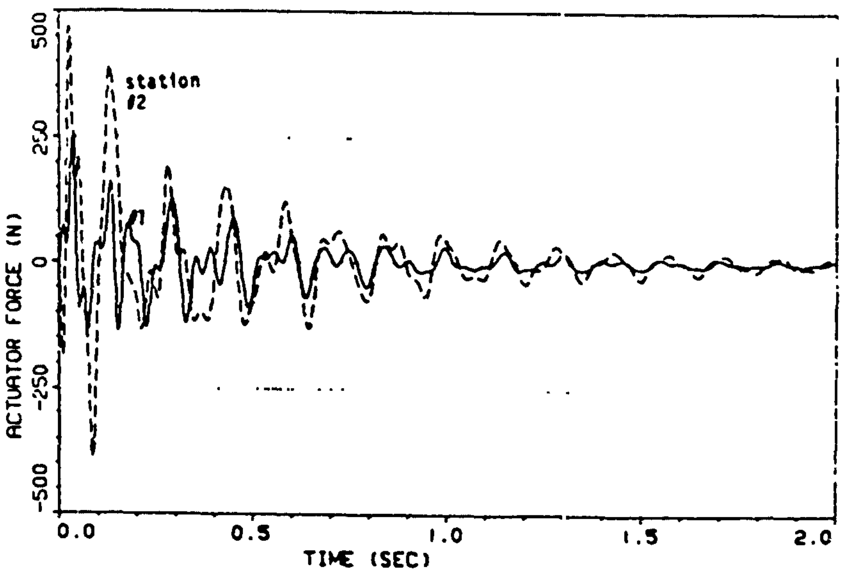

Figure 2.10b REQUIRED ACTUATOR CONTROL FORCE INPUT

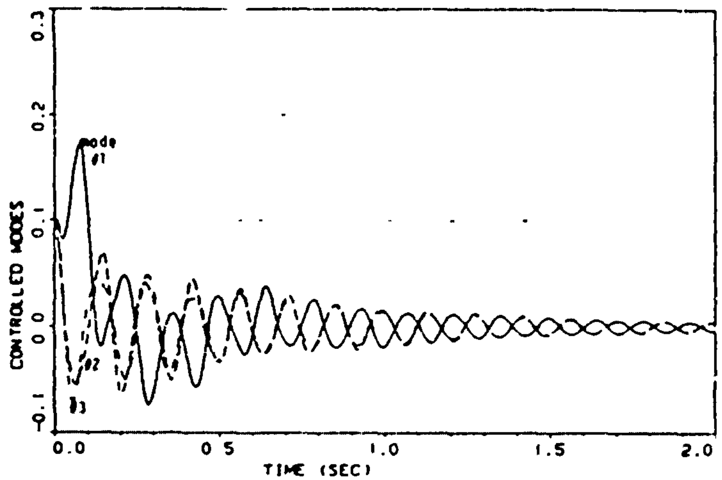

Figure 2.10c CONTROLLED MODES RESPONSE (3 MODES)

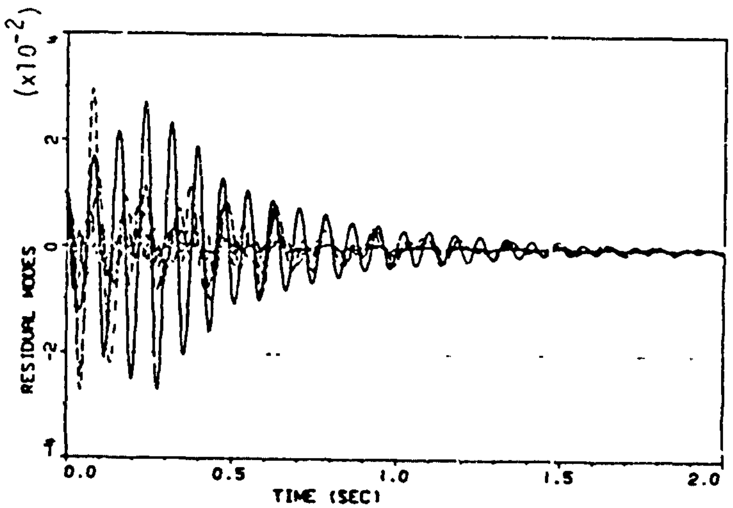

Figure 2.10d RESIDUAL MODES RESPONSE (7 MODES)

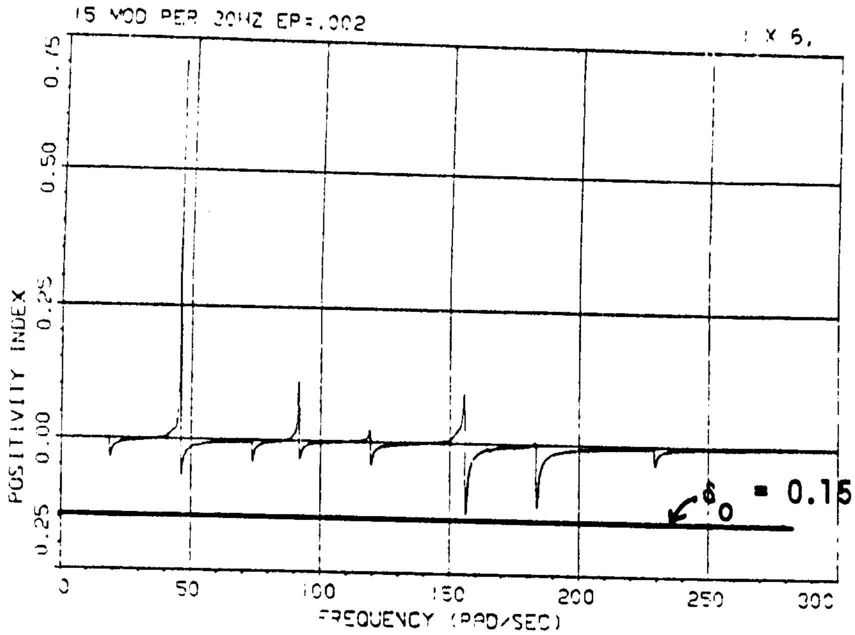

Figure 2.11 Positivity Index For Plate With Actuators and Sensors

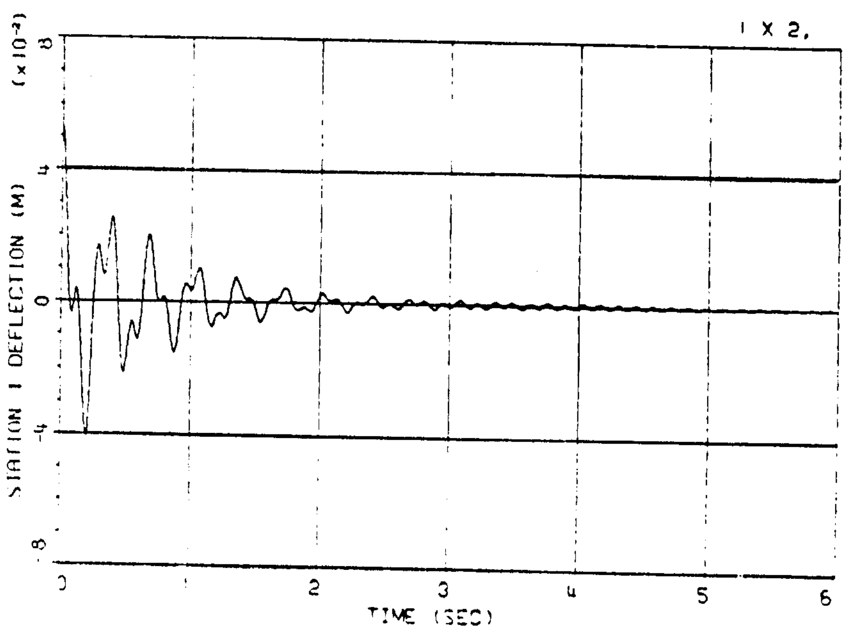

Figure 2.12a Output Transient of Plate At Station #1

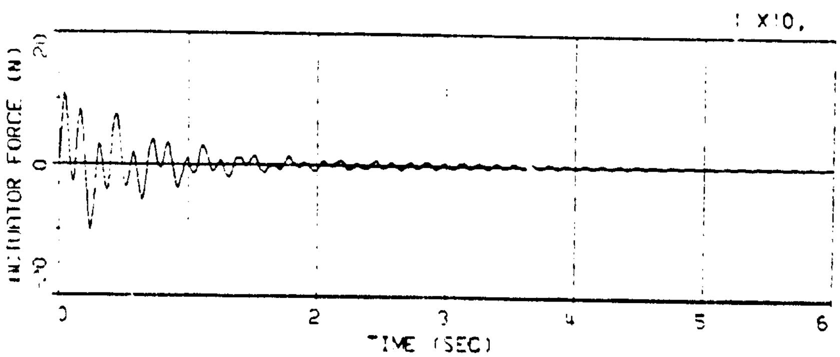

Figure 2.12b Control Force At Station #1 of Plate

Figures 2.12a and b show the simulated transient response of the designed system. Figure 2.12a shows the transient is stable. Figure 2.12b shows that the control effort is very modest. It is interesting to compare these simulation results with those of the idealized system, figure 2.10a-d. The transient in the present design is half as fast and the control effort is reduced by a factor of 50. These results make good intuitive sense since one is now dealing with finite bandwidth actuators and sensors.

2.2.3 Frequency Domain Precompensation Example

Using the same flat plat as an example, the combined precompensations and "D" embedding technique outlined on page 2-20 will be used to show how one can manipulate the characteristic gains and the positivity index.

The characteristic gains for the plate, shown in Figure 2.13a, lead one to believe that the system has sufficient stability margins to permit high loop gains. However, the positivity index, shown in Figure 2.13b has not decreased at high frequencies, a region where high uncertainty exists in the modal data. Hence, one needs to use low loop gains in order to accommodate for a conservative estimate of the δ_0 used during the "D" embedding operation. This of course is at the expense of performance. To avoid this problem, one would like to shape the loci so that a decreasing positivity index is obtained at high frequencies. If this is done such that there is little or no effect on the controlled modes, it would permit a less conservative estimate of δ_0, the latter permitting higher loop gains. The approach that has been used is to shape the characteristic gains and the positivity index by using a commutative compensator [6].

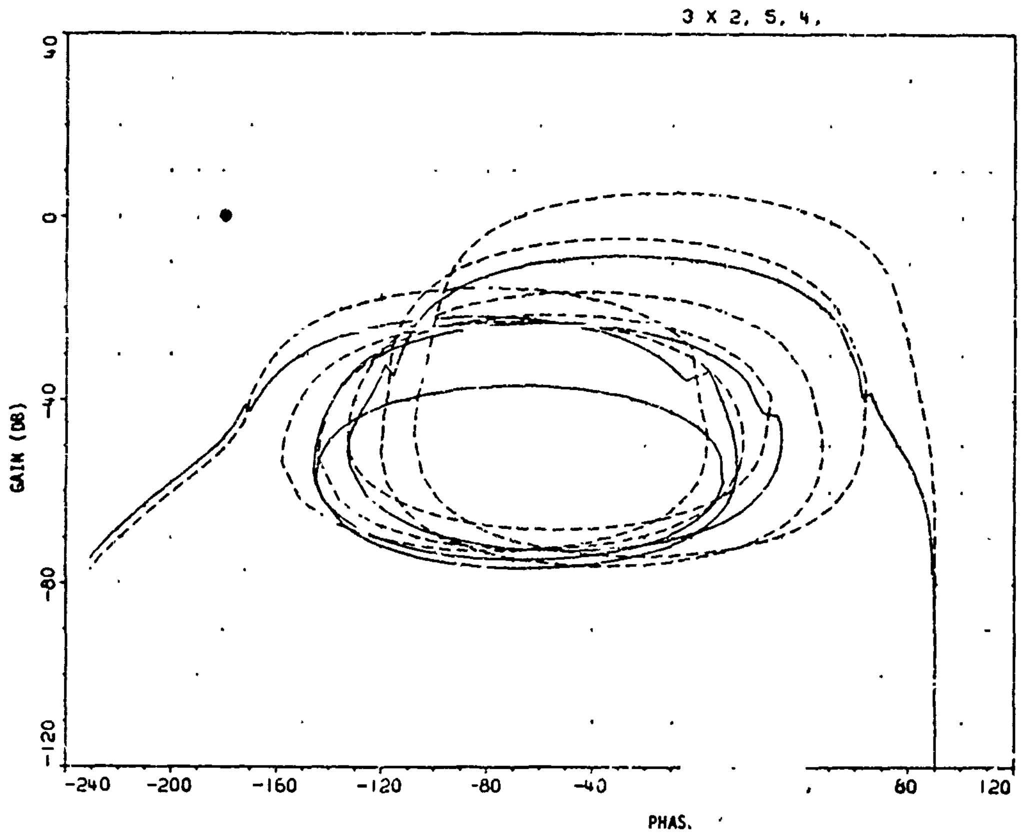

Figure 2.13a PLATE EXAMPLE: CHARACTERISTIC GAINS FOR UNCOMPENSATED SYSTEM.

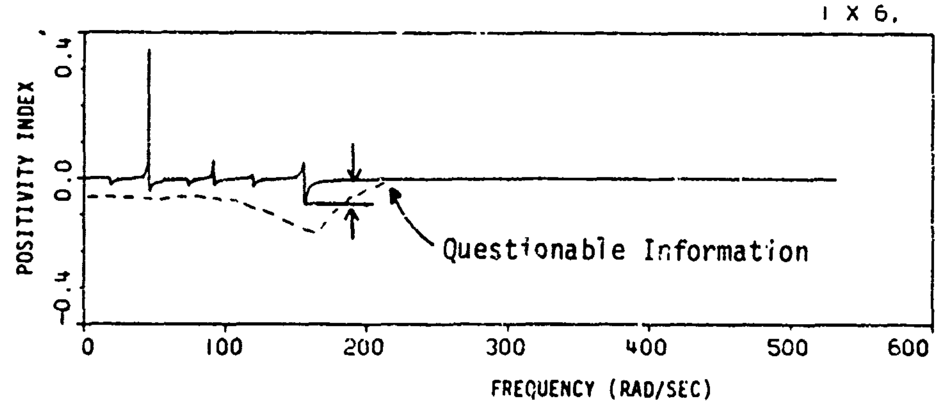

Figure 2.13b POSITIVITY INDEX FOR UNCOMPENSATED SYSTEM

The Figures 2.14a and b show the effect of 4th order compensation. This compensation was optimized for attenuation of the last two modes and the final "cross-over", and for minimum phase lag at the controlled mode frequencies. The compensa' characteristic gains and positivity index show that this objective was met. The index at the highest frequency has been reduced by a factor of three. Thus permitting a less conservative estimate of δ_0 to be used without risking instability at some unmodeled high frequency mode.

2.3 DRAPER MODEL #2 EXAMPLE

In this section, the Draper Model #2*, shown in Figure 2.15a will be used as a test evaluation structure for the positivity design approach. The objectives are two-fold. One is to demonstrate how the technique can be applied to establish the stability of the structure, inclusive of actuator and sensor dynamics and rigid body control. The second is to show how one can couple the technique with on-orbit tuning to create a stability ensuring design methodology that can meet stringent performance goals.

The performance goals for Draper Model #2 are to maintain the line-of-sight (LOS) rotation and DEFOCUS errors below .05 μ rad and 25 μ m, respectively. This accuracy is to be maintained even though sinusoidal disturbances are acting directly on the structure. Figure 2.15b shows the locations and amplitudes of these disturbances.

Conceptual Design. One way to understand the LSS control problem is to think of the LSS and the surrounding environment as a closed system wherein energy is stored, transformed and dissipated. The vibration suppression problem is, in these terms, to simultaneously maximize energy dissipation within the "clean" structure, and minimize the vibrational energy created in, and transmitted to it from the outside. Ideally, the latter would need, to be totally performance robust, to spatially isolate the whole clean structure from the outside over all energy frequencies. This cannot be done in

* A description of Draper Model #2 is given in Appendix A

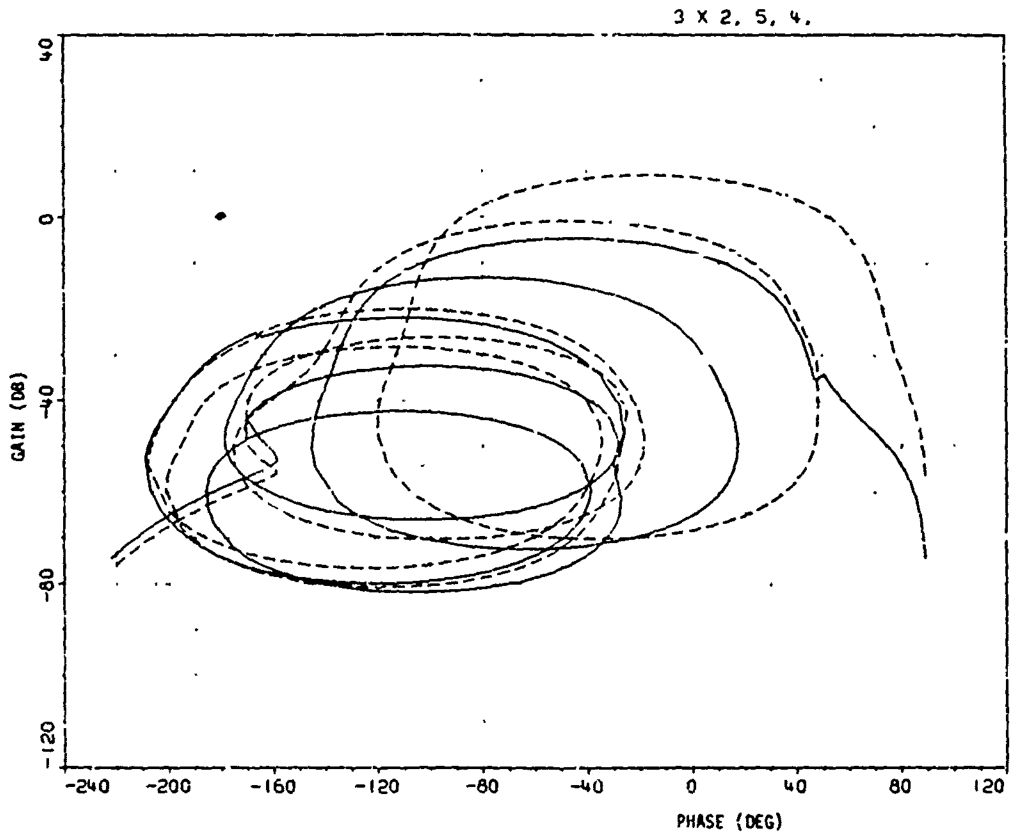

Figure 2.14a PLATE EXAMPLE: Characteristic Gains After Compensation

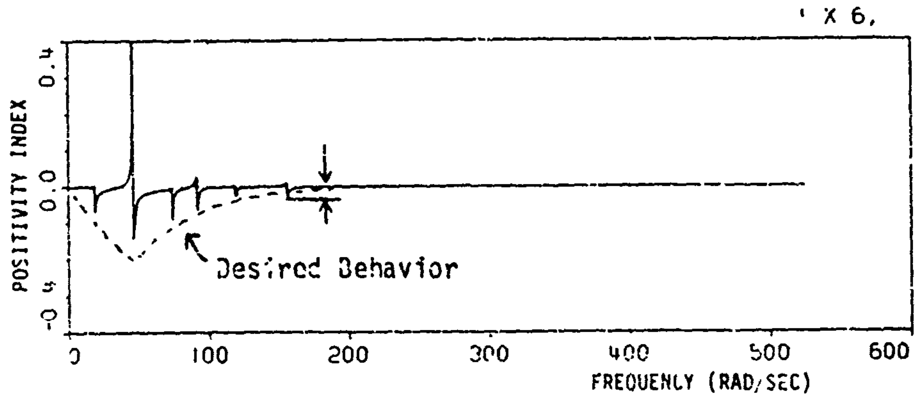

Figure 2.14b Positivity Index For Compensated System

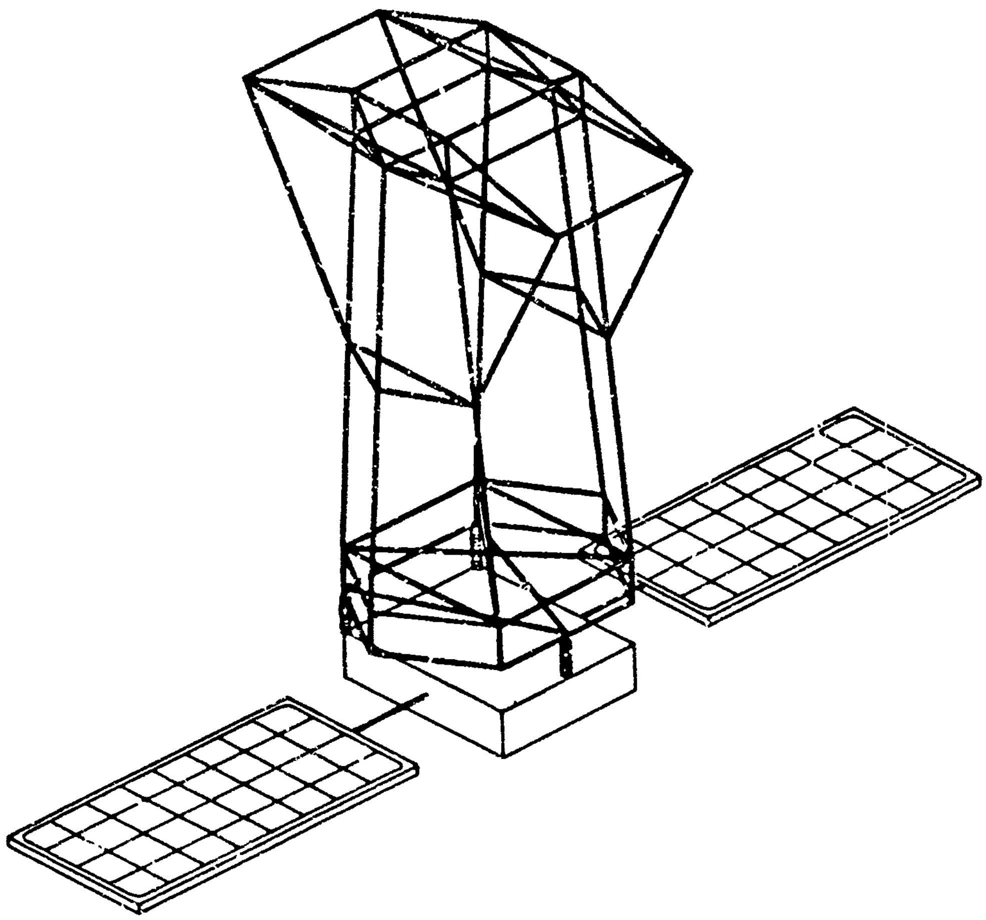

Figure 2.15a DRAPER MODEL #2

DESIGN GOALS

.05 μrad LOS ERROR (X-AXIS)
.05 μrad LOS ERROR (Y-AXIS)
25 μm DEFOCUS ERROR

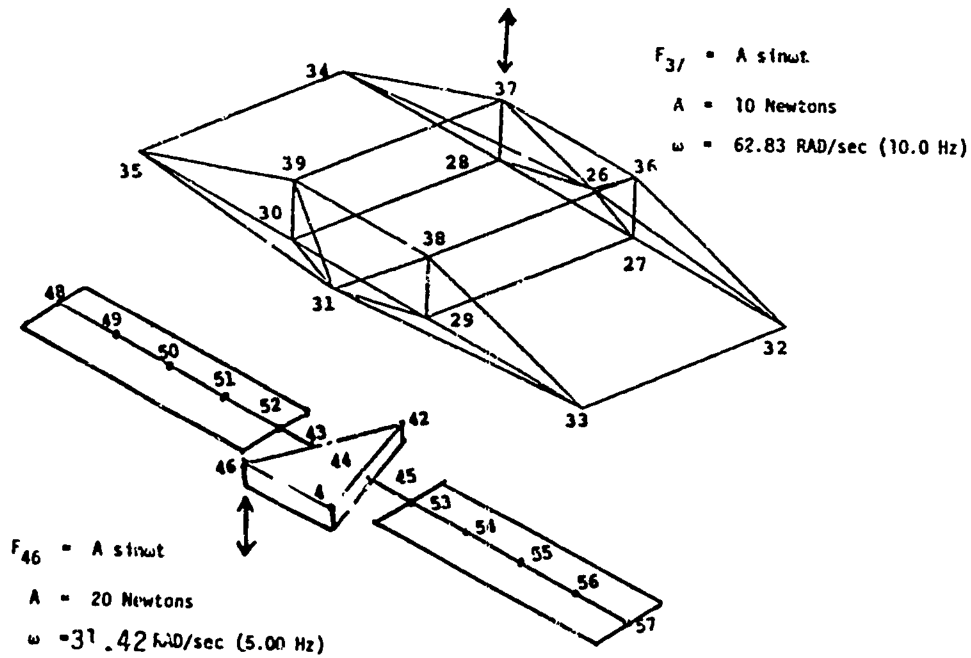

Figure 2.15b DRAPER MODEL #2 Disturbance Source Locations and Design Goals

general, however, because total active spatial isolation would need to be continuously distributed and have infinite bandwidth. Fortunately, in practice, the most energetic sources are spatially localized and a large percentage of the emitted power is over a specific band of frequencies. Hence, a practical solution to the isolation problem exists when energy sources can be identified as to content and locale. A tradeoff between the amount of isolation of the "clean" structure from the equipment (dirty) section and amount of dissipation also exists, the amount of dissipation required depending on the energy "leaked" by the isolating mechanism.

The strategy for Draper Model #2 will be to put the burden of the problem upon the isolators. This will take advantage of the fact that the locale and energy content of the disturbance sources are well known. A passive isolator system will therefore first be used to isolate the clean structure from the disturbances in the dirty box; then, spatial locations for passive damping will be chosen so that leaked energy in the disturbance band will be maximally dissipated; the rigid body controller will then be designed to provide attitude control and isolation to the entire structure from low frequency disturbances emanating from the environment; finally, the clean structure disturbance will be locally dissipated and isolated from the "spatial entity" LOS. It is important to note that vibration in the entire clean structure need not be suppressed. It is sufficient to suppress only the spatial entity described by line-of-sight.

<u>Physical Considerations</u>. As in any other feedback control system, the quality of the actuators and sensors must be commensurate with the desired closed-loop performance. This leads to some prerequisites that must be met by the actuators and sensors if the overall performance of .05 μrad error is to be achievable.

With respect to the sensors, the desire to point with LOS errors less than .05 μrad means that one must have at least one <u>inertial</u> sensor capable of providing a reference down to this level Second, the proper control of structural vibrations will require the active control sensors

to be sensitive enough to measure the expected deflections and rotations incurred at the sensing station during a .05 μ rad LOS deviation. Finally, the disturbance rejection requirements imply that the active control sensor bandwidth must exceed the disturbance bandwidth by a factor of 5-20. The latter depending upon the type of expected disturbance, the bandwidth of the actuators, and the mode shapes and spacings of the modal frequencies between the control bandwidth and the actuator bandwidth. Similar bandwidth considerations must be given to the actuator mechanisms. However, the actuator must first be capable of acting upon an LOS deviation of .05 μ rad. This means that its deadband must be narrower than the expected deflections and rotations incurred at the control stations during the LOS deviation.

The decision of whether or not an actuator-sensor pair should work on a relative or inertial basis also has to be considered carefully. Intuitively, an inertial disturbance (ex., moving masses in a cryo-cooler) acting on a totally rigid object can only be counteracted using inertial controls. Relative control, on the other hand, for use in vibration suppression is as likely to redirect energy as much as dissipate it. After all, this controller has its inputs connected to a moving system. Hence the controller can only dissipate energy as fast as its reference permits it. Inertial control is, however, referenced to something that is theoretically not moving, an inertial frame where ideally no dissipation rate limits will exist. It seems reasonable to expect, therefore, that inertial disturbances will require a higher number of relative controllers than inertial controllers for an equivalent rate of dissipation.

<u>Determining Modes, Nodes and Truss Members To Be Controlled</u>. Previous esperience by TRW on the control of flesible spacecraft and missiles (ex., TDRS and Minuteman) has shown that the G-factor gives a good measure of the relative amplitude of a mode at a particular node. The G-factor is defined as the d.c. gain of the transfer function between two nodes at a modal frequency of interest, i.e.,

$$\left.\frac{\phi_i^k \phi_j^k}{s^2 + 2\zeta_n \omega_n s + \omega_n^2}\right|_{s=0} = \frac{\phi_i^k \phi_j^k}{\omega_n^2}$$

where i, j are node members

n is the mode number

k identifies the spatial coordinate (e.g. translation: x, y, z; rotation λ_x, λ_y, λ_z ; or along a truss direction).

The TRW computer program MDLSFT automates the sifting process. It will go through all the modal data and will

1) Rank modes by G-factor given important nodes or mode shapes.

2) Rank nodes by G-factor given important modes.

3) Rank relative node members given important modes (those nodes connected by a truss member) by G-factor along the line connecting the nodes.

2.2.1 Control Topology For Rigid Body and Active Structure Control

A functional block diagram of the control topology used on Draper Model #2 is shown in Figure 2.16. The controller H(s) is partitioned as shown in Figure 2.17. $H_F(s)$ controls the flexible dynamics and $H_R(s)$ controls the rigid body attitude. The idea here is to make use of the fact that if both $H_R(s)$ and $H_F(s)$ are positive, then the composite controller

$$H(s) = \left[\begin{array}{c:c} H_R(s) & 0 \\ \hdashline 0 & H_F(s) \end{array}\right]$$

is also positive. These controllers can therefore be designed separately and because each one is positive, either H_F of H_R may be set to zero without destabilizing the system.

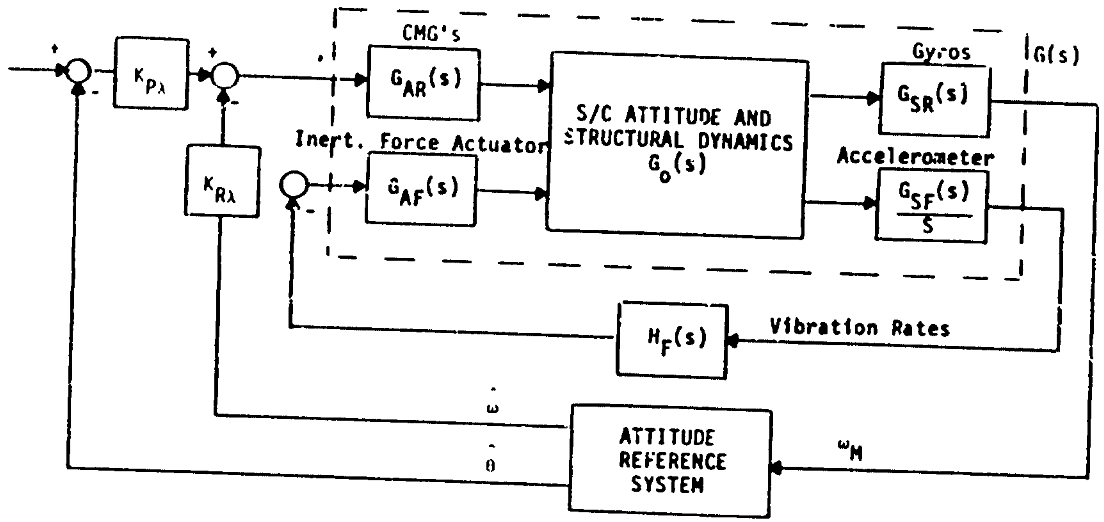

Figure 2.16 Controller Topology For Draper Model #2

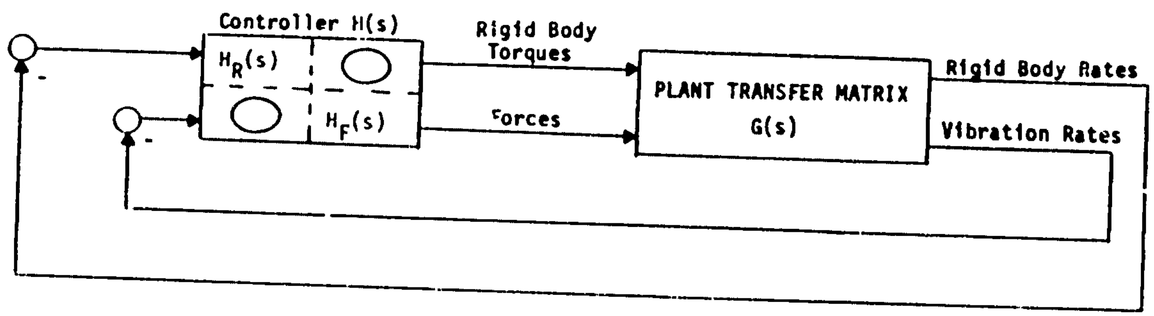

Figure 2.17 Controller Partitioning For Draper Model #2

In order to make the plant as positive as possible, over the largest frequency range, the rigid body controller assumes only rate is measured. Attitude control, however, will require some position feedback. $H_R(s)$ is therefore chosen as

$$H_R(s) = K_{R\lambda} + \frac{K_{P\lambda}}{s}$$

Now $H_R(s)$ is positive real for $K_{R\lambda}, K_{P\lambda}$ positive semi-definite and the positivity theorem with embedding can be easily applied. Note here that for spacecraft using integrated gyro rate for attitude reference, $H_R(s)$ models the true physical situation.

2.3.2 The Positivity Design

Following the conceptual design procedure, the approach consisted of: 1) the passive isolator design; 2) the passive member damper design; 3) the rigid body design; and finally 4) the active damping design.

The first quantities that were computed are the LOS disturbance rejection requirements. This was computed by normalizing the dB scale according to 0dB** = 1 rad/N. Here, .05 μ rad/N represents -146 dB, so for the 20N and 10N disturbances considered in this study, it can be shown that the requirements are equivalent to:

	@ 31.42 rad/sec	@ 62.83 rad/sec
From Top (Node 3.)	-	-166 dB
From Bottom (Node 46)	-172 dB	-

Passive Isolator Design. The passive isolator design is an example of the ideal positivity design. Here, rate gain is the implicit feedback parameter, and, since there are no actuator and sensor dynamics, the dashpots create a natural positive definite feedback gain matrix.

---

* Gain in dB will refer to 20 LOG_{10} [magnitude] unless specifically stated otherwise.

The approach used to determine the actual isolator dashpot constants is based on the multivariable frequency domain approach of Mac Farlane [6]. For the problem here, this requires that one determine the characteristic gains and transmission zeros* of the system. The characteristic gains were used as a guide in the selection of loop gains resulting in desirable sensitivity and damping properties. The transmission zeros were used to determine which eigenvalues will become real.

If one looks at the frequency response of a normalized 2nd order transfer function with $\zeta=1$, one will notice

$$\text{PHASE @ } 2\omega_n \ - \ \text{PHASE @ } \frac{1}{2}\omega_n = 75°$$

Hence, a plot of the characteristics gains in the Nichols chart allows one to approximately determine the gains g_i for which the eigenvalues will first touch the real axis. That is, when the closed-loop phase contours changes between +38° and -38° as ω changes between $\frac{1}{2}\omega_n$ and $2\omega_n$.

An eigenvalue analysis for loop gains $\frac{1}{2}$ g_i, g_i and $2g_i$ then permits a quick check to see if isolator damping is adequate, and also supplies a selection of possible alternatives. Final selection of gains was based on the set providing the best combination of overall damping and isolation.

The frequency response plots in Figures 2.18a and b show the results of the design. The responses are from the disturbance source locations to the line-of-sight outputs. The defocus error is not shown as it easily meets the 25 μm design goal.

Passive Member Damper Design. The passive member damper design is another example of the ideal positivity design. Damper values were therefore determined by using the same procedure outlined in the passive isolator design. The critical part was determining which and how many truss members

---

* Eigenvalues of the system as the feedback gains approach infinity.

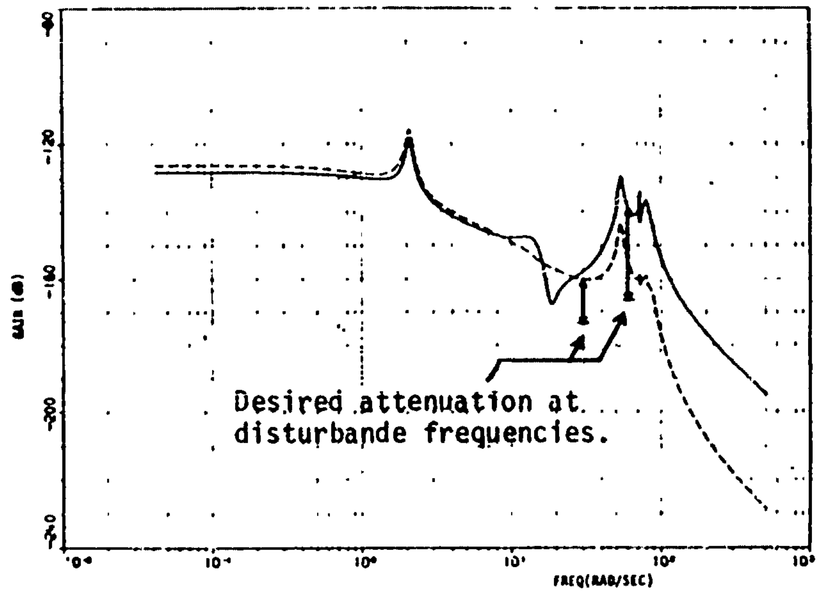

Figure 2.18a Frequency Response From Disturbance Sources to LOS X-Axis

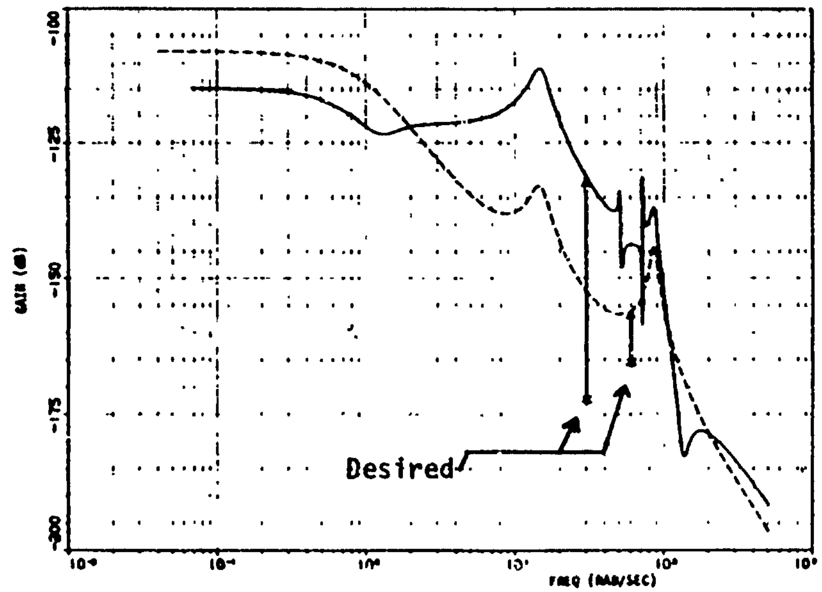

Figure 2.18b Frequency Response From Disturbance Sources To LOS Y-Axis

———————— Disturbance At Node 37

------------ Disturbance At Node 46

NOTES:

1) The design model consisted of modes: 7, 8, 9, 10, 11, 13, 15, 17, 21, 28, 30, 34, 35, 37(ζ=.001)
2) The dashpot locations were: connecting/between nodes 4,42 (x,y,x): Nodes 4,46 (x,y,z): Nodes 3,46 (x,y,z)
3) The dashpot gains were: 2231 N/m/sec (x and y axis); 10,000 N/m/sec (z-axis).
4) Due to the large dimensions of the models involved, the frequency response plots are only a first order approximation to the true response. The approximation is based on ignoring the modal coupling introduced by the insertion of the isolator.

were to have the dashpots in-line with themselves. In order to determine this, the MDLSFT was run using two options: 1. Given important mode shapes (LOS), rank modes by G-factor; these resulting modes were then used as the important modes in the option. 2. Given important modes, rank relative node members by G-factor. The member dampers were then chosen from this list according to the magnitude of their modal influence and the number of modes they influenced. The number of members was determined as the minimum number to have influence on all the critical modes.

Four member dampers resulted using the above procedure. The frequency response plots in Figure 2.19a and b show the results. These figures indicate improvement in the disturbance rejection response, but active control is still required to meet specifications.

Rigid Body (Attitude) Control Design. The rigid body controller is the first place in the Model #2 design wherein active control will be required. The ACS is located on node 44 of the dirty box and it is composed of CMG's, rate gyros and a three axis controller. The CMG's were assumed to have a 5 Hz bandwidth, the gyros 10 Hz. This controller was designed using the "D" embedding design procedure outlined earlier. The main design steps were to:

1) Compute the positivity index

$$\delta_G(\omega) = \lambda_{min} \left\{\frac{1}{2}\left[G^*(j\omega) + G(j\omega)\right]\right\} \forall\ \omega \epsilon\ [o,\infty)$$

where
$G(j\omega)$ is the input-output transfer matrix of the rigid body of the structure including actuator and sensor dynamics.

2) Determine a fictitious diagonal operator $D(j\omega) = I \cdot d(j\omega)$ such that $\delta_G(\omega) + \text{Real}\ [d(j\omega)] \geq 0$ for all ω.

3) Physically implement a positive controller $H(j\omega)$ that remains positive even after fictitious positive feedback $D(j\omega)$ has been wrapped around it.

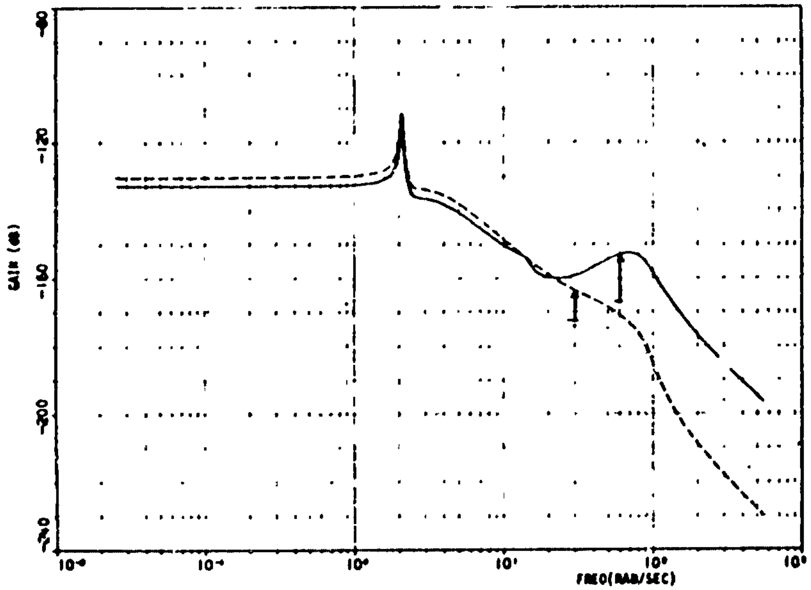

Figure 2.19a Frequency Response From Disturbance Sources to LOS X-Axis

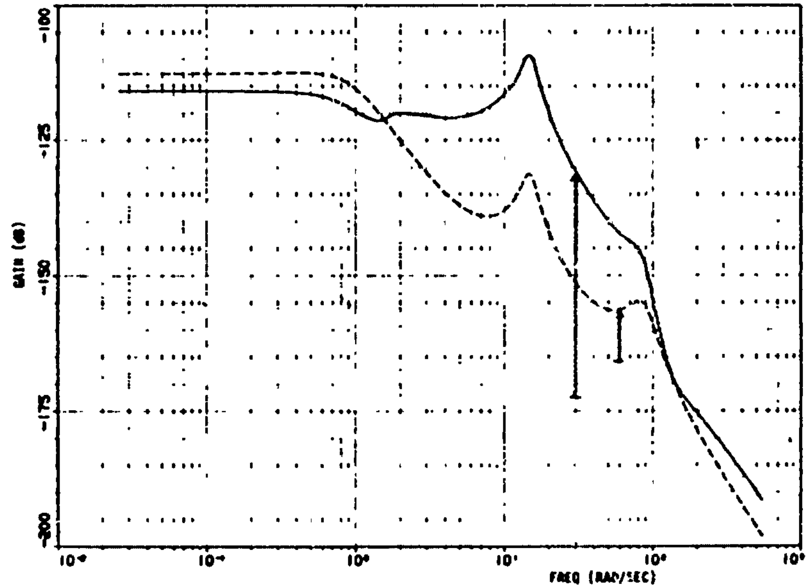

Figure 2.19b Frequency Response From Disturbance Sources to LOS Y-Axis

__________ DISTURBANCE AT NODE 37

---------- DISTURBANCE AT NODE 46

NOTES: 1) The design model consisted of modes: 7, 8, 9, 10, 11, 12, 13, 15, 17, 21, 28, 30, 34, 35, 37, ($\zeta = .001$)

2) The isolator was included in the design model.

3) The member damper locations were along trussess 5, 96, 82 and 119.

4) The dashpot gains were: 10^5 N/m/sec (trusses 5 & 119); 5×10^5 N/m/sec (trusses 96 and 82)

In the present design the rigid body controller was assumed to be of the form

$$H_R(s) = K_{R\lambda} + \frac{K_{P\lambda}}{s}$$

where $K_{R\lambda} = I \cdot k_{R\lambda}$ and $K_{P\lambda} = I \cdot k_{p\lambda}$. It can be shown that with $k_{R\lambda} = 1.2 \times 10^6$ N-m sec/rad and $k_{p\lambda} = 8 \times 10^5$, N-m/rad, $H_R(s)$ will remain positive with fictitious "D" embedding tracking the $-\delta_G(\omega)$ curve. Figures 2.20a and b show the positivity index $\delta_G(\omega)$ and the Nichols plot of the characteristic gains for the rigid body. Also shown on Figure 2.20b is the resulting rate loop operating point.

Active Damping System (Positivity Design). The design methodology for the active damping system is the same as in the rigid body design. The objective here, however, is to maximally isolate/dissipate the energy emanating from the disturbance sources.

The active control locations were chosen to be those nodes closest to the disturbances (46 and 37). It can be argued that these locations may be sensitive to disturbance location, but, it can also be argued that they are the most robust w.r.t. to the modal data. Placement in real situations would therefore depend on trading the degree of expected spatial uncertainty for the degree of expected modal data uncertainty.

Ideally one model should be used for determining the positivity index of the active control system. However, the large number of modes within the actuator/sensor bandwidth* made this difficult. Instead, two models were determined for computing a worst case index. One model was based on G-factor rankings of those modes affecting node 37 the most, and the other on those affecting node 46 the most. The resulting positivity plot, Figure 2.21a shows the node 46 model, which is the most "negative". Rate gains and position compensation were therefore based on this model.

Figure 2.21b shows the rate loop operating point in the Nichols plot for the active system model. The position compensator was chosen as

*Actuator/sensor bandwidth is 100 Hz.

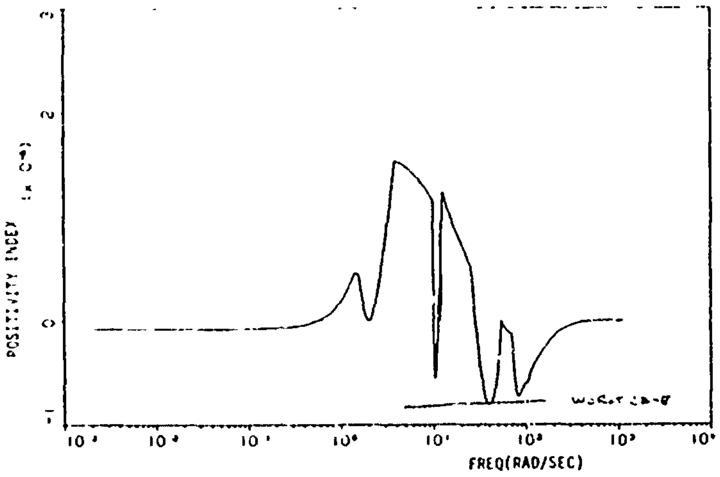

Figure 2.20a Positivity Index-Rate Loop Open

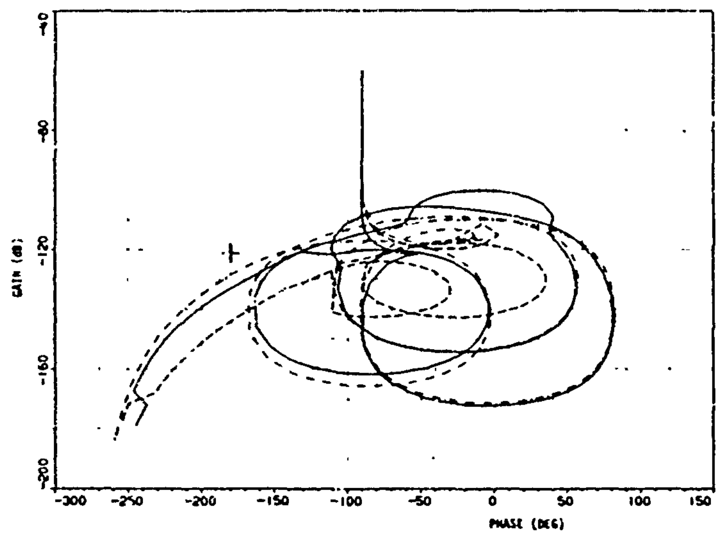

Figure 2.20b Characteristic Gains For Rigid Body Rate Loop

NOTES:
1) The design model consisted of modes: 1-17, 21, 22, 23, 24, 26, 29, 33, 36, 40, 44, 45 (ζ=.001).
2) The design model includes the isolator and the passive member dampers.
3) The controller location is at Node 44 (λ_x, λ_y, λ_z)
4) The actuator bandwidth is 30 Rad/Sec.
5) The rate sensor bandwidth is 120 Rad/Sec.
6) $K_{r\lambda} = 1.2 \times 10^6$ N/m/sec/rad · I ; $K_{p\lambda} = 8 \times 10^5$ N/m/rad.

Figure 2.20 Positivity Index and Characteristic Gains for ACS

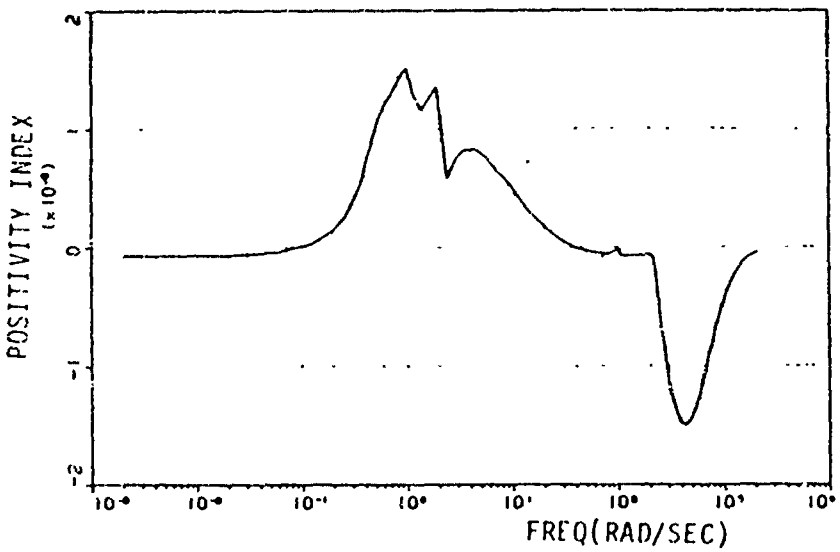

Figure 2.21a Positivity Index Using Worst-Case G-Factors For Node 46.

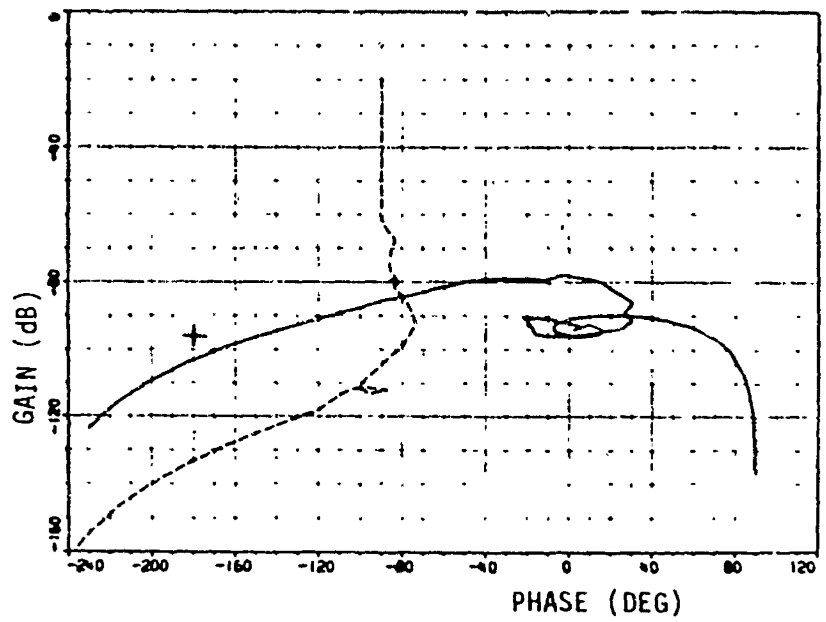

Figure 2.21b Characteristic Gains Using Worst-Case Node 46 Model

NOTES:
1) The design model consisted of modes: 1-14, 16, 18, 22, 26, 29, 36, 39, 57, 61
2) The design model includes the isolator, the passive member dampers and the rigid body controller.
3) The actuator/sensor (proof mass actuator/accelerometer) locations are at nodes 37(z) and 46(z).
4) The actuator and sensor bandwidth is 600 rad/sec (ω_{AA}, ω_{AS})
5) The rate gains are $K_{R37} = K_{R46} = 6.7 \times 10^4$ N-sec.
6) The position compensator is 1.66×10^6 N-m/m $\bullet \left[\frac{S^2 + 9.48s + 561.69}{S^2 + 6.68s + 1115.56}\right]$

Figure 2.21 Positivity Index and Characteristic Gains For Active Damping System

th.: o.ıı ⁝ 2nd order filter which would simultaneously boost the gain at 30 and 60 rad/sec to +9 dB and minimize high frequency gain. This choice permits frequency selective high loop gains at the frequencies requiring the most disturbance rejection. Higher order filters could have been chosen here for greater selectivity, but a better characterization of the uncertainty in the disturbances would have been required. If the disturbances were truly sinusoidal and at exactly the given frequencies, the optimal compensator would have had one undamped pole for each sinusoidal disturbance frequency.

2.3.3 Results For The Positivity Design

Figure 2.22 shows a block diagram of the entire Draper Model #2 positivity designed system. This system was analyzed and simulated to check the robustness and performance of the design.

To analyze the positivity design performance, a nominal evaluation model retaining the largest G-factors in the LOS was constructed. The frequency response of this model, shown in Figures 2.23a, b, c was then computed from various points of interest. The nominal design yielded a rigid body bandwidth of at least .4 rad/sec, and disturbance rejections from disturbance source to LOS as shown below. Clearly, the specification could not quite be attained with the untuned positivity design. This was more or less expected, since the positivity design is conservative.

	LOS x	LOS y	req'd to meet spec
From top (node 37) at 62.83 rad/sec	-152 dB	-145 dB	-166 dB
From bottom (node 46) at 31.42 rad/sec	-170 dB	-158 dB	-172 dB

The root-sum-squared prediction based on this data is LOS x error = .258 μrad and LOS y error = .751 μrad. These predictions agree with those obtained through simulation, as shown in Figures 2.24a, b, c. Figures 2.24d and e show that the required actuator force is a very reasonable 25N, which can be implemented with a linear momentum exchange device(proof mass actuator) weighing about 5 Kg.

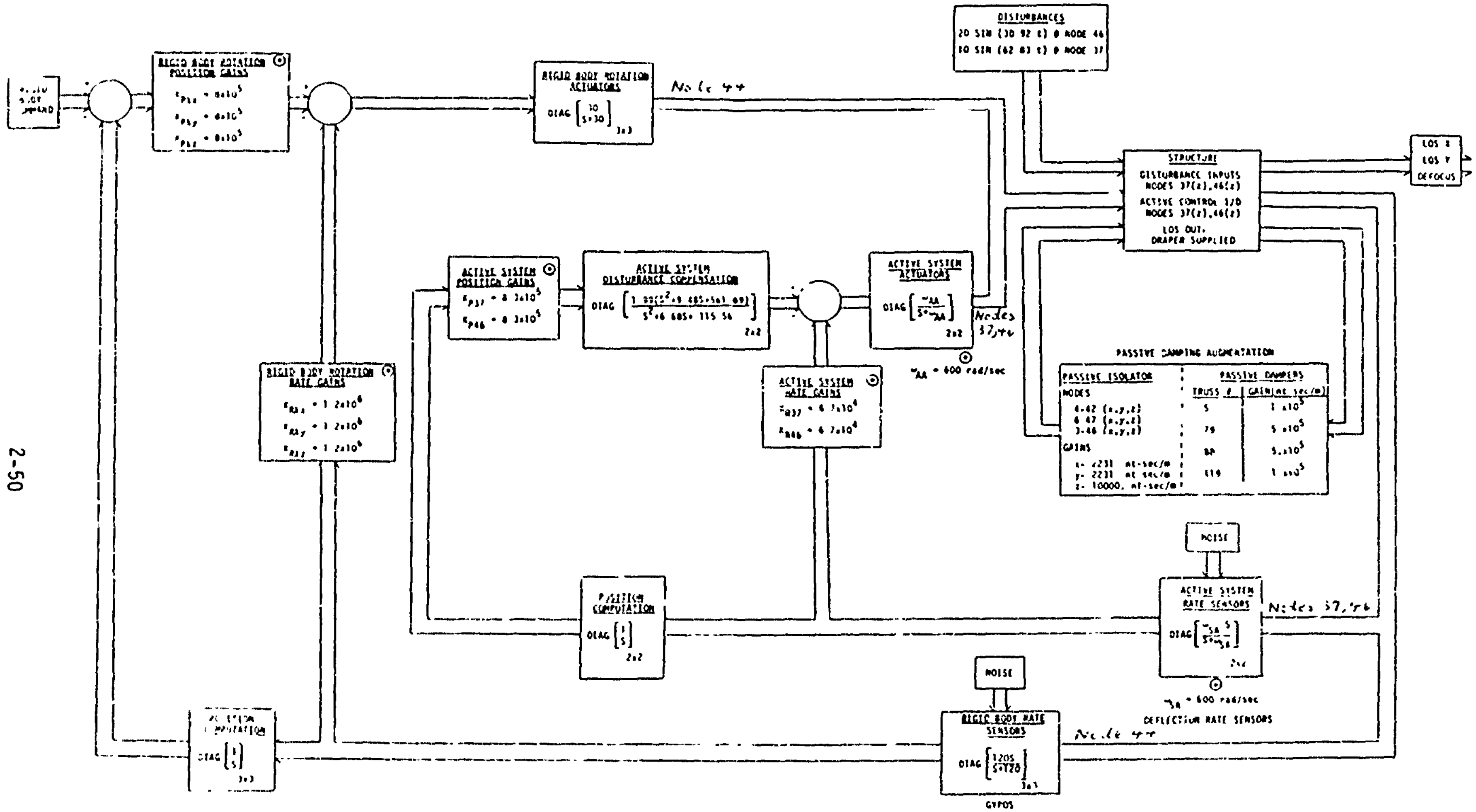

⊙ THESE GAINS/PARAMETERS WERE LATER CHANGED DURING THE TUNE-UP PROCEDURE.

Figure 2.22 Block Diagram of DRAPER Model #2 Design

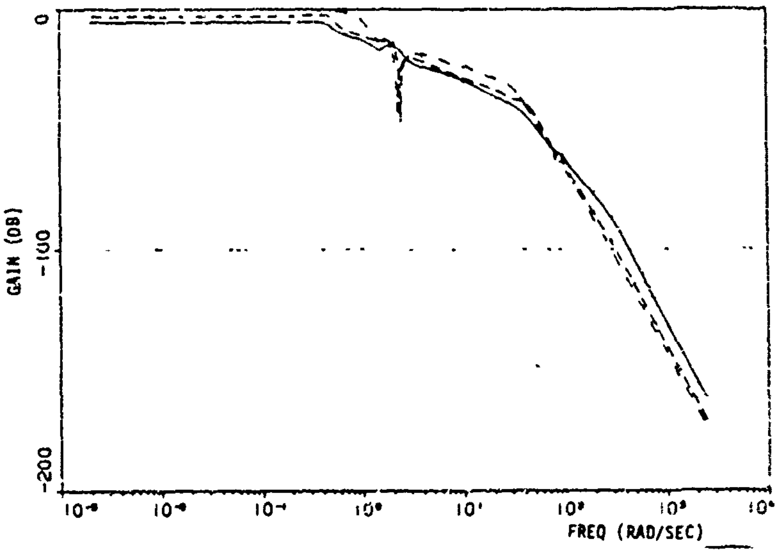

Figure 2.23a

Rigid Body Command To Rigid Body Sensor Frequency Response.

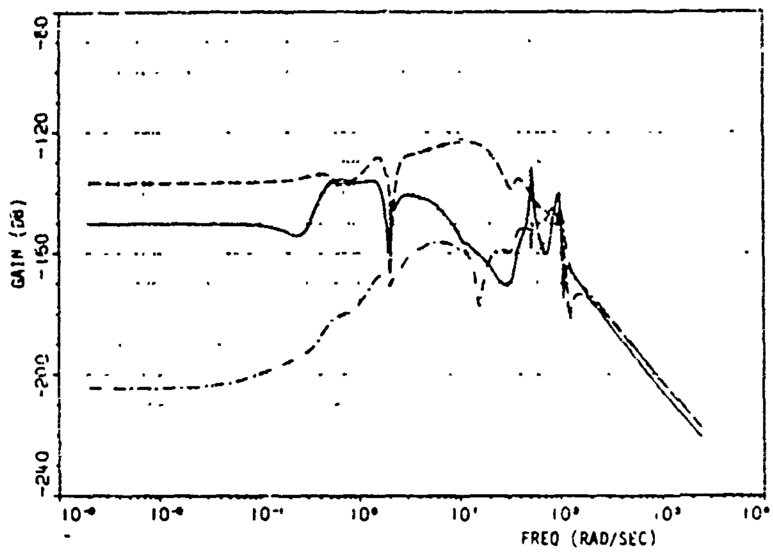

Figure 2.23b

Disturbance Rejection From Node 37 to LOS

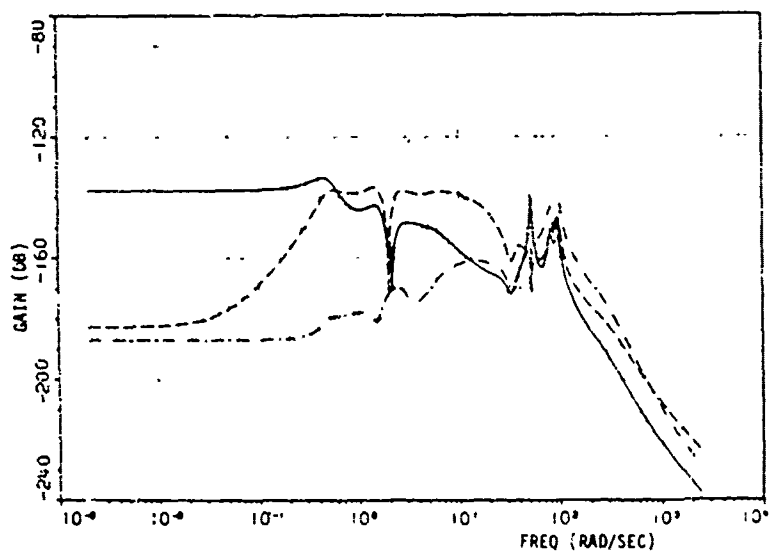

Figure 2.23c

Disturbance Rejection From Node 46 to LOS

NOTES: Model retains modes 4-7, 21, 28, 30, 34, 35, 37, 39, 40, 41

——— θ_z

– – – – θ_y

—— – —— θ_y

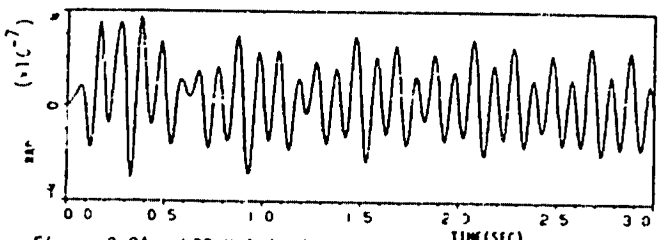

Figure 2.24a LOS X-Axis Error

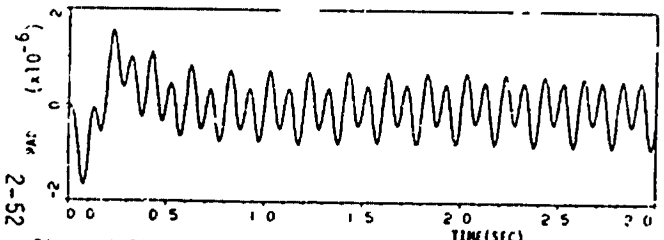

Figure 2.24b LOS Y-Axis Error

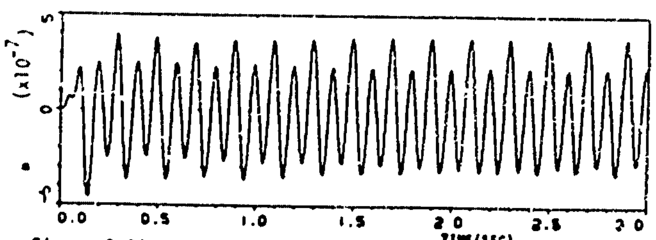

Figure 2.24c DEFOCUS Error

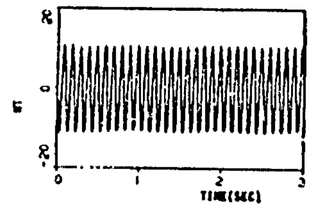

Figure 2.24d Control Effort of Actuator at Node 37

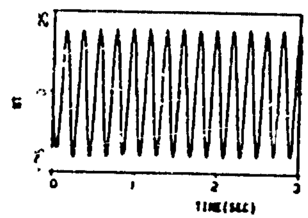

Figure 2.24e Control Effort of Actuator at Node 46

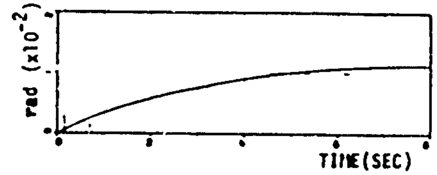

Figure 2.24f λ_x "Rigid Body" Transient (Node 44)

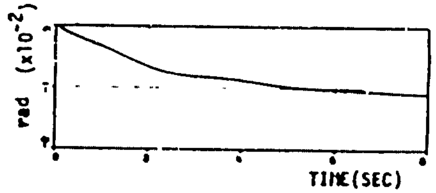

Figure 2.24g λ_y "Rigid Body" Transient (Node 44)

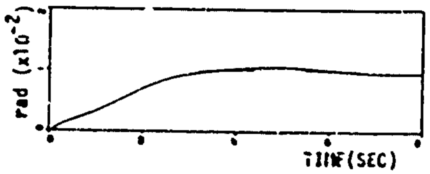

Figure 2.24h λ_z "Rigid Body" Transient (Node 44)

Figure 2-24 Simulation Results Using The Positivity Design
Positivity Design

Figures 2.24f-h show the ACS step-input transient. λ_x, λ_y, and λ_z, were simultaneously commanded .01, -.01 and .01 rad, respectively. These Figures show a stable, smooth rise in less than 5 seconds and with little ringing from the multitude of bending modes.

In order to demonstrate the robustness of the positivity design, the nominal evaluation model was perturbed as described in Appendix A. The simulation results using perturbed Model #2 and #4 show that the system is stable. Moreover, the performance change from the nominal case is imperceptable*. See Figures 2.25a-f.

2.3.4 Positivity Design "Tune-up"

The results of the previous design indicate that the disturbance tracking has to be improved in order to meet all the performance requirements. Since the open and closed-loop characteristic gains of this design are related analogously to the Bode/Nyquist single-input-single-output case, the improvement in tracking is realized by increasing the magnitude of the characteristic gains,

i.e., for large $\lambda(s)$,

$$\text{tracking error} = \frac{\lambda(s)}{1 + (K_p + K_R s)\,\lambda(s)} \approx \frac{1}{K_p + K_R s} \quad \Big\} \begin{array}{c} s \text{ in the} \\ \text{disturbance} \\ \text{band} \end{array}$$

It was now assumed that the characteristic gains in Figures 2.20b and 2.21b resulted from ground processing of post on-orbit test data and describes the system accurately (note that the transfer matrix can be obtained from on-orbit frequency response data via the FFT). Therefore much more elaborate embedding can be used, or if the system can be assumed to be linear, multivariable frequency domain techniques can be applied. The locus in Figure 2.21b predicts, then, that the DC gain increase required to meet specification would result in an unstable system. So, either additional compensation or increased actuation/sensing bandwidth is required. In the interest of time, we doubled the active system actuator/sensor BW to 1200 rad/sec so that we could assure that the required loop gains would not destabilize the system.

* As measured by steady state peak-to-peak error.

PERTURBED MODEL NO. 2

PERTURBED MODEL NO. 4

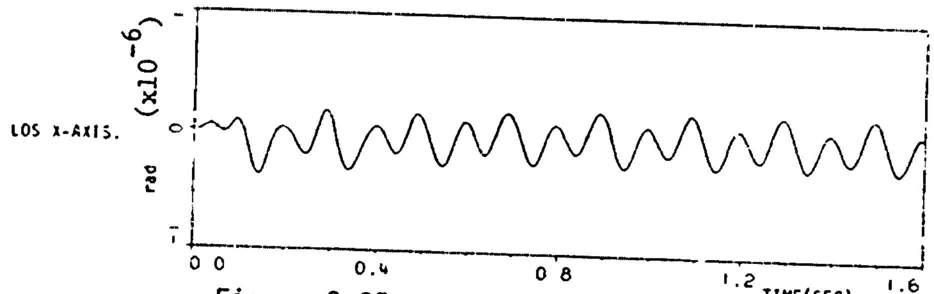

Figure 2.25a

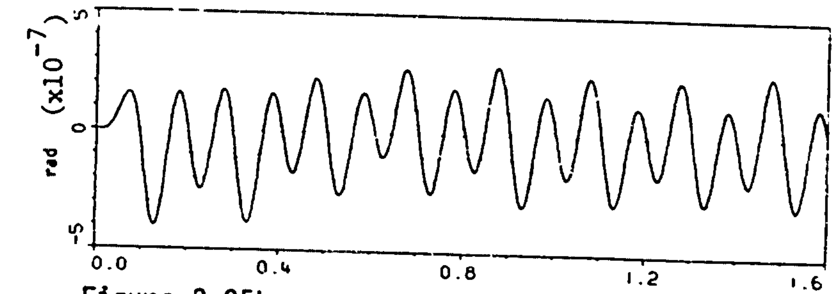

Figure 2.25b

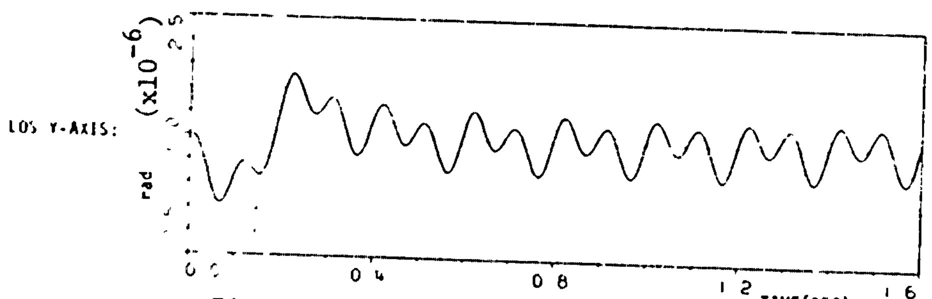

Figure 2.25c

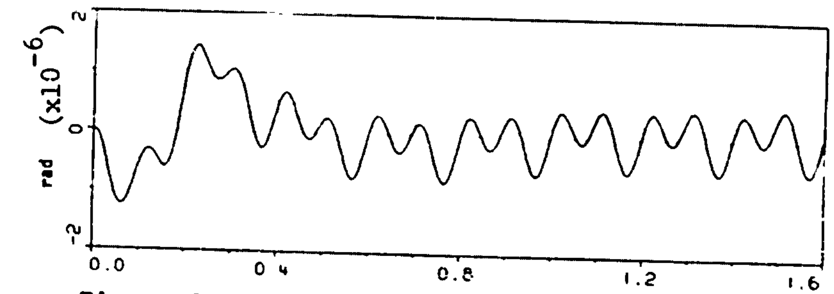

Figure 2.25d

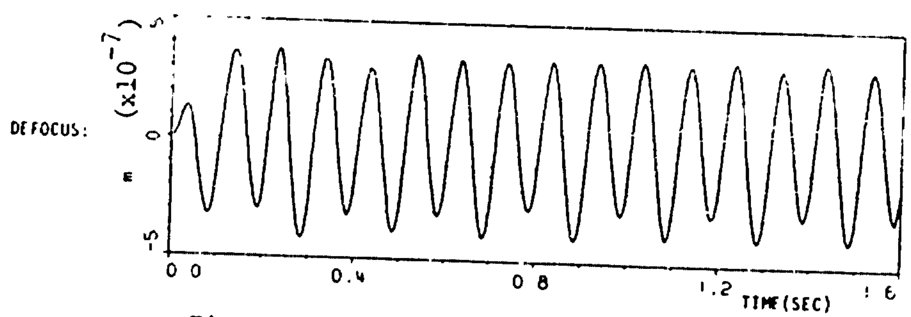

Figure 2.25e

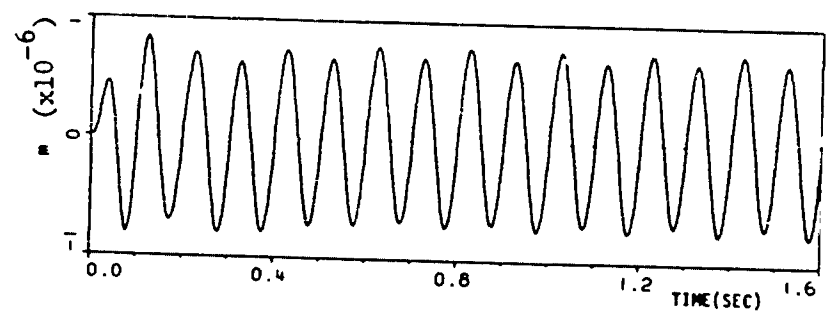

Figure 2.25f

Figure 2.25 Perturbed Models No. 2 and 4

Figures 2.26 a-c show the LOS errors for the "tuned-up" system as simulated on the computer. The tune-up design meets all specifications.

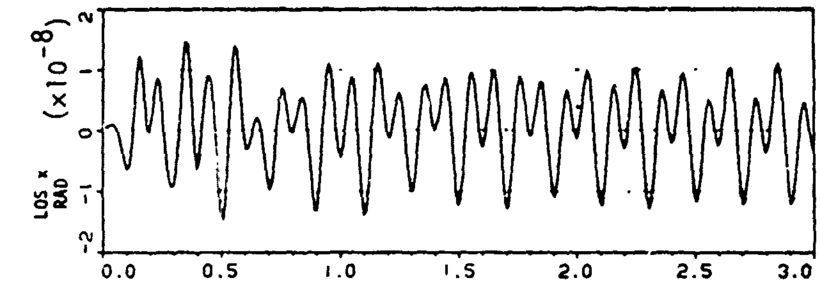

Figure 2.26a

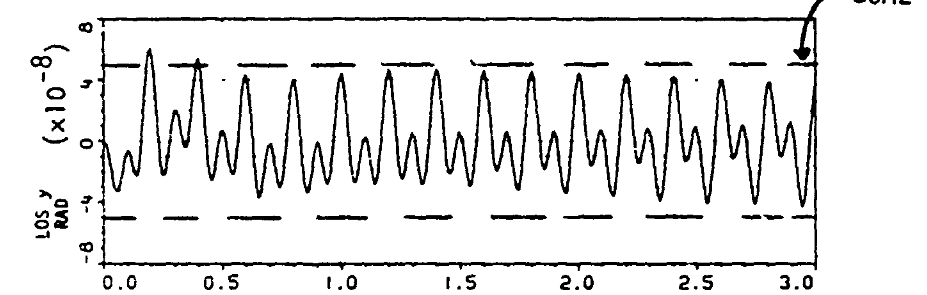

Figure 2.26b

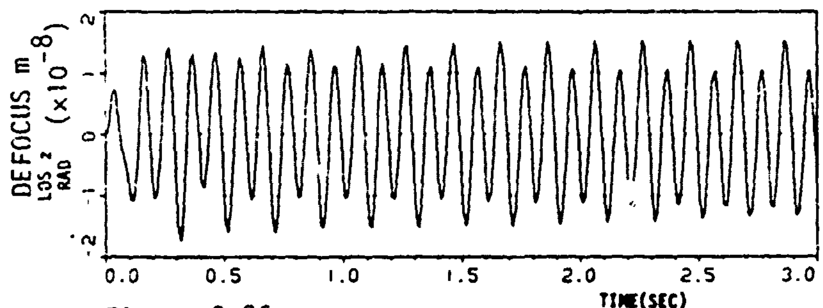

Figure 2.26c

NOTES: 1) Same configuration as Figure 2.22

2) The new gains are:

$K_{R\lambda x} = 3x10^6$ N-m/rad/sec $\qquad K_{P\lambda x} = 3x10^7$ N-m/rad

$K_{R\lambda y} = 1.05x10^6$ N-m/rad/sec $\qquad K_{P\lambda y} = 1x10^7$ N-m/rad

$K_{R\lambda z} = 9x10^5$ N-m/rad/sec $\qquad K_{P\lambda z} = 1x10^7$ N-m/rad

and

$K_{R37} = 1x10^6$ N/m/sec $\qquad K_{P37} = 1.75x10^8$ N/m

$K_{R46} = 3x10^5$ N/m/sec $\qquad K_{R46} = 3.5x10^7$ N/m

Figure 2.26 Steady State Disturbance Response of Tuned-Up System

3. ON-ORBIT TEST AND SYSTEM IDENTIFICATION

3.1 INTRODUCTION

The prime motivation for conducting on-orbit tests and system identification is the uncertainties in the finite dimensional model that approximates the dynamics of the large space structure. The finite element method is often used to obtain this finite dimensional model which, from past experience, is expected to contain errors greater than 20% in the predicted modal frequencies and mode shapes of some of the modes. As a consequence, the active controllers which are computed on the basis of this inaccurate model will not achieve their designed performance. Hence it is desirable to obtain a more accurate model by testing the actual spacecraft on-orbit. Ground-based tests for large and flexible structures are not always feasible; besides, the test environment on the ground is not representative of on-orbit conditions. For the above reasons, on-orbit tests and system identification are important issues in the active control technology for the large space structures.

System identification is the problem of determining the dynamic model of an uncertain system based on measurements of inputs and outputs. It is a very broad problem which even includes the case where the order of the system is unknown. However in this report, a finite order, parametric description of the dynamic models is used where certain coefficients in the dynamic equations are unknown. A parameter estimation technique is then used to solve the system identification problem.

The concept of on-orbit tests and controller tuning is shown in Figure 3-1. In this approach, LSS on-orbit input-output data are transmitted to ground where the parameter estimation algorithm is applied to update the LSS parameters. The improved LSS model is then used to recompute new control parameters in order to tune the controller to achieve the desired performance. A ground-based estimator will relieve much of the computational burden from the spacecraft and allow more sophisticated parameter estimation techniques to be applied.

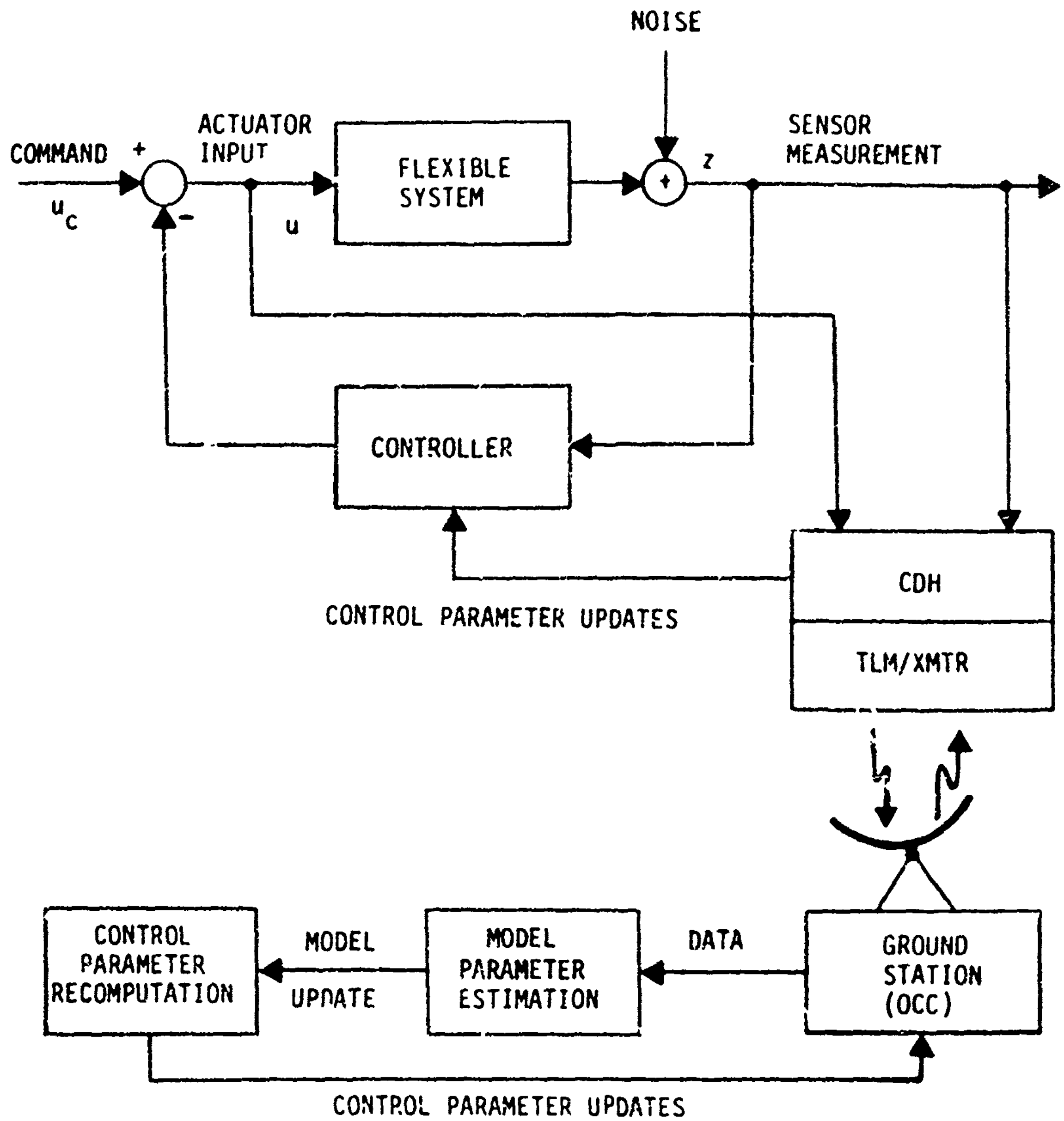

Figure 3-1. On-Orbit System Identification and Controller Tuning

3.2 PARAMETER ESTIMATION METHODS

Several existing parameter estimation methods are evaluated qualitatively for their suitabilities of performing on-orbit parameter estimation.

(A) Cross-Correlation Method

The error between the measured output and the computed output is cross-correlated with the signal in the model that is an input to the parameter to be identified. The output of the cross-correlation integral then adjusts the corresponding parameter value in the system. The main advantage is that it can be implemented for on-line parameter estimation. But there remains some difficulties for multiple-input-multiple-output systems.

(B) Linear Prediction Method

The parameters in an auto regression model are selected so that the mean square prediction error is minimized. There are efficient computational algorithms to compute the estimates. However, this method is sensitive to non-white measurement noise and non-zero initial states.

(C) Transfer Function Method

The magnitude square of the LSS transfer function is obtained from the ratio of the power spectral density of measured output to that of the input signal through the use of Fast Fourier Transforms (FFTs). Although this method is sensitive to non-white measurement noise and non-zero initial states, it is simple, easy to implement, and can be used to obtain the "first-cut" solution.

(D) Kalman Filtering Method

Parameters are treated as states and the parameter estimation problem is formulated as a non-linear state estimation problem. The extended Kalman filtering algorithm is then applied. Consequently, this algorithm can be used for on-line parameter estimation, but the method is complex computationally and may lead to biased estimates.

(E) Maximum Likelihood Method

The parameters are chosen so that the likelihood functional is maximized. When the underlying statistics is Gaussian, the maximum likelihood method and the least squares method are equivalent. This method is known to yield asymptotically unbiased and consistent estimates.

Among the methods presented above, the maximum likelihood method and the transfer function method are believed to be most suitable for on-orbit parameter estimation.

3.3 MAXIMUM LIKELIHOOD PARAMETER ESTIMATION FOR LARGE SPACE STRUCTURES

This section presents the maximum likelihood method [1] and its applications in the estimation of LSS physical and modal parameters. The effects of data length are also discussed.

3.3.1 Maximum Likelihood Method

The three major problems in applying the maximum likelihood method to LSS are:

1) obtaining an approximated finite dimensional model for the LSS, and determining which parameters are to be adjusted;

2) deriving an expression for the likelihood cost functional[+]; and

3) selecting an algorithm to minimize the likelihood cost functional

These three problems and the properties of the maximum likelihood estimates are discussed below.

Modeling LSS Dynamics

The large space structure is a distributed parameter system with point actuators and point sensors. The dynamics of a LSS can be described completely by partial differential equations (PDEs) in the general form:

+ If an approximated model is obtained for the LSS, the derived likelihood cost functional will also be an approximation

$$\frac{d}{dt} X(t) = AX(t) + Bu(t) \tag{3.1a}$$

$$s(t) = CX(t) \tag{3.1b}$$

where A is the infinitesimal generator of a strong continuous semigroup over a separable Hilbert space; X(t) is in D(A); B and C are influence operators for point actuators and point sensors; u(t) is the input vector; and s(t) is the ideal (noise-free) output vector. The actual sensor measurement is

$$z(t) = s(t) + n(t) \tag{3.2}$$

where n(t) is zero mean white Gaussian noise with positive covariance matrix G.

Except for simple structures such as thin plates and thin beams, the exact solution of equation (3.1) for a complex LSS will be very complicated, if not impossible to obtain. Hence, one would like to approximate the dynamics of a LSS by a finite dimensional model. The finite element method [2] is often used to obtain such a model.

In the finite element method, the structure is discretized into small basic elements connected at node points. The motions of the node points can be described by a set of simultaneous, second order differential equations (with damping terms omitted for the moment),

$$M\ddot{q}(t) + Kq(t) = B_p u(t) \tag{3.3a}$$

$$y(t) = C_p q(t) \tag{3.3b}$$

where q(t) is the physical coordinates of the node points, M is the mass matrix, K is the stiffness matrix, B_p and C_p are input and output influence matrices, u(t) is input vector, and y(t) is the output vector predicted from the model.

Let Λ and Φ be the eigenvalues matrix and the corresponding eigenvector matrix of the eigenvalue problem

$$M\Phi\Lambda = K\Phi$$

Equation (3.3) can be transformed into a set of decoupled equations

$$\ddot{\eta}(t) + \Lambda\eta(t) = B_m u(t) \tag{3.4a}$$

$$y(t) = C_m \eta(t) \tag{3.4b}$$

where

$$q = \Phi\eta$$

$$B_m = \Phi^T B_p$$

$$C_m = C_p \Phi$$

$$\Lambda = \text{diag}\,[\omega_1^2, \omega_2^2, \ldots \omega_n^2]$$

Viscous damping can now be modeled in terms of damping ratios, ζ_i $i = 1, 2, \ldots, n$. Including damping terms and reordering the state variables, one can rewrite equation (3.4) as

$$\dot{x}(t) = Ax(t) + Bu(t) \tag{3.5a}$$

$$y(t) = Cx(t) \tag{3.5b}$$

where

$$x = \begin{bmatrix} \eta_1 \\ \dot{\eta}_1 \\ \vdots \\ \dot{\eta}_n \end{bmatrix} \qquad A = \left[\begin{array}{cc|cc} 0 & 1 & & \\ -\omega_1^2 & -2\zeta_1\omega_1 & & 0 \\ \hline & & \ddots & \\ & 0 & 0 & 1 \\ & & -\omega_n^2 & -2\zeta_n\omega_n \end{array}\right]$$

$$B = \left[\begin{array}{c} 0 \\ \hline (B_m)_1 \\ \hline 0 \\ \hline (B_m)_2 \\ \vdots \end{array}\right] \qquad C = \left[\begin{array}{c|c|c|c} (C_m)_1 & 0 & (C_m)_2 & \cdots \end{array}\right]$$

Equation (3.5) is a finite dimensional approximation of the actual LSS dynamics described in equation (3.1). As mentioned before, this finite dimensional model is expected to have errors in modal frequencies, damping ratios, and mode shapes. The errors can be minimized by adjusting the parameters in equation (3.5). Figure 3-2 shows two ways to tune

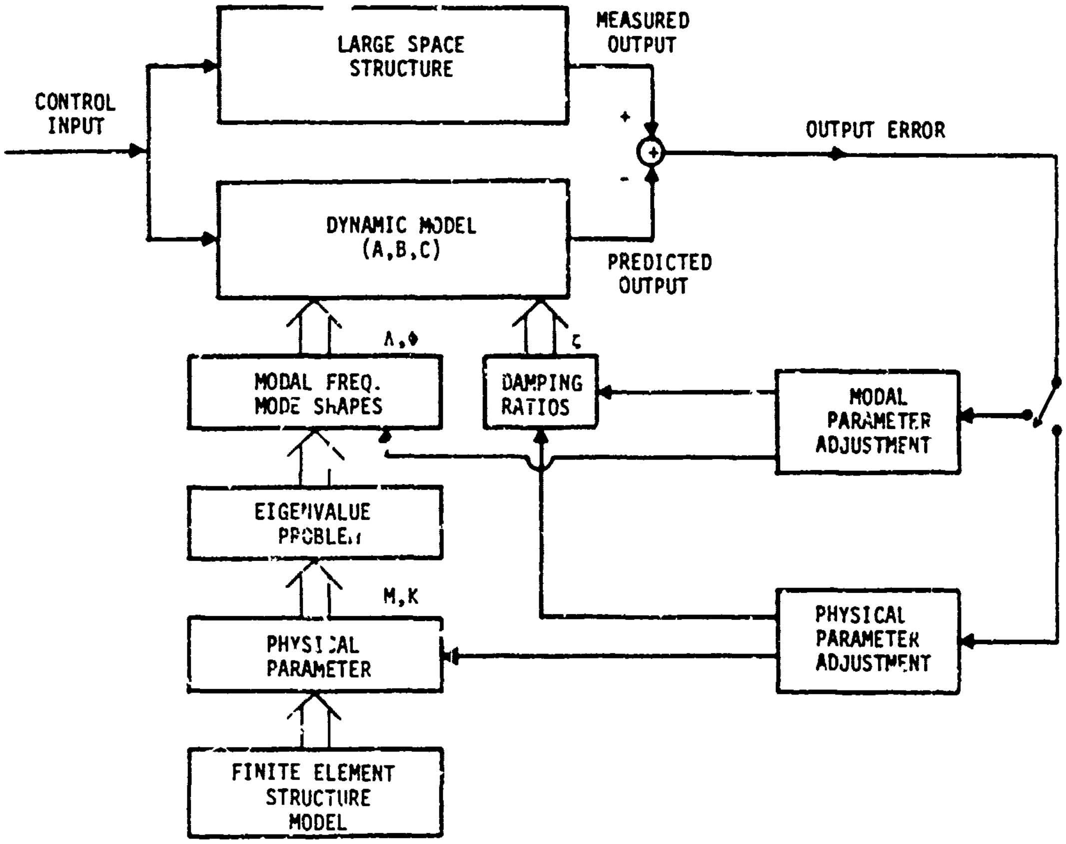

Figure 3-2. Modal Parameter Estimation and Physical Parameter Estimation

the model. The first approach is to adjust the modal frequencies, damping ratios, and mode shapes, called modal parameters, in equation (3.5) directly. The other approach is to adjust the parameters in matrices M and K, called physical parameters, in equation (3.3). Examples of physical parameters are Young's modulus of structural material, mass distributions on the structure, etc. Changes in M and K will influence the values of modal frequencies and mode shapes via the eigenvalue problem. Damping ratios can be adjusted with physical parameters at the same time.

Likelihood Cost Functional

Let the actual LSS dynamics and sensor measurement be described by equations (3.1) and (3.2). Then the likelihood cost functional for a record of LSS input-output measurements {u(t), z(t)} during the time interval [0,T] is [3]

$$\tilde{J} = \frac{1}{2} \int_0^T [z(t) - s(t)]^T G^{-1} [z(t) - s(t)] dt \tag{3.6}$$

where s(t) is the ideal sensor measurement described in equation (3.1).

The above likelihood cost functional which involves the solution of PDE is difficult to evaluate. However, it can be approximated by

$$J(\theta) = \frac{1}{2} \int_0^T [z(t) - y(\theta;t)]^T G^{-1} [z(t)-y(\theta;t)] dt \tag{3.7}$$

where $y(\theta,t)$ is the output estimated by the finite dimensional model (equation (3.5)) which is parameterized as

$$\frac{d}{dt} x(\theta;t) = A(\theta)\, x(\theta;t) + B(\theta)\, u(t) \tag{3.8a}$$

$$y(\theta,t) = C(\theta)\, x(\theta;t) \tag{3.8b}$$

and $\theta = [\alpha_1, \alpha_2, \ldots, \alpha_p]^T$ is a vector of unknown parameters (modal or physical) in matrices A, B, and C.

The maximum likelihood estimates $\hat{\theta}$ is the θ which minimizes $J(\theta)$. The parameter estimation problem now becomes a non-linear minimization problem. The modified Newton-Raphson method can be used to perform the minimization numerically.

Modified Newton-Raphson Method

Let θ_1 denotes the a-priori value of the unknown parameter θ, e.g., the nominal parameter values. The Newton-Raphson method is an iteractive procedure in which the new estimate θ_{n+1} is computed from the present estimate θ_n:

$$\theta_{n+1} = \theta_n - H^{-1}(\theta_n) \ \nabla J(\theta_n) \tag{3.9}$$

where $\nabla J(\theta)$ is the gradient of $J(\theta)$ with respect to θ, and $H(\theta)$ is the Hessian matrix. If all the second derivatives in $H(\theta)$ are omitted, then this procedure is called the modified Newton-Raphson method.

Let

$$\theta = [\alpha_1, \alpha_2, \text{---------}, \alpha_p]^T,$$

then for modified Newton - Raphson method:

$$\nabla J(\theta) = \begin{bmatrix} \frac{\partial J(\theta)}{\partial \alpha_1} \\ \cdot \\ \cdot \\ \cdot \\ \cdot \\ \frac{\partial J(\theta)}{\partial \alpha_p} \end{bmatrix}$$

$$\frac{\partial J(\theta)}{\partial \alpha_i} = -\int_0^T \left[\frac{\partial y(\theta;t)}{\partial \alpha_i}\right]^T G^{-1} \left[z(t) - y(\theta;t)\right] dt \tag{3.10}$$

and

$$H(\theta) = [h_{ij}(\theta)]$$

$$h_{ij}(\theta) = \int_0^T \left[\frac{\partial y(\theta;t)}{\partial \alpha_i}\right]^T G^{-1} \left[\frac{\partial y(\theta;t)}{\partial \alpha_j}\right] dt \tag{3.11}$$

where

$$\frac{\partial y(\theta;t)}{\partial \alpha_i}$$

is the output sensitivity with respect to parameter α_i.

In order for the modified Newton-Raphson iteration to converge, the matrix $H(\theta)$ should be positive definite in a region containing the true parameter. This is the identifiability condition for the maximum likelihood method.

The output sensitivity is important in calculating the gradient and the Hessian matrix. The computation of the output sensitivity for physical and modal parameters will be discussed later.

Properties of Maximum Likelihood Estimates

It is known that the maximum likelihood estimates are asymptomatically unbiased and consistent.

Let θ_0 be the true parameter and θ be the maximum likelihood estimate, then the covariance matrix of the estimation error

$$E \left\{ (\theta-\theta_0)\ (\theta-\theta_0)^T \right\} \leq H^{-1} \tag{3.12}$$

where H is the Fisher information matrix. The elements of H is described in equation (3.11). The matrix H^{-1} is the Cramer-Rao lower bound.

3.3.2 Physical Parameter Estimation

Output Sensitivity With Respect to Physical Parameters

Consider the physical representation of a LSS dynamic model (equation (3.3)).

$$M(\theta)\ \ddot{q}(\theta;t) + K(\theta)\, q\ (\theta;t) = B_p u(t) \tag{3.13a}$$

$$y(\theta;t) = C_p \; q(\theta;t) \tag{3.13b}$$

$$\theta = [\alpha_1, \alpha_2, \text{----} , \alpha_p]^T$$

The output sensitivity can be obtained by differentiating equation (3.13) with respect to the unknown parameter α_i,

$$M(\theta) \frac{\partial q(\theta;t)}{\partial \alpha_i} + K(\theta) \frac{\partial q(\theta;t)}{\partial \alpha_i} = - \frac{\partial K(\theta)}{\partial \alpha_i} q\,(\theta;t)$$

$$+ \frac{\partial M(\theta)}{\partial \alpha_i} \; M^{-1}(\theta) \;\; [K(\theta)\, q(\theta;t) - B_p u(t) \,] \tag{3.14a}$$

$$\frac{\partial y(\theta;t)}{\partial \alpha_i} = C_p \; \frac{\partial q(\theta;t)}{\partial \alpha_i} \tag{3.14b}$$

For complex structures, the dimensions of equations (3.13) and (3.14) could become very large, and it would be numerically advantageous to transform both equations into sets of decoupled equations in the modal coordinates. Table 3-1 describes the transformations. Equation (3.13) is transformed into modal coordinates by the modal matrix. Except for the input part, equation (3.14) is similar to equation (3.13) hence; it can also be transformed into a set of decoupled equations.

The block diagram in Figure 3-3 illustrates the use of finite element model in the maximum likelihood estimation of LSS physical parameters. Initial or updated unknown physical parameters and other fixed parameters are fed in a finite element modal analysis program which generates new system matrices for LSS dynamics and output sensitivity computations. The finite element program can be a special subroutine written for a particular LSS structure, or it can be a "canned" program such as NASTRAN which will be capable of handling various large and complicated structures. Currently, a special finite element subroutine is used. Also note that when enough mechanical isolations are provided among different parts of the whole structure, the finite element program needs only to model those parts whose physical properties are of interest. This will be demonstrated later in

Table 3-1. Output Sensitivity Computation For Physical Parameters

	STRUCTURAL REPRESENTATION	RELATION	MODAL REPRESENTATION
LSS DYNAMIC MODEL	$M\ddot{q} + Kq = B_p u$ (3.13) $y = C_p q$	$q = \Phi \eta$ $\longleftrightarrow$	$\ddot{\eta} + \Lambda \eta = \Phi^* B_p u$ $y = C_p \Phi \eta$
OUTPUT SENSITIVITY	$M \frac{\partial \ddot{q}}{\partial \alpha_i} + K \frac{\partial q}{\partial \alpha_i} = - \frac{\partial K}{\partial \alpha_i} q$ $+ \frac{\partial M}{\partial \alpha_i} M^{-1} [Kq - B_p u]$ (3.14) $\frac{\partial y}{\partial \alpha_i} = C_p \frac{\partial q}{\partial \alpha_i}$ $i = 1,2,\ldots,P$	$\frac{\partial q}{\partial \alpha_i} = \Phi \xi_i$ $\longleftrightarrow$	$\ddot{\xi}_i + \Lambda \xi_i = \Phi^* \frac{\partial M}{\partial \alpha_i} [\Phi \Lambda \eta - M^{-1} B_p u]$ $- \Phi^* \frac{\partial K}{\partial \alpha_i} \Phi \eta$ $\frac{\partial y}{\partial \alpha_i} = C_p \Phi \xi_i$ $i = 1,2,\ldots,P$

- UNKNOWN PARAMETER $\theta = [\alpha_1, \alpha_2, \ldots, \alpha_p]^*$, α_i in M or K
- Λ AND Φ SATISFY THE EIGENVALUE PROBLEM $K\Phi = M \Phi \Lambda$

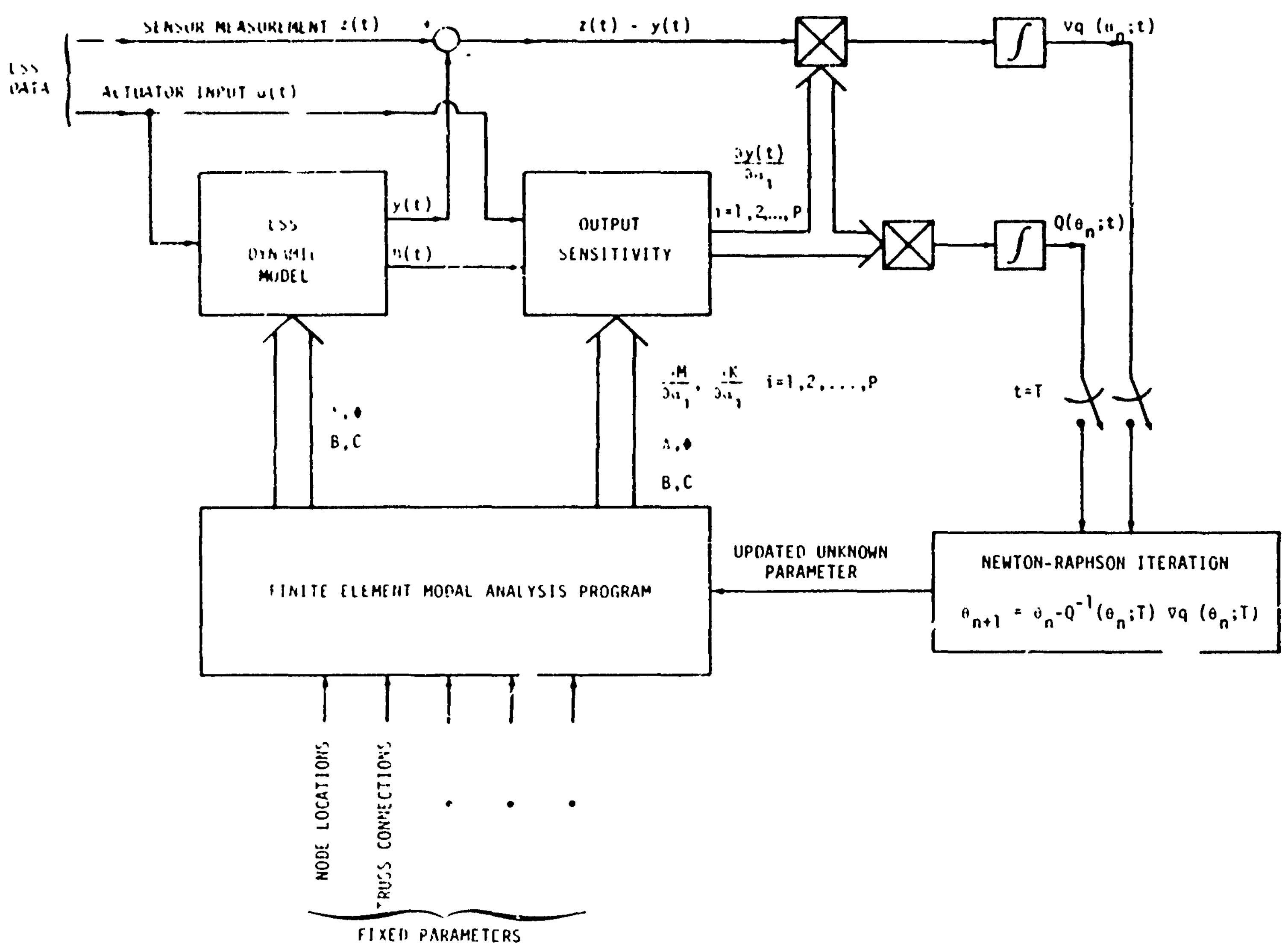

Figure 3-3 Maximum likelihood with Newton-Raphson Iteration For Physical Parameter Estimation

Section 3.6.

Output Sensitivity W.R.T Damping Ratios

The damping ratios, ζ_i's, are, strictly speaking, modal parameters, but they can be estimated with other physical parameters at the same time. This is because the damping ratios are not involved in the underlying eigenvalue problem, and the corresponding output sensitivities can be obtained by differentiating the LSS modal equations with respect to damping ratios. The damping ratio for each mode can be treated as individual independent unknown parameter. This will drastically increase the number of unknown parameters. Hence for any practical applications, it is desirable to divide damping ratios into small number of groups so that damping ratios in each group are constraint to have the same value. This will reduce the number of unknown parameters. In the subsequent simulation tests, all the damping ratios in the precision structure are considered as one unknown parameter. The output sensitivity for this case is computed as follows:

Let $\quad \zeta_1 = \zeta_2 = \dots = \zeta_n = \zeta$

Then the output sensitivity for damping ratio can be obtained by differentiate equation (3.5) with respect to ζ,

$$\frac{d}{dt}\left(\frac{\partial x\ (t)}{\partial \zeta}\right) = A\ \frac{\partial x(t)}{\partial \zeta} + \frac{\partial A}{\partial \zeta}\ x(t) \tag{3.15a}$$

$$\frac{\partial y(t)}{\partial \zeta} = C\ \frac{\partial x(t)}{\partial \zeta}$$

$$\frac{\partial A}{\partial \zeta} = \begin{bmatrix} \frac{\partial A_1}{\partial \zeta} & \emptyset \\ \emptyset & \frac{\partial A_n}{\partial \zeta} \end{bmatrix} \qquad \frac{\partial A_i}{\partial \zeta} = \begin{bmatrix} 0 & 0 \\ 0 & -2\omega_i \end{bmatrix}$$

3.3.3 Direct Estimation of Modal Parameters

Accurate modal parameters (modal frequencies, mode shapes) for all modes of interest can be computed from the estimated physical parameters via finite-element modal analysis program. But the estimation of physical parameters may be too complicated if one only wants to estimate the modal data of a small number of modes, or physical parameter estimation loses meaning because of the complexity of the structure. The maximum likelihood method can be applied to estimate those modal parameters directly.

The output sensitivities for damping ratios are shown before. For modal frequencies and mode shapes, the output sensitivity can be computed in a similar manner; i.e.,

$$\frac{d}{dt}\frac{\partial x(t)}{\partial \alpha_i} = A\frac{\partial x(t)}{\partial \alpha_i} + \frac{\partial A}{\partial \alpha_i}x(t) + \frac{\partial B}{\partial \alpha_i}u(t) \tag{3.16a}$$

$$\frac{\partial y(t)}{\partial \alpha_i} = C\frac{\partial x(t)}{\partial \alpha_i} + \frac{\partial C}{\partial \alpha_i}x(t) \tag{3.16b}$$

where

α_i is a modal parameter.

3.3.4 Effect of Data Length

It is known that the accuracies of the estimates can be improved by using longer data measurements. The large space structure is a very lightly damped system. The corresponding cost functional that must be minimized to obtain a good parameter estimate has a component of the sinc-function type as shown in Figure 3-4.

For long data measurements the minimum of this function is well defined, as shown in curve (a), and the modified Newton-Raphson method

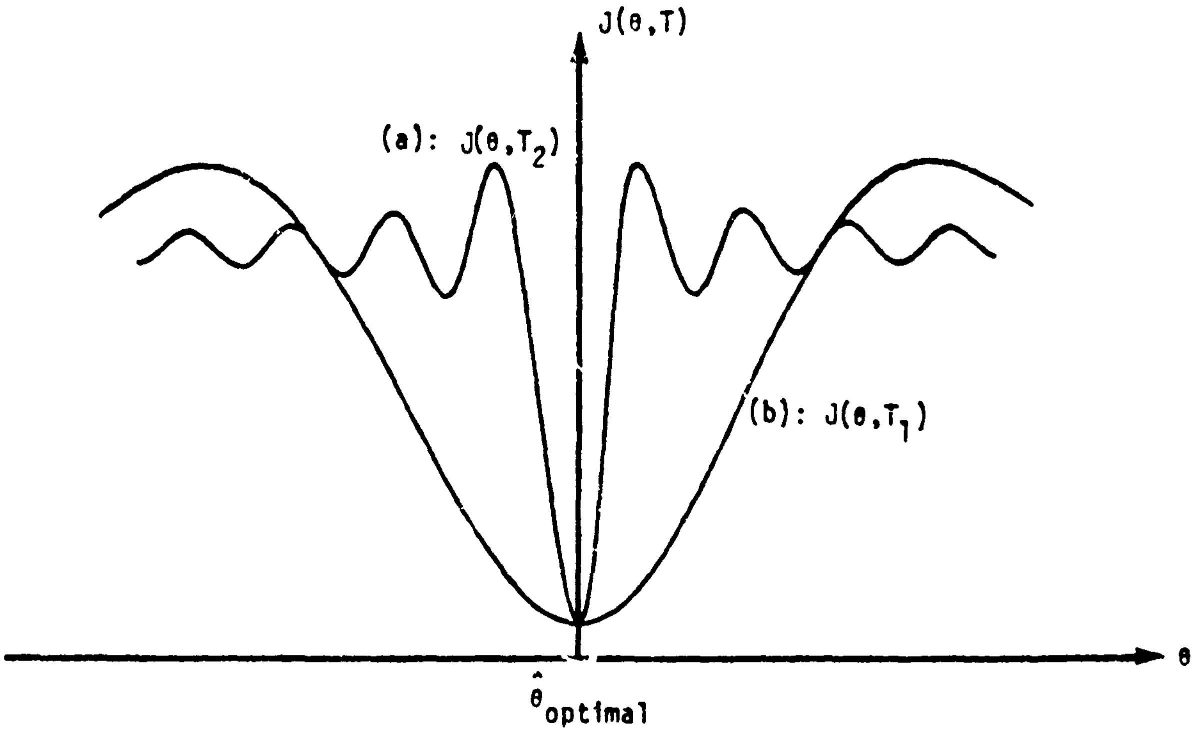

Figure 3-4. Cost Functional For Maximum Likelihood Estimation ($T_1 << T_2$)

will rapidly converge, provided the a priori (initial) estimate θ_0 was within the convex part of the global minimum. Otherwise, the algorithm will diverge to a local minimum of the quadratic cost function. For data measurements of short length, the sinc function is broad as shown in curve (b) and the absolute minimum is not well defined for a gradient search technique. Thus, initially the a priori parameter estimates should be merely improved by processing relatively short pieces of measurement data. Thereafter, the data length should be increased to provide better noise rejection and a "sharp" convergence to more accurate parameter estimates.

One can expect that longer data length will increase the accuracies of the estimated parameter, however, the initial estimates will be required to be closer to the true parameter valves in order for the maximum likelihood algorithm to converge.

Simple Example

The effect of data length can be further illustrated by a simple example. Consider the mass-spring system, shown in Figure 3-5, with **true** dynamics

$$m_0 \; x(t) \; + \; k_0 \, x(t) = F(t) \qquad\qquad m_0 = 1, \;\; k_0 = 1$$

and model

$$m \, x(t) \; + \; k \;\; x(t) = \; F(t)$$

For an impulse input, $F = \delta(t)$, the displacement of the mass is

$$x(t) \;\; = \;\; \frac{1}{\sqrt{m_0 k_0}} \; \sin \sqrt{\frac{k_0}{m_0}} \;\; t \qquad = A_0 \sin \omega_0 t$$

Similarly, the estimated response is found to be

$$\hat{x}(t) \;\; = \;\; \frac{1}{\sqrt{mk}} \;\; \sin \sqrt{\frac{k}{m}} \;\; t \qquad = A \sin \omega t$$

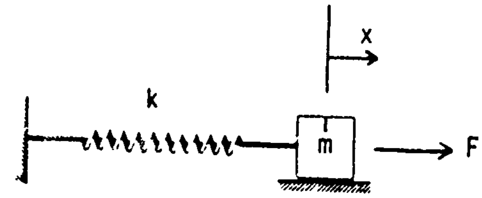

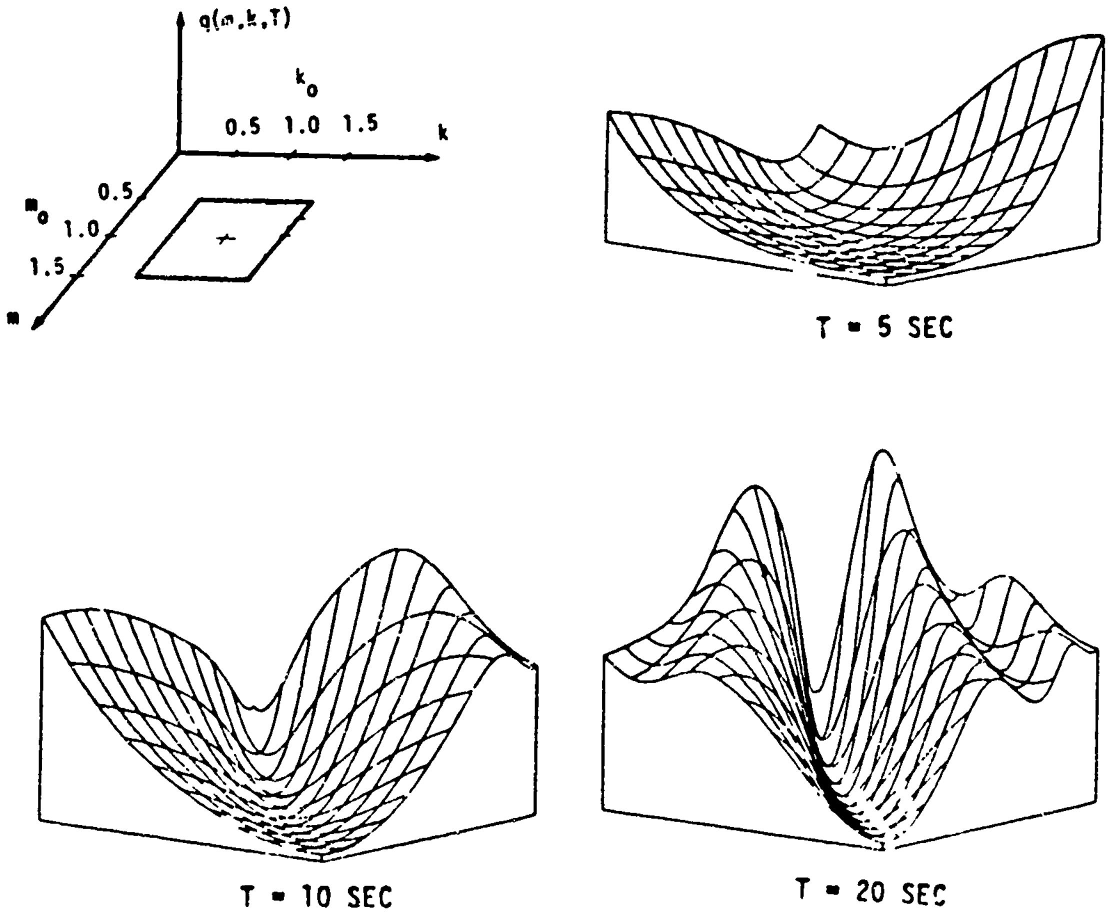

Figure 3-5. Cost Functional of Mass-Spring System For Data Length T=5, 10 And 20 Seconds ($0.5 \leq m \leq 1.5$, $0.5 \leq k\ 1.5$)

This cost functional can be expressed as

$$q(T) = \frac{1}{2T} \int_0^T (x(t) - \hat{x}(t))^2 \, dt$$

$$= \frac{1}{4} [A_0^2 + A^2] - \frac{1}{4} \left[A_0^2 \frac{\sin 2\omega_0 T}{2\omega_0 T} + A^2 \frac{\sin 2\omega T}{2\omega T}\right]$$

$$+ \frac{1}{2} AA_0 \frac{\sin (\omega_0 + \omega)T}{(\omega_0 + \omega) T} - \frac{1}{2} AA_0 \frac{\sin (\omega_0 - \omega)T}{(\omega_0 - \omega)T}$$

The cost functional for $0.5 \leq m \leq 1.5$, $0.5 \leq k \leq 1.5$, and $T = 5, 10, 20$ are shown in Figure 3-5.

It can be seen that as T increases the cost functional becomes sharper around the true values - higher accuracies, but one has to start at a point closer to the true values - smaller region of convergence.

3.4 SELECTION OF CRITICAL PARAMETERS

It is known that too many unknown parameters will decrease the accuracies of the estimated values and even cause identifiability problem in some cases. One need to determine which parameters are critical and must be estimated. All other parameters are fixed at their nominal values. The physical parameters are usually small in number and hence pose less difficulties. Two criteria that can be used to select critical modal parameters are presented in this section.

3.4.1 Controller Performance Sensitivity Criterion

Consider the modal representation of a LSS dynamic model:

$$\dot{x}_c = A_c x_c + B_c u$$

$$\dot{x}_r = A_r x_r + B_r u$$

$$y = C_c x_c + C_r x_r$$

where X_c is the controlled mode and X_r is the residual mode.

The actuator input signal is u(t), and the sensor measurement is y(t). For the following analysis, it is assumed that the actuators and sensors are collocated, hence $B_C^T = C_c$ and $B_r^T = C_r$.

The feedback controller selected for the sensitivity study is the one that satisfies both positivity design and LQG design. This particular design may not meet the controller performance requirement, but it provides the generic structure of both positivity and LQG designs.

$$\dot{\hat{x}}_c = (\hat{A}_c - \hat{G}_c \hat{C}_c) \hat{x}_c + \hat{G}_c y$$

$$u = - \hat{K}_c \hat{x}_c$$

where

$$\hat{G}_c = \hat{B}_c$$

$$\hat{K}_c = \hat{G}_c^T \hat{P}$$

$$\hat{P} (\hat{A}_c - \hat{G}_c \hat{C}_c) + (\hat{A}_c - \hat{G}_c \hat{C}_c)^T p = - [\hat{Q} + 2\hat{B}_c \hat{B}_c^T]$$

$$\hat{Q} = \mathrm{Diag}\, [\hat{Q}_j]$$

$$\hat{Q}_j = \begin{bmatrix} 0 & \cdot \\ 0 & 4\zeta_j \omega_j \end{bmatrix}$$

The symbol "^" is used to denote those quantities that are function of unknown parameters.

The controller equations and the LSS dynamics can be combined to form an augmented system,

$$\frac{d}{dt}\begin{bmatrix}\hat{x}_c \\ x_c \\ x_r\end{bmatrix} = \underbrace{\begin{bmatrix}\hat{A}_c - \hat{B}_c\hat{C}_c & \hat{B}_c C_c & \hat{B}_c C_r \\ -B_c \hat{B}_c^T \hat{P} & A_c & 0 \\ -B_r \hat{B}_c^T \hat{P} & 0 & A_r\end{bmatrix}}_{A} \underbrace{\begin{bmatrix}\hat{x}_c \\ x_c \\ x_r\end{bmatrix}}_{X}$$

$$\dot{X} = AX \qquad X(o) = X_0$$

The controller performance index (not the performance index for controller design) is taken to be

$$J = \int_0^\infty X^T(t)\, R^T R\, X(t)\, dt = X_0^T \int_0^\infty e^{A^T t} R^T R\, e^{At}\, dt\, X_0$$

Where the matrix R can be chosen so that RX represents the quantity to be minimized, e.g., RX could be line-of-sight error. The performance index, J, is a function of both A and X_0. A usual mathematical procedure to eliminate the dependence on the initial states x_0 is to average J over the n-dimensional unit sphere of initial states. This leads to the average performance index $\hat{J}$

$$\hat{J} = n\,E\{J\} = \text{Trace}\left[\int_0^\infty e^{A^T t} R^T R\, e^{At}\, dt\right] = \text{Trace}\,[\,L\,]$$

where L is the solution of a Liapunov equation

$$A^T L + L A + R^T R = 0$$

Let $\alpha_1, \alpha_2, \text{------}, \alpha_p$ be modal parameters, then the sensitivity of performance index $\hat{J}$ to parameter α_i is

$$\frac{\partial \hat{J}}{\partial \alpha_i} = \text{Trace}\left[\frac{\partial L}{\partial \alpha_i}\right] \qquad i = 1,2,\ldots,p$$

where $\frac{\partial L}{\partial \alpha_i}$ satisfies

$$A^T \frac{\partial L}{\partial \alpha_i} + \frac{\partial L}{\partial \alpha_i} A + \left[\frac{\partial A^T}{\partial \alpha_i} L + L \frac{\partial A}{\partial \alpha_i}\right] = 0$$

Note that for physical parameters the computation of sensitivity is more complicated, due to the fact that the controller is designed through the use of modal representation. For physical parameters $\beta_1, \beta_2, \ldots, \beta_\ell$, the sensitivity of performance index is

$$\frac{\partial \hat{J}}{\partial \beta_j} = \sum_{i=1}^{p} \frac{\partial \hat{J}}{\partial \alpha_i} \frac{\partial \alpha_i}{\partial \beta_j}$$

where $\frac{\partial \hat{J}}{\partial \alpha_i}$ is sensitivity to modal parameters, and $\frac{\partial \alpha_i}{\partial \beta_j}$ involves eigenvalue problems but can be approximated by using Jacobi's formula.

The performance sensitivity of each parameter is itself an indication of importance, however one can not compare the performance sensitivity of mode frequency with the performance sensitivity of damping ratio.

Let ΔJ be the total allowed degradation in the performance index

$$\Delta \hat{J} = \frac{\partial \hat{J}}{\partial \alpha_1} \Delta\alpha_1 + \frac{\partial \hat{J}}{\partial \alpha_2} \Delta\alpha_2 + \ldots + \frac{\partial \hat{J}}{\partial \alpha_p} \Delta\alpha_p$$

where $\Delta\alpha_i$ is the change in parameter α_i.

The degradation of $\Delta\hat{J}$ will not be exceeded if $\Delta\alpha_i$'s are such that

$$|\Delta\alpha_i| \leq \frac{\left|\frac{\Delta \hat{J}}{p}\right|}{\left|\frac{\partial \hat{J}}{\partial \alpha_i}\right|} \qquad i = 1,2,\ldots,p$$

The percent change in parameter values are bounded by

$$\left|\frac{\Delta\alpha_i}{\alpha_i}\right| \le \frac{\left|\frac{\Delta\hat{J}}{p}\right|}{\left|\frac{\partial\hat{J}}{\partial\alpha_i}\alpha_i\right|} = \frac{\text{CONST.}}{\left|\frac{\partial\hat{J}}{\partial\alpha_i}\alpha_i\right|}$$

Therefore, in order to assure controller performance robustness, those parameters with small $\left|\frac{\Delta\alpha_i}{\alpha_i}\right|$ values (or equivalently high $\left|\frac{\partial\hat{J}}{\partial\alpha_i}\alpha_i\right|$ values) should be selected for parameter estimation. For instance, if one wants to estimate m parameters, then the first m parameters with highest $\left|\frac{\partial\hat{J}}{\partial\alpha_i}\alpha_i\right|$ values should be estimated.

Example (DRAPER Tetrahedral Truss Structure)

This parameter sensitivity analysis technique of selecting critical system parameters is applied to the Draper tetrahedral truss structure (See Section 4-2)

Controlled Modes: Modes 1-8

Residual Modes: Modes 9-12

$$\hat{A}_c = \begin{bmatrix} A_1 & & \phi \\ & A_2 & \\ \phi & & \ddots A_8 \end{bmatrix} \qquad A_i = \begin{bmatrix} 0 & 1 \\ -\omega_i^2 & -2\zeta_i\,\omega_i \end{bmatrix}$$

$$\hat{B}_c = \begin{bmatrix} 0 & 0 & \cdots & 0 \\ b_{1,1} & b_{1,2} & \cdots & b_{1,6} \\ 0 & 0 & \cdots & 0 \\ b_{2,1} & b_{2,2} & & \vdots \\ \vdots & & \ddots & \\ b_{8,1} & & & b_{8,6} \end{bmatrix} \qquad \hat{C}_c = \hat{B}_c^T$$

Table 3-2. Parameters With Significant Influence On Performance For The Draper Tetrahedral Truss Structure Example.

	Parameter	Nominal Value (α_i)	$\left\| \frac{\partial J}{\partial \alpha_i} \right\|$	$\left\| \frac{\partial J}{\partial \alpha_i} \alpha_i \right\|$
1	ω_1	1.34	.589	.790
2	$b_{2,4}$	.111	6.008	.672
3	$b_{2,5}$	.111	6.008	.672
4	ω_2	1.66	.348	.580
5	ζ_1	.01	41.4	.414
6	$b_{1,6}$	.067	5.57	.373
7	$b_{1,3}$	-.067	5.57	.373
8	ζ_2	.01	30.0	.300
9	$b_{2,1}$	-.068	3.70	.255
10	$b_{2,2}$	-.068	3.70	.255
11	$b_{1,1}$	.043	3.64	.159
12	$b_{1,2}$	-.043	3.64	.159
13	ω_5	3.39	.0356	.121
14	ω_4	2.95	.039	.115
15	ω_7	4.66	.0173	.080
16	ω_3	2.89	.0203	.058
17	ω_8	4.75	.0118	.056
18	$b_{1,4}$	-.023	1.93	.044
19	$b_{1,5}$	.023	1.93	.044
20	$b_{5,1}$	.351	.088	.031
21	$b_{5,2}$	.351	.088	.031

$$\text{Performance Index:} \quad RX = \begin{bmatrix} LOS\ X \\ LOS\ Y \end{bmatrix}$$

The modal parameters are the modal frequencies (ω_i), the mode shapes ($b_{i,j}$) and the damping ratios (ζ_i) in the controlled modes.

Table 3-2 lists the first 21 parameters (out of 64) according to their $\left| \frac{\partial \hat{J}}{\partial \alpha_i} \alpha_i \right|$ values. Large values in the last column means significant influence on performance.

3.4.2 Residual Power Spectral Density Criterion

In previous criterion, the critical parameters are selected independent of the actual input-output measurements of the LSS. Some parameters may be very close to their true values already and need not be estimated. Another criterion of selecting critical parameters is to examine the Power Spectral Density (PSD) plots of the residuals (output errors). Those modes whose frequencies are closest to the spikes in the residual PSDs are chosen for parameter estimation. One mode or several modes can be estimated at the same time, and update the modal data. This process can be repeated until desired error levels are achieved.

The application of this criterion is illustrated later on the DRAPER Model #2.

3.5 DESIGN OF ON-ORBIT TEST SIGNALS

In general, the input signal to a LSS should be "sufficiently rich" so that the modes of interests are excited. A more systematic approach is to examine the resulting Fisher information matrix H (equations (3-11) and (3.12)). The inverse of H is an accuracy measure on the estimated parameters. It would be beneficial to find an input signal which optimizes functionals of H subject to some energy constraint. Examples of functionals

are: (Det(H), Trace (H), and Trace (H^{-1}). This is the optimal input signal design problem.

The optimal input signal can assure the identifiability condition and improve the estimation accuracies. In other words, the same levels of estimation accuracies can be achieved with shorter LSS input-output measurement data. Hence, the time required in on-orbit testing and parameter estimation can be reduced.

But optimal input design, in general, is a difficult problem to solve. The results depend on the unknown parameters, and may violate the spacecraft mission requirement, structure load constraint, or linearity assumption. An alternative approach to input design problem can be as follows. Several input signals which satisfy the mission requirement and the structure load constraint are selected as candidates. The one with highest Det(H) value is used to excite the LSS.

3.6 APPLICATIONS TO DRAPER MODEL #2

Computer simulation tests were conducted to verify the performance of the maximum likelihood parameter estimator as it applied to the Draper Example Structure Model #2 (see Appendix A). The results of estimating physical parameters and modal parameters are presented.

3.6.1 Draper Model #2

The Draper example structure Model #2 and its actuator and sensor locations are shown in Figure 3-6. The actuator is of force type, and it can only act in the truss axial direction. The sensor measures the relative position displacement of two nodes in the direction of the line connecting them. Two collocated actuator/sensor pairs are placed on truss members connecting nodes 27 to 30, and 9 to 10. Two additional sensors are from nodes 29 to 32 and 28 to 35 which has no connecting truss members. The actuator and sensor from node 27 to 30 is denoted as "actuator 27-30" and "sensor 27-30", respectively.

Note that the actuator/sensor locations differ from that of the active control (Section 2). This is because the control studies and identification studies are conducted independently at the same time. In practice, one should attempt to perform parameter estimation using the same set of actuators and sensors that are selected for control. If the actuators and sensors for control are not sufficient for identification, additional actuator/sensor should be placed.

The perturbed Model #2 is taken to be the true system. The input signal for actuator 27-30 is shaped pulse (100Hz bandwidth) of magnitude 1 Newton, duration .02 second, and period .25 second. Same input signal with .02 second time delay is applied to actuator 9-10. The simulated sensor measurements are generated by using the perturbed Model #2 which contains 84 modes. A small amount ($\sigma = 3 \times 10^{-9}$ m) of independent white Gaussian noise is added to the simulated sensor measurements. The highest modal frequency is at 247 Hz, but the modes of interests have modal frequencies below 50 Hz. The sampling rate is taken to be 1000 Hz which is fast enough so that the continuous time formulation for the maximum likelihood estimator is essentially valid for this set of data.

3.6.2 Physical Parameter Estimation

Problem Statement

The objective is to extract physical parameters from the simulated data. The unknown parameters are the Young's modulus, E, of all truss members in the precision section and the mass distributions at upper and lower support structures. The initial and true parameter values are listed in Table 3-3. In order to reduce the number of unknown parameters the masses at some nodes are constraint to have identical weights. The shearing modulus of elasticity, G, is also constraint so that G=0.3E. It is assumed that the estimator has correct information on the values of A, I, and J for all truss members.

The damping ratio was fixed at its true value in the intial tests and was estimated alone with other unknown paramet[illegible] in later test runs.

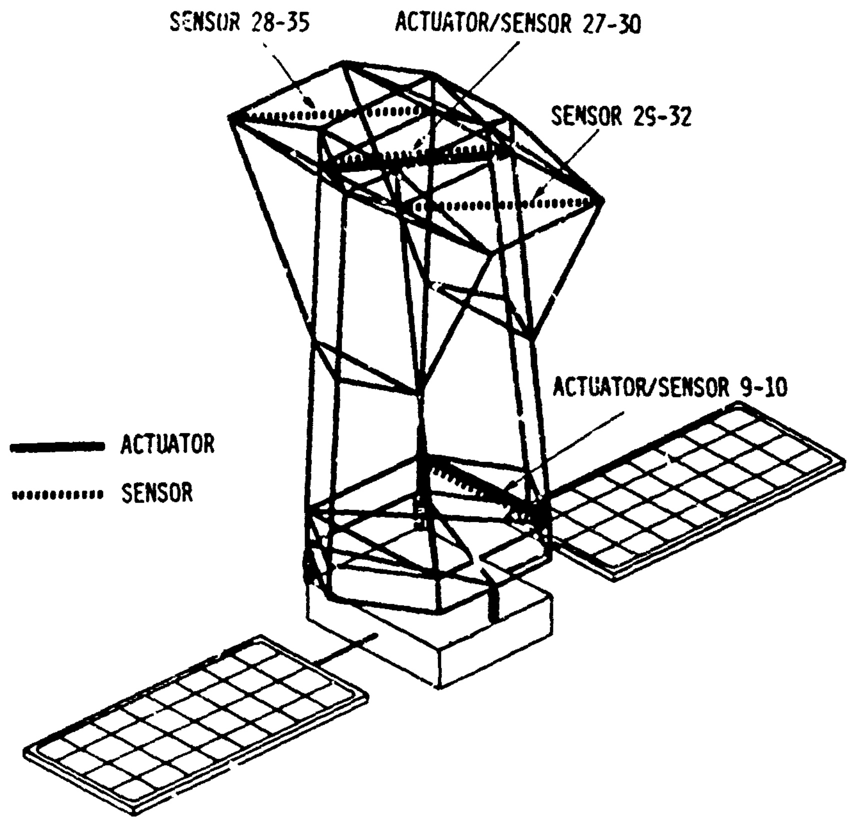

Figure 3-6. Locations of Actuators and Sensors For Parameter Estimation

Table 3-3. Draper Model #2 Physical Parameter For Identification

PARAMETER	INITIAL PARAMETER VALUES	TRUE PARAMETER VALUES	UNIT
YOUNG'S MODULUS (E), ALL TRUSSES	1.00×10^{11}	1.24×10^{11}	N/M^2
MASS, NODE 9,10,11,12	500	500	KG
MASS, NODE 27,28,29,30	375	350	KG
MASS, NODE 32	500	500	KG
MASS, NODE 33	500	550	KG
MASS, NODE 34	250	300	KG
MASS, NODE 35	250	250	KG

Simplified Structural Model for Physical Parameter Estimation

Since precision section and equipment section are connected by isolators and only the structural properties of the precision section are of interest, the finite element model for the estimator can be simplified to the model shown in Figure 3-7. The equipment section and solar panels are omitted. The precision section is mounted on isolators to inertially fixed rigid support. The mode frequencies of this simplified model and the complete model are also shown in the figure. All the mode frequencies of the simplified model (except 6 isolator modes) can be found in the mode frequencies of the complete model (denoted by "Δ"). In fact, this simplified model keeps all the modes associated with the precision section intact while reducing the number of modes from 84 to 54.

Simulation Results

A total of 14 test runs were made. Runs 1 through 11 used .1 second of simulated data. Runs 12 through 14 used .5 second of simulated data. Damping ratio was fixed (not estimated) for runs 1 through 10, and was estimated alone with other unknown parameter for the last 4 runs. The results are summarized in Table 3-4. Each individual run is highlighted below.

(A) Runs 1-5

Run 1 used .1 second of data. The estimation algorithm starting from the standard initial values converged in 6 iteration. Figure 3-8 compared the time histories of the simulated measurements with the estimated measurements generated by the estimator using standard initial parameter values. Similar comparisons were shown in Figure 3-9 in which the estimated measurements were obtained from the final estimates of Run 1. It appears that the estimator has made significant improvements in the estimated sensor measurements. The residuals (differences of simulated and estimated measurements) of Figure 3-9 are shown in Figure 3-10. It can be seen that the residuals consist primarily of sensor noise.

Simplified Model For Identification

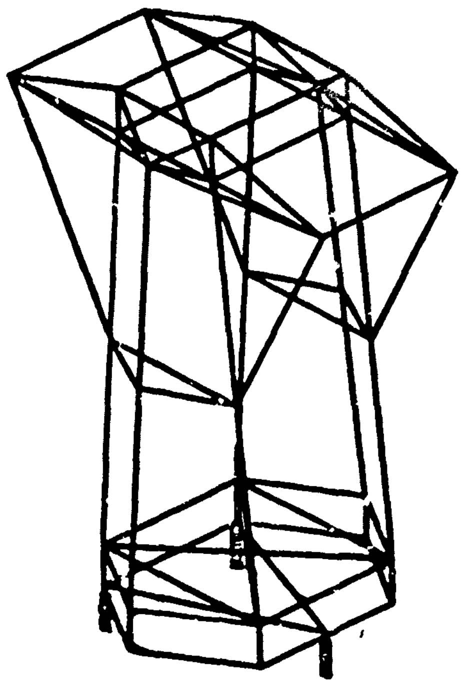

MODAL FREQUENCIES (RAD/SEC)

SIMPLIFIED MODEL	ISOLATOR MODES	3.387E-01	5.373E+01	1.077E+02	1.754E+02	2.590E+02	9.507E+02
		4.644E-01	7.223E+01	1.120E+02	1.793E+02	2.908E+02	1.015E+03
		1.375E+00	7.988E+01	1.198E+02	1.931E+02	3.008E+02	1.015E+03
		1.847E+00	8.607E+01	1.493E+02	2.062E+02	3.208E+02	1.189E+03
		2.972E+00	8.894E+01	1.534E+02	2.114E+02	3.968E+02	1.189E+03
		3.132E+00	9.823E+01	1.628E+02	2.167E+02	3.974E+02	1.309E+03
		1.075E+01	1.008E+02	1.656E+02	2.364E+02	5.794E+02	1.313E+03
		1.482E+01	1.038E+02	1.695E+02	2.404E+02	5.794E+02	1.552E+03
		5.086E+01	1.052E+02	1.748E+02	2.548E+02	9.465E+02	1.552E+03

COMPLETE MODEL	9.043E-05	3.653E+00	2.864E+01	▲8.608E+01	▲1.656E+02	▲2.404E+02	6.924E+02
	5.192E-05	7.689E+00	2.922E+01	8.894E+01	1.661E+02	2.548E+02	7.000E+02
	3.588E-05	8.029E+00	4.370E+01	9.823E+01	▲1.695E+02	2.590E+02	▲9.465E+02
	2.699E-05	8.168E+00	4.645E+01	1.008E+02	▲1.748E+02	2.908E+02	9.507E+02
	3.459E-05	1.048E+01	▲5.086E+01	1.038E+02	▲1.754E+02	3.008E+02	1.015E+03
	1.119E-04	▲1.077E+01	▲5.373E+01	1.052E+02	▲1.792E+02	3.208E+02	1.015E+03
	9.144E-01	1.143E+01	5.538E+01	1.077E+02	1.798E+02	3.968E+02	1.189E+03
	1.654E+00	1.143E+01	5.538E+01	1.120E+02	▲1.931E+02	▲3.974E+02	1.189E+03
	1.994E+00	▲1.481E+01	7.129E+01	1.198E+02	▲2.062E+02	4.537E+02	1.309E+03
	2.092E+00	1.745E+01	▲7.223E+01	1.493E+02	▲2.114E+02	4.552E+02	1.313E+03
	2.785E+00	1.995E+01	▲7.988E+01	1.534E+02	▲2.167E+02	▲5.794E+02	1.552E+03
	3.631E+00	2.128E+01	8.535E+01	▲1.628E+02	▲2.364E+02	▲5.794E+02	▲1.552E+03

Figure 3-7. Simplified Draper Model #2 And The Corresponding Modal Frequencies

Table 3-4. Summary of Results on Estimating Physical Parameters

		RUN 1,2,3,4	RUN 5	RUN 6	RUN 7	RUN 8	RUN 9	RUN 10	RUN 11	RUN 12	RUN 13,14	TRUE VALUES
DATA LENGTH (SECOND)		.1	.1	.1	.1	.1	.1	.1	.1	.5	.5	
NO. OF ITERATIONS		6,6,8,8	12	8	8	8	8	8	9	9 (DIVERGE)	6,9	
PARAMETER	YOUNG'S MODULUS (N/M^2) E	1.24E11	1.24E11	1.24E11	1.21E11	1.24E11	1.24E11	1.24E11	1.24E11	2.59E11	1.24E11	1.24E11
	MASS (KG) NODES 9,10,11,12	498.4	496.1	498.4	474.0	499.7	501.1	500.3	499.9	832.9	500.1	500.0
	MASS (KG) NODES 27,28,29,30	350.1	350.3	350.1	342.1	350.8	351.5	350.5	350.5	1283.7	350.1	350.0
	MASS (KG) NODE 32	499.0	499.4	499.0	471.7	499.7	513.3	519.2	499.4	50.0	501.2	500.0
	MASS (KG) NODE 33	557.7	557.6	557.6	556.8	557.8	559.4	567.7	557.7	1147.0	550.0	550.0
	MASS (KG) NODE 34	299.1	298.9	299.1	294.8	298.8	304.8	284.4	298.9	164.3	299.8	300.0
	MASS (KG) NODE 35	248.1	248.6	248.1	234.9	249.5	248.7	248.9	248.8	50.0	250.1	250.0
	DAMPING RATIO (-) ζ	—	—	—	—	—	—	—	.075%	1.0%	.102%	.100%

RUN 1: INITIAL PARAMETER VALUES ARE: 1.00E11, 500.0, 375.0, 500.0, 500.0, 250.0, 250.0
RUN 2: INITIAL PARAMETER VALUES ARE: 1.50E11, 550.0, 375.0, 550.0, 450.0, 200.0, 300.0
RUN 3: INITIAL PARAMETER VALUES ARE: 1.00E11, 600.0, 375.0, 600.0, 400.0, 150.0, 350.0
RUN 4: INITIAL PARAMETER VALUES ARE. 1.00E11, 800.0, 400.0, 550.0, 400.0, 150.0, 300.0
RUN 5: INITIAL PARAMETER VALUES ARE: 1.80E11, 250.0, 300.0, 400.0, 400.0, 200.0, 200.0
RUN 6: INITIAL PARAMETERS SAME AS RUN 1; 12 HIGHEST FREQUENCY MODES ARE TRUNCATED (36 MODES)
RUN 7: INITIAL PARAMETERS SAME AS RUN 1; 18 HIGHEST FREQUENCY MODES ARE TRUNCATED (30 MODES)
RUN 8: INITIAL PARAMETERS SAME AS RUN 1; DAMPING RATIOS ARE FIXED AT .05%
RUN 9: INITIAL PARAMETERS SAME AS RUN 1; MASSES AT NODES 14,15,16,17,18 AND 19 ARE SET TO BE 14 KGS (TRUE VALUES ARE 8,17,17,17,17, AND 8 KGS, RESPECTIVELY)
RUN 10: INITIAL PARAMETERS SAME AS RUN 1; MEASUREMENTS FROM SENSOR 28-35 ARE NOT USED (SENSOR FAILURE)
RUN 11: INITIAL PARAMETERS SAME AS RUN 1; INITIAL VALUE FOR DAMPING RATIO IS .05%
RUN 12: INITIAL PARAMETERS SAME AS RUN 11; ESTIMATOR DOES NOT CONVERGE AFTER 9 ITERATIONS
RUN 13: INITIAL PARAMETERS ARE THE FINAL ESTIMATES OF RUN 11
RUN 14: INITIAL PARAMETERS ARE: 1.15E11, 480.0, 365.0, 485.0, 535.0, 285.0, 235.0, .075%

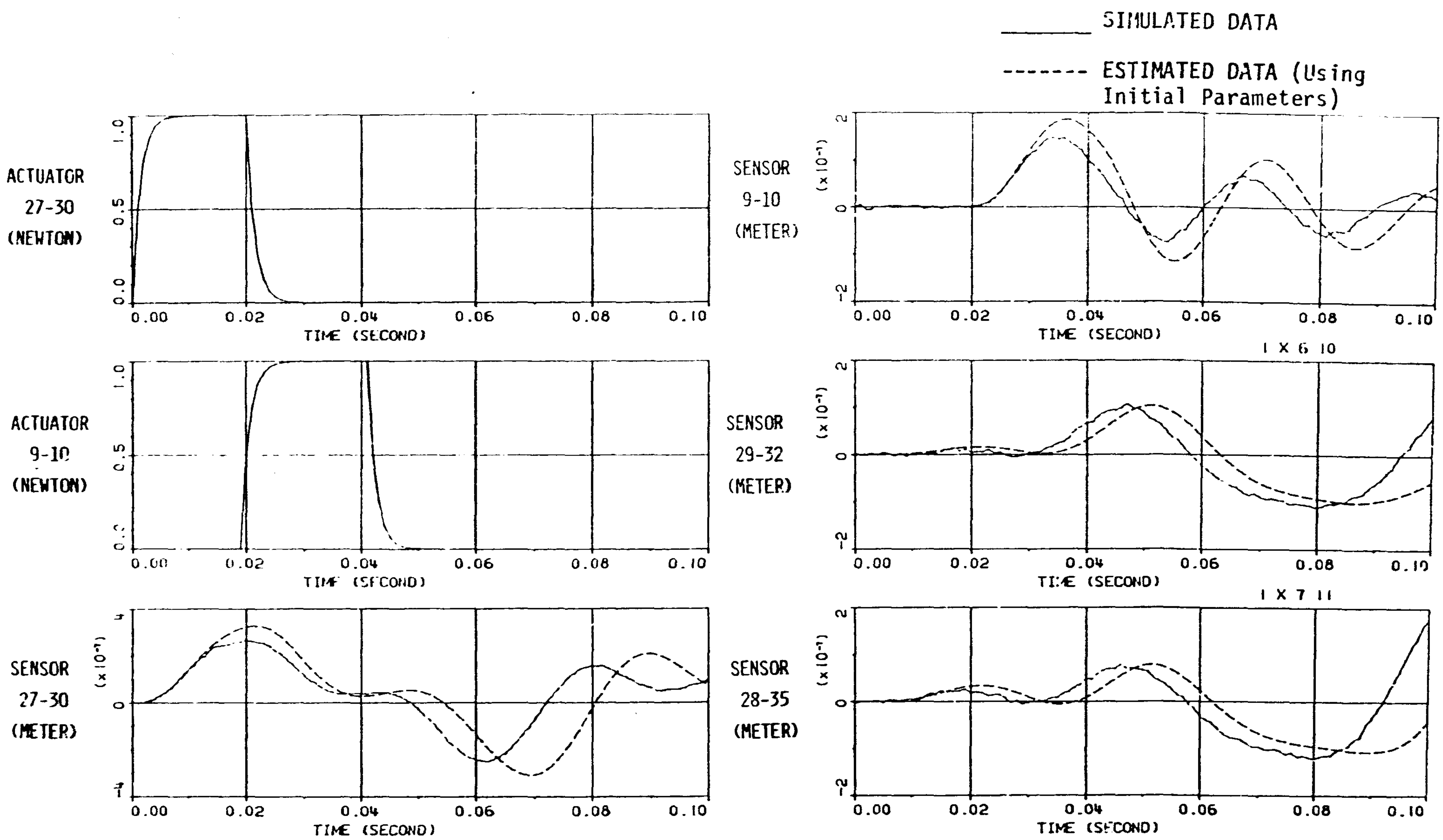

Figure 3-8. Comparisons Of Simulated Measurements With Measurements Predicted By The Model Using Initial Parameters

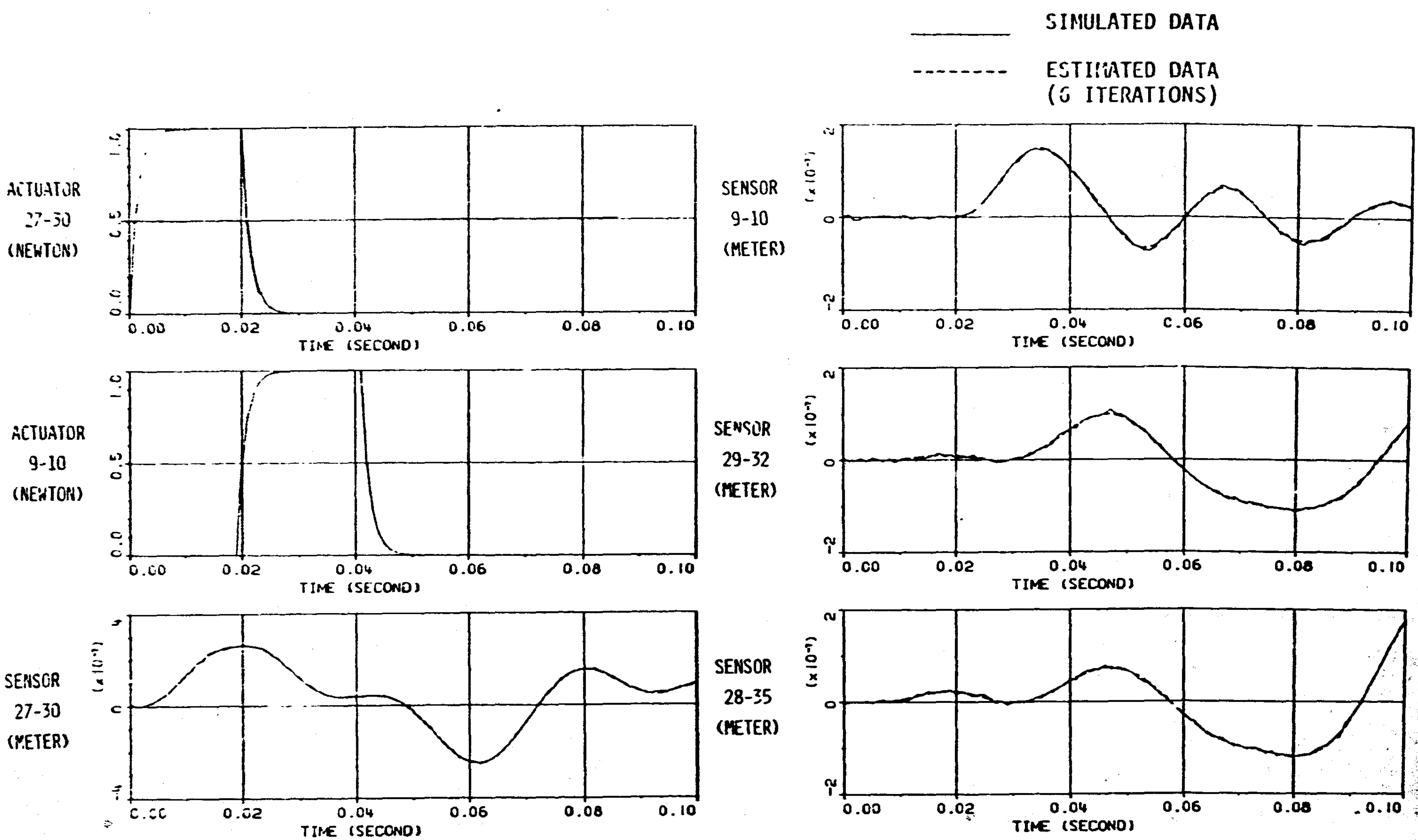

Figure 3-9. Comparisons Of Simulated Measurements With Measurements Predicted By The Model Using Estimated Parameters Obtained in Run 1.

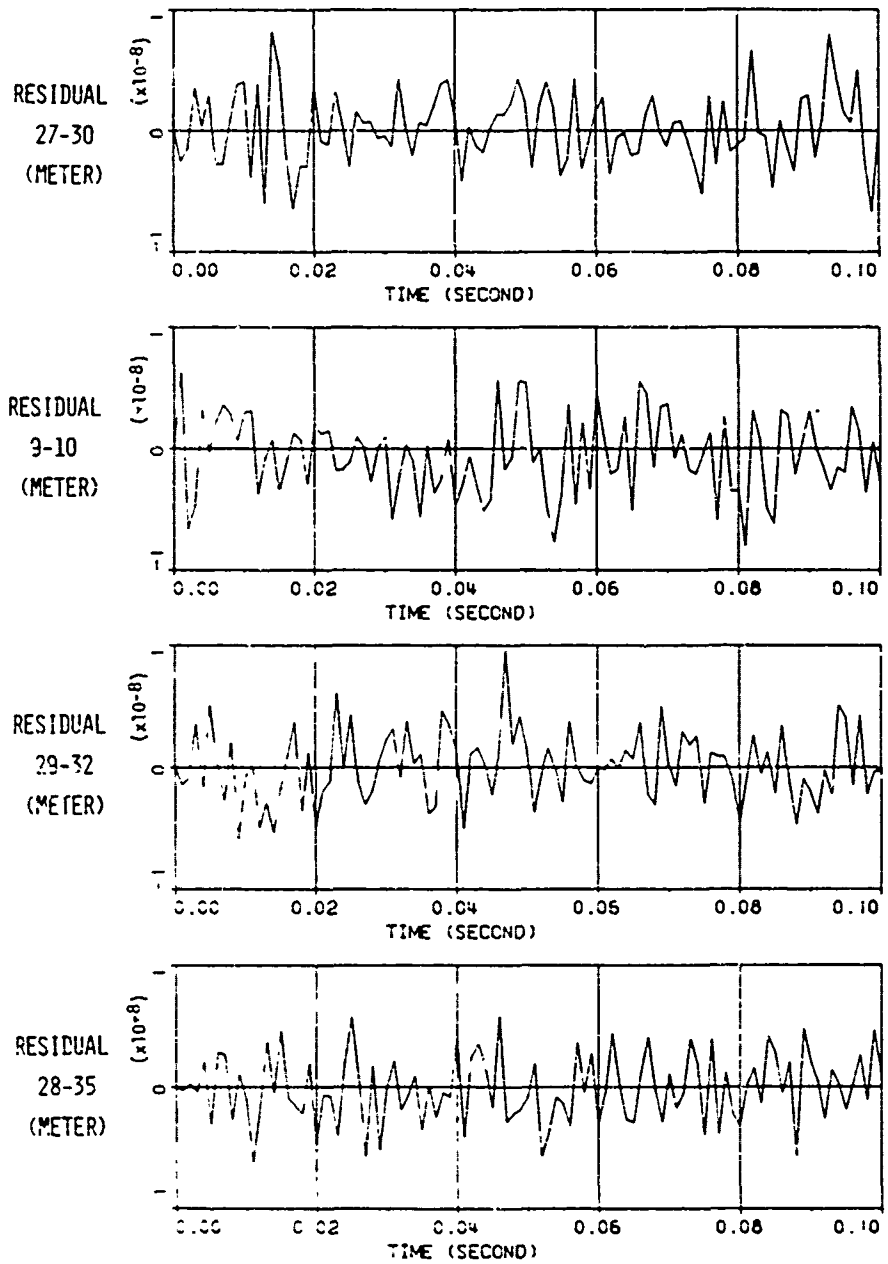

Figure 3-10. Residuals Of Run 1

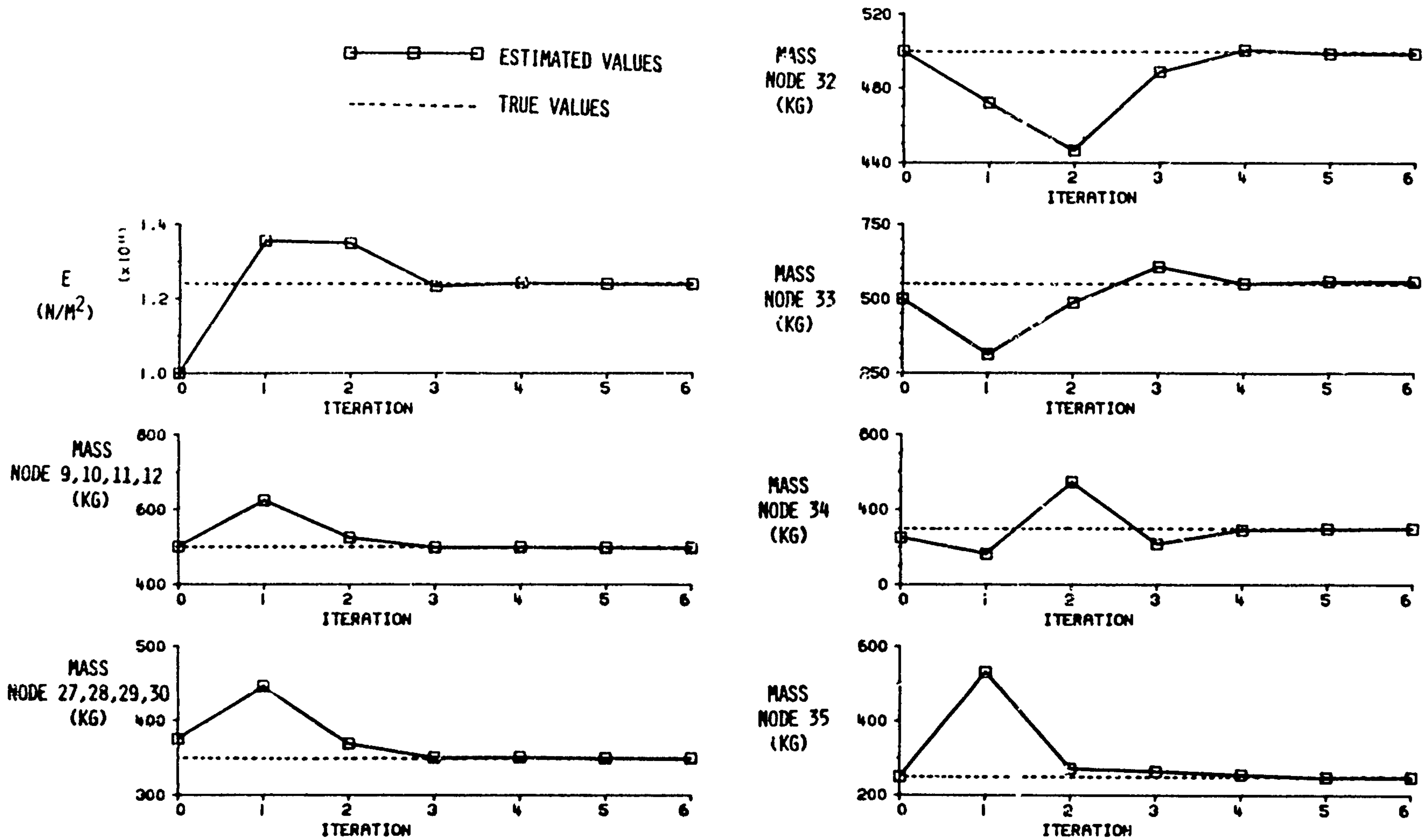

Figure 3-11. Convergence of Estimated Parameters for Run 1

Table 3-5. Convergence of Esti ed Parameters for Run 1.

PARAMETER	ITERATION INITIAL						FINAL	TRUE VALUE
	0	1	2	3	4	5	6	
YOUNG'S MODULUS (N/M^2)	1.00×10^{11}	1.35×10^{11}	1.34×10^{11}	1.23×10^{11}	1.24×10^{11}	1.24×10^{11}	1.24×10^{11}	1.24×10^{11}
MASS, NODE 9,10,11,12 (KG)	500.0	624.7	524.7	498.2	499.6	498.4	498.4	500.0
MASS, NODE 27,28,29,30 (KG)	375.0	446.1	369.3	350.8	351.3	350.1	350.1	350.0
MASS, NODE 32 (KG)	500.0	472.0	446.5	488.9	500.7	498.9	499.0	500.0
MASS, NODE 33 (KG)	500.0	313.3	487.1	605.7	550.2	557.6	557.7	550.0
MASS, NODE 34 (KG)	250.0	163.1	549.4	217.3	291.9	299.1	299.1	300.0
MASS, NODE 35 (KG)	250.0	531.6	272.1	264.5	255.8	248.3	248.1	250.0

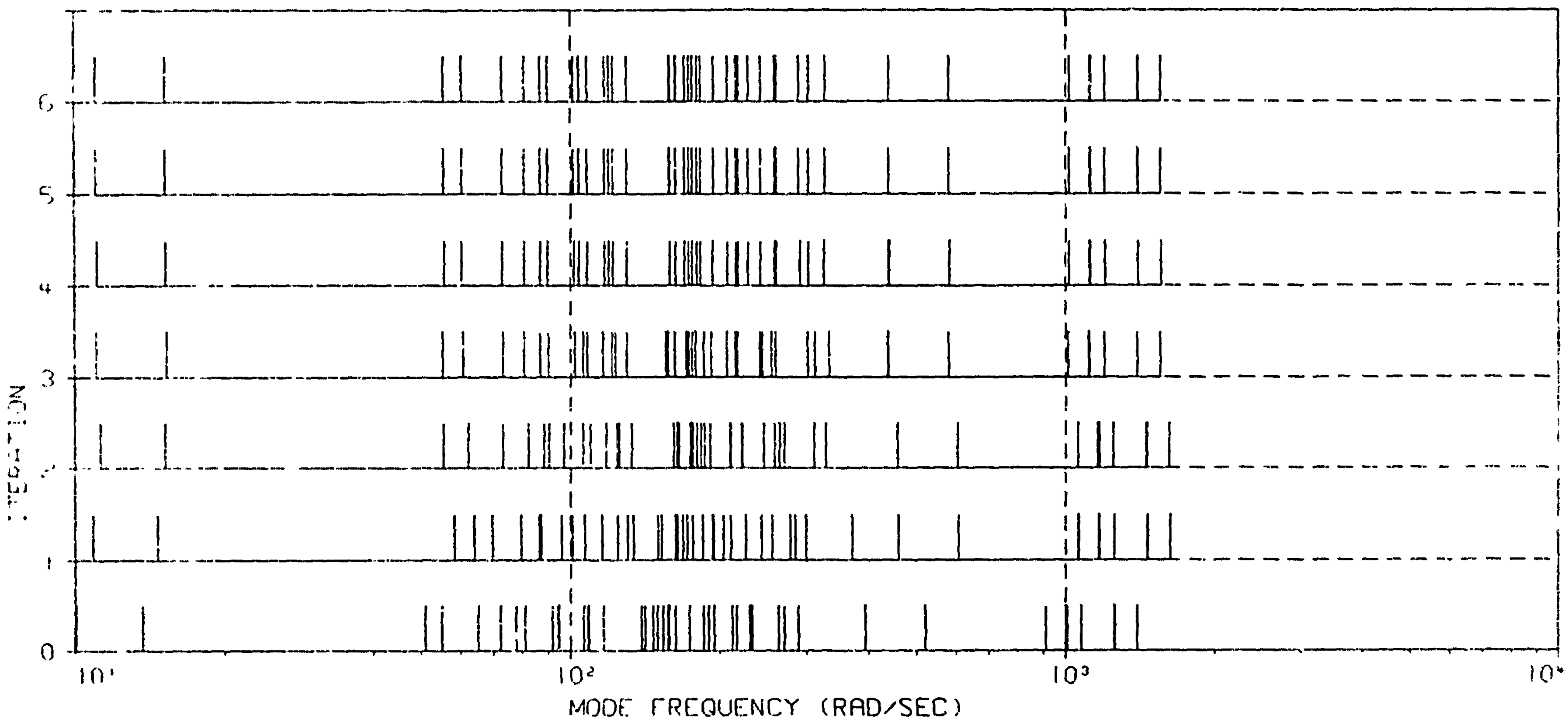

Figure 3-12. Corresponding Modal Frequencies For Each Iteration in Run 1

The convergence of the estimated parameter in each iteration is plotted in Figure 3-11. The numerical values are listed in Table 3-5. The estimated parameter converge after 6 iterations.

Although the mode frequences and mode shapes are not estimated directly, they can be computed from the estimated physical parameters via modal analysis program. The corresponding mode frequencies for each iteration are shown in Figure 3-12.

To test the ability of the identification algorithm to converge from other intial parameter values, RUNS 2, 3, 4, and 5 are made on the same simulated data. RUNS 2, 3, and 4 converge in 6 to 8 iterations. RUN 5 which is the worst case (up to 50% error in initial parameter values) converged in 12 iterations.

(B) Runs 6, 7

In Run 6, 12 highest frequency modes are truncated. This has very little effect on the estimated values. However in RUN 7, with 18 highest frequency modes truncated, there are noticeable degradations in the estimated parameter values. It is possible to truncate more modes, but it has to be done selectively, i.e. dominant modes should be retained.

(C) Runs 8-10

In RUN 8 all damping ratios are set to be .05% while true values are .1%. There are very little changes in the estimates, and this indicates that the damping rations will be difficult to estimate from this set of data.

In RUN 9, the estimator has incorrect values for the masses in the metering truss. RUN 10 simulates when sensor 28-35 fails, and the measurements from it are not used in the estimator. Both runs show some degradations in the estimated parameter values.

(D) Run 11

In RUN 11, the damping ratio ζ (for all structural modes) is estimated, in addition to other physical parameters, using 0.1 second of data.

It is assumed that the value of ζ is known to lie between 0.01% and 1.00%. The estimator converges in 9 iterations. The damping ratio is the last parameter to converge and its final estimate is .075% (true value =.100%). But according to the C-R Bound (standard deviation =.05%) this final estimate is a very reasonable value for 0.1 second of data. To obtain better estimates, longer data are to be used.

(E) Runs 12-14

To obtain more accurate estimates, the maximum likelihood estimator is applied to 0.5 second of simulated data. The first 0.1 second of this data is identical to the data used in previous test cases.

RUN 12 has the same initial parameter values as RUN 11, but after 9 iterations, the estimator shows no signs of convergence. The divergence is caused by too large errors in the initial parameter values relative to data length (discussed in Section 3.3.4). Hence, in RUN 13, the final estimate of RUN 11 are used as the initial estimates. The estimator converges in 6 iterations. All the final estimates are very close to the true values, especially for the damping ratio. The time histories of simulated and estimated measurements are compared in Figure 3-13.

The initial parameter values for RUN 13 are very close to the true values already. RUN 14 represents a case between two previous runs as far as initial parameter errors are concerned. The estimator converges in 9 iterations. The final estimates are the same as RUN 13.

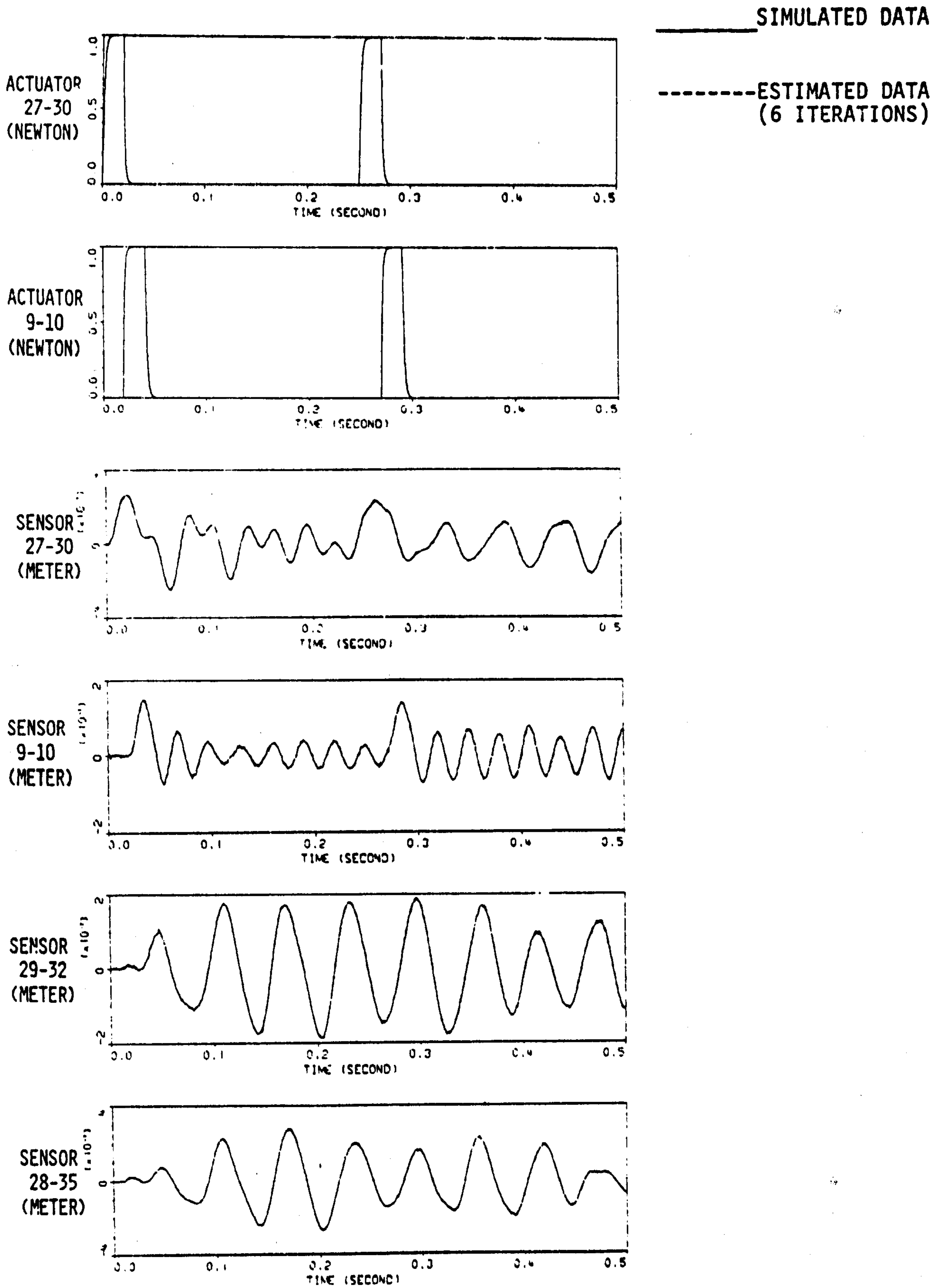

Figure 3-13. Comparisons Of Simulated Measurements With Measurements Predicted By The Modal Using Estimated Parameters Obtained in Run 13.

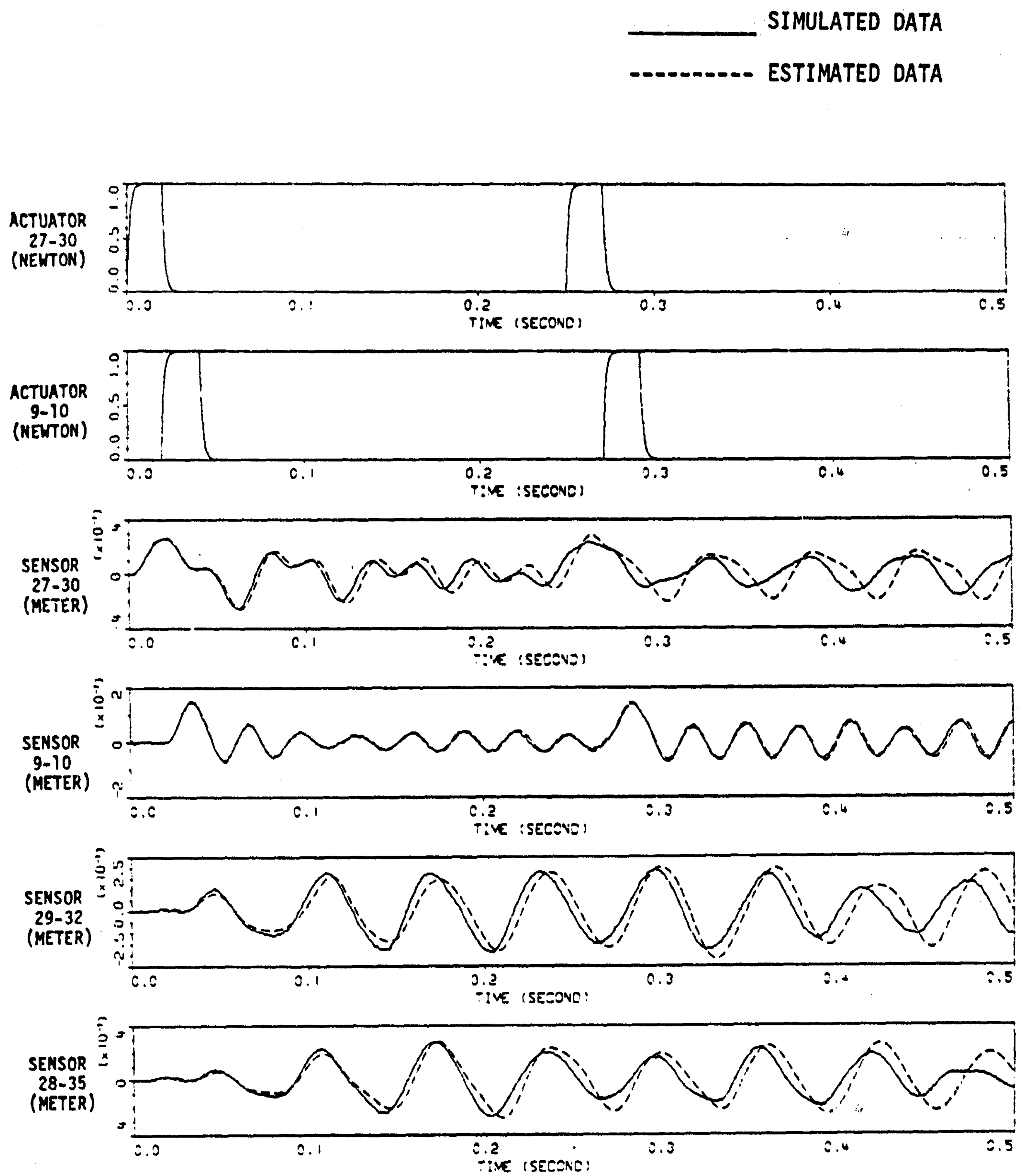

Figure 3-14. Comparisons Of Simulated Measurements With Measurements Predicted By 3-Mode Model Using Nominal Modal Data.

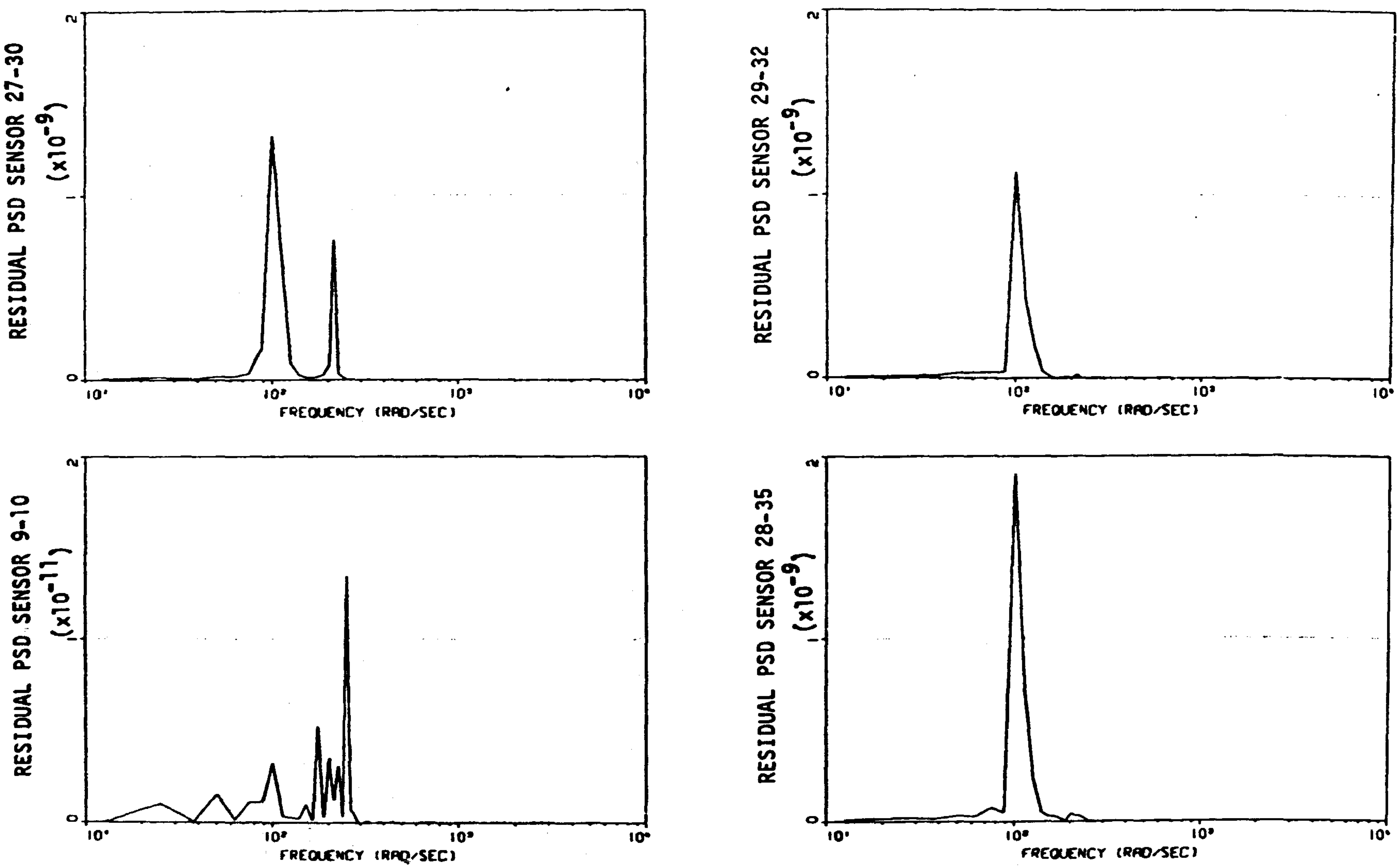

Figure 3-15. Residual Power Spectral Density Functions For Nominal Modal Data.

3.6.3 Direct Estimation of Modal Parameters

The objective is to improve the nominal modal data by estimating the modal parameter of few critical modes which are selected via the residual power spectral density (PSD) function criterion described in Section 3.4.2.

Simulation Results

The estimator has a dynamic model containing 30 dominant modes: modes 17, 21, 28, 30, 34-49, 51-54, and 56-61. The simulated measurements (.5 second) are the same as before. Initially, all 30 modes in the estimator are set to their nominal values. The estimated measurements from nominal values are compared to the simulated measurements. The time histories are shown in Figure 3-14. The residuals PSD functions are shown in Figure 3-15. From the residual PSD plots, all sensors, except sensor 9-10, show large errors at frequencies of 100 rad/sec (mode 41) and 210 rad/sec (mode 58).

The modal parameters of mode 41, except $C_{2,41}$, are estimated. The new residual PSD plots are examined, and mode 58 is chosen for further parameter estimation. After modes 41 and 58 are identified, the time histories comparisons, and the residual PSD plots are shown in Figure 3-16, and 3-17, respectively. It appears that the maximum likelihood estimator reduces the residuals by a factor of 10 in power (3 in magnitude).

The numerical values of final estimates for modes 41 and 58 are listed in Table 3-6. The estimates are not as close to their true values as seen in previous cases where physical parameters are estimated. This is because all other parameters are at their erroneous nominal values, and exact convergence cannot be expected. Nevertheless, a very significant improvement in the knowledge of critical modes has been achieved.

Damping ratio cannot be estimated to the desired accuracy from this set of data. However, a run is made where all modes are artificially set to their true values, except the ones to be estimated, all parameters including damping ratios converge to the true values.

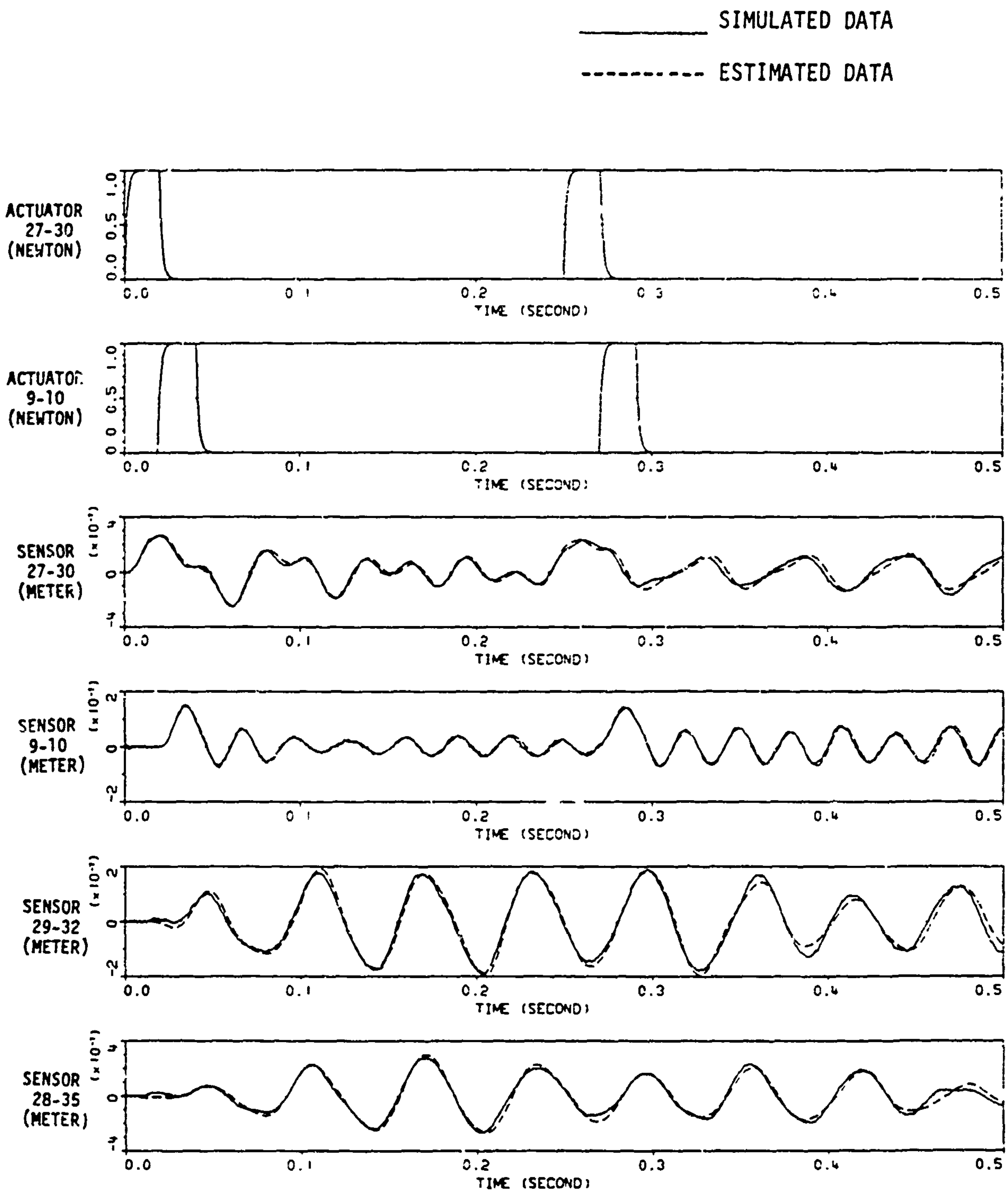

Figure 3-16. Comparisons Of Simulated Measurements With Measurements Predicted by 30-Mode Model After Estimation of Modes 41-58.

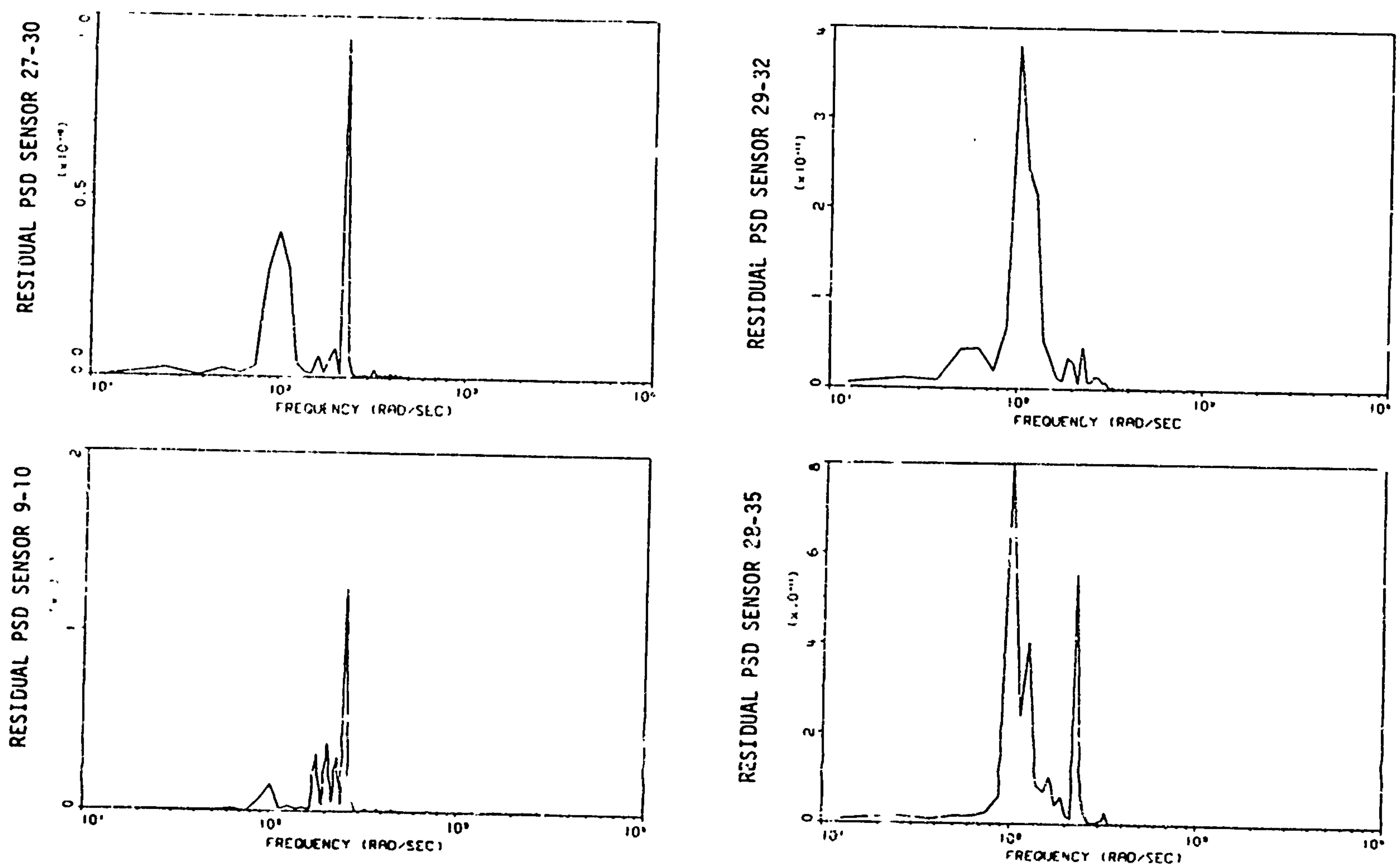

Figure 3-17. Residual Power Spectral Density Functions After Estimation of Modes 41 and 58.

Table 3-6. Summary of Results on Estimating Modal Parameters

PARAMETER		NOMINAL VALUES	EST. MODE 41	EST. MODE 58	TRUE VALUES
MODE 41	ω_{41}	103.83	109.7	-	108.0
	$b_{41,1};c_{1,41}$	.0184	.0215	-	.0272
	$c_{3,41}$	-.0167	-.0239	-	-.0257
	$c_{4,41}$	-.0216	-.0272	-	-.0308
MODE 58	ω_{58}	211.43	-	215.7	215.58
	$b_{58,1};c_{1,58}$	.0498	-	.0466	.0486
	$c_{3,58}$	.0069	-	.0091	.0086
	$c_{4,58}$	.0141	-	.0044	.0080

3.7 SYSTEM DESIGN CRITERIA

The operations for proposed on-orbit parameter identification are: collecting LSS data on-orbit, transmitting data to ground, and estimating data on-ground. Since estimations are done on-ground, there will be only moderate software/hardware requirements for the spacecraft. The areas pertaining to system design are in control system interfacing, actuator/sensor placements, actuator/sensor dynamics and data gathering and handling:

- Identification Phase

  It should be determined whether input-output data obtained from LSS normal maneuvers are sufficient for parameter identification. If identification should be included as a phase of LSS operations, it should be decided that the control loop be open, closed, or closed with reduced gain.

- Actuator/Sensor Placement

  Check whether the number of actuators/sensors for control system are sufficient for parameter identification. If not, where and what type of additional actuators/sensors should be placed.

- Actuator/Sensor Bandwidth

  Actuator/sensor bandwidth is preferred to be much higher than the important mode frequencies. If bandwidth and mode frequencies are in the same order of magnitude, the actuator/sensor transfer functions should be known to high degrees of accuracies. Sensor noise level should be known within an order of magnitude.

- Input Signal

  Input signals should be "sufficiently rich" (e.g., high Det(H) value) and still within safety constraint.

- Data Handling

  Tradeoffs between data length and estimation accuracies should be studied. Other topics such as the quantization level, sampling rate, data storage space, and synchronization among the signals of actuators and sensors should also be determined.

3.8 CONCLUSIONS

The maximum likelihood method presented in this section has shown significant promise for estimating LSS parameters from input-output measurement data obtained on-orbit. Simulation studies were conducted for both physical parameter and modal parameter estimation. Excellent results for estimating physical parameters were obtained. Significant improvements on nominal modal data were also achieved by estimating the modal parameters directly. Modal parameters require a relatively simple algorithm for estimation, but they are large in number and become "over-parameterized" easily. On the other hand, the physical parameters are usually small in number, but the identification algorithm (which involves finite element modeling) is more complicated.

Another important subject studied was the effects of measurement data length. The accuracies of estimated parameters can be improved by using longer data measurements. But it is known in theory, and is also observed in the simulation tests (RUNS 11, 12, and 13), that for longer data, the initial parameter estimates have to be closer to their true values in order for the maximum likelihood estimator to converge.

4.0 COMPARISON OF DIRECT ADAPTIVE CONTROL WITH FIXED GAIN CONTROL

The study of direct adaptive control is motivated by its ability to account for system changes and modelling errors. These errors arise in LSS control through modelling inaccuracies, component failures, depletion of consumables, changes in the working environment (e.g., thermal), and through reorientation of possibly large articulated payloads. In most cases, the on-orbit identification procedure described in Section 3 can be combined with standard, fixed gain, control techniques* to solve these problems. Direct adaptive controls may provide, however, an on-board autonomous alternative which, under some circumstances (e.g., extended periods of no communication with ground links), is more desirable.

In this section direct adaptive control will be compared with two fixed-gain control approaches. Positivity constrained, direct adaptive control theory will be summarized first. Then fixed-gain control, direct adaptive controls and identification followed by fixed-gain control will be compared. The approach will be to use the Draper Tetrahedron as representative of a large space structure; design a control system for each type of control such that equivalent performance under nominal conditions is obtained; make performance comparisons using a perturbed model.

4.1 POSITIVITY CONSTRAINED ADAPTIVE CONTROL THEORY

This section will outline the theory behind positivity constrained adaptive control. First, the required extension of the positivity theorem used in Chapter 2 will be described. Second, since digital control will be the rule rather than the exception in future applications, the discrete time analogs to the concepts used in Chapter 2 will be summarized. Third, it will be shown how the adaptive control used here evolves naturally from well established principles. Finally, it will be shown how the adaptive controller is mechanized so that it can be implemented with current microprocessor technology.

---

* This design approach is generally termed "indirect" adaptive control.

4.1.1 Positivity Theory For Non-Linear Systems

The adaptive controls to be considered here are highly nonlinear and time-varying and therefore require a more generalized approach to establish stability. As alluded to in Chapter 2, positivity* is a general concept not limited to linear time-invariant systems, and is therefore very able of treating the problem here.

The following definitions will be required to state the general positivity theorem:

Definition 1: Truncated Function:

$$f_T(t) = \begin{cases} f(t), & 0 \le t \le T \\ 0 & , t > T \end{cases}$$

Definition 2: Extended Hilbert Space $\mathcal{H}_e$: The space of all functions f(t) such that $f_T(t)$ belongs to the Hilbert space $\mathcal{H}$, i.e.,

$$f \ \varepsilon \mathcal{H}_e \Rightarrow f_T \ \varepsilon \mathcal{H}$$

Definition 3: Positive operator: An operator with a domain and range in an extended Hilbert space $\mathcal{H}_e$ is positive/strictly positive if for $f \varepsilon \mathcal{H}_e$,

$$\langle f_T, Hf_T \rangle \ge 0 \quad (>0)$$

Positive operators are useful because they have the following properties:

1) The inverse of a positive operator is positive.

2) The sum of positive operators is positive.

3) Positivity Theorem [1, 12]: The negative feedback systems shown in Figures 3-1a and 3-1b are bounded-input-bounded

* Recently Willems [9,10] and others [11] have made further extensions to the theory by using the more general concept of energy dissipation.

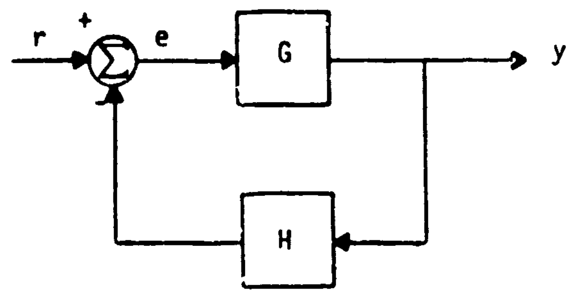

Figure 4.1a   Negative-Feedback System

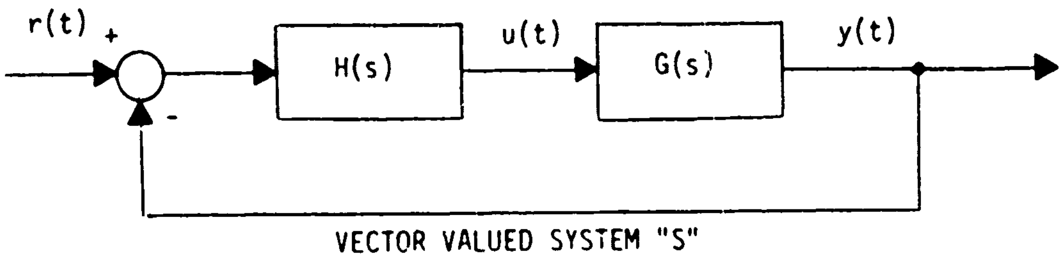

Figure 4.1b   Unity Negative-Feedback System

output stable for all inputs in $\mathcal{H}_e$ if both G and H are positive operators and at least one of them is also strictly positive.

Like the positivity theorem in Section 2, the advantage of this test is that it permits one to infer closed-loop stability from the individual properties of the controller and plant. Also, like in Chapter 2, when the theorem cannot be applied directly, the same embedding techniques discussed earlier can be used to establish stability.

Finally, we note in passing, that the term "Positive Real" refers to a positive operator that is also linear time-invariant, and, the term "Hyperstability" refers to the positivity theorem when at least one of the subsystems G or H is positive real, while the other may be nonlinear and/or time-varying.

4.1.2 Modifications Imposed By Digital Positivity Designs

Any control system to be considered for LSS control will likely be digital. This is particularly true for adaptive control designs where, because of the algorithmic complexity, the cost and flexibility advantages offered by microprocessors are prevalent. The controller comparisons made here, therefore assume digital adaptive and fixed-gain controls.

The generality offered by positivity theory permits stability assurance of digital designs without additional technical difficulties.* For example, Anderson's discrete time analog to the continuous time domain positivity test is:

Let A, B, C, D be a minimal realization of G (z). i.e., define

$$G(z) = D + C\,(z\,I-A)^{-1}\,B$$

* The inner product $\langle f_{T_o}, H f_{T_o} \rangle$ merely changes from $\int_0^{T_o} f^*(t) \cdot [Hf(t)]\,dt$ to $\sum_{i=0}^{n} f^*(iT)\,[Hf(iT)]$ where $nT=To$.

where

$$X_{n+i} = A \quad X_n + BU_n$$

$$Y_n \quad = C \quad X_n + DU_n$$

then G(z) is positive real if and only if there exists a symmmetric L and W such that

i) $A^T PA - P = -LL^T$

ii) $A^T PB = C^T - LW$

iii) $W^T W = D + D^T - B^T PB$

Similarly, the analogous frequency domain positivity index for sampled data systems is:

$$\delta(\omega) = \lambda_{min} \left\{ \frac{1}{2} [G(z) + G^*(z)] \right\} , \; z = e^{j\omega T}, \; \omega \varepsilon [o, 2\pi)$$

where

$\delta(\omega)$ is always >0 implies G(z) is strictly positive real

$\delta(\omega)$ is always $\geq$0 implies G(z) is positive real

$\delta(\omega)$ can be $\leq$0 implies G(z) is not positive.

The stability of sampled data systems is therefore handled by using the stated definitions in the positivity theorem. Design, including embedding, is handled with methods directly analogous to the methods of Chapter 2.

Unlike in the continuous case, discrete time systems almost always require embedding. This occurs because sampling plus the zero-order-hold introduces sufficient phase lag to destroy positivity, even when ideal actuators and rate sensors are assumed. It is noteworthy, however, that once embedded, aliasing does not affect stability as long as the system is

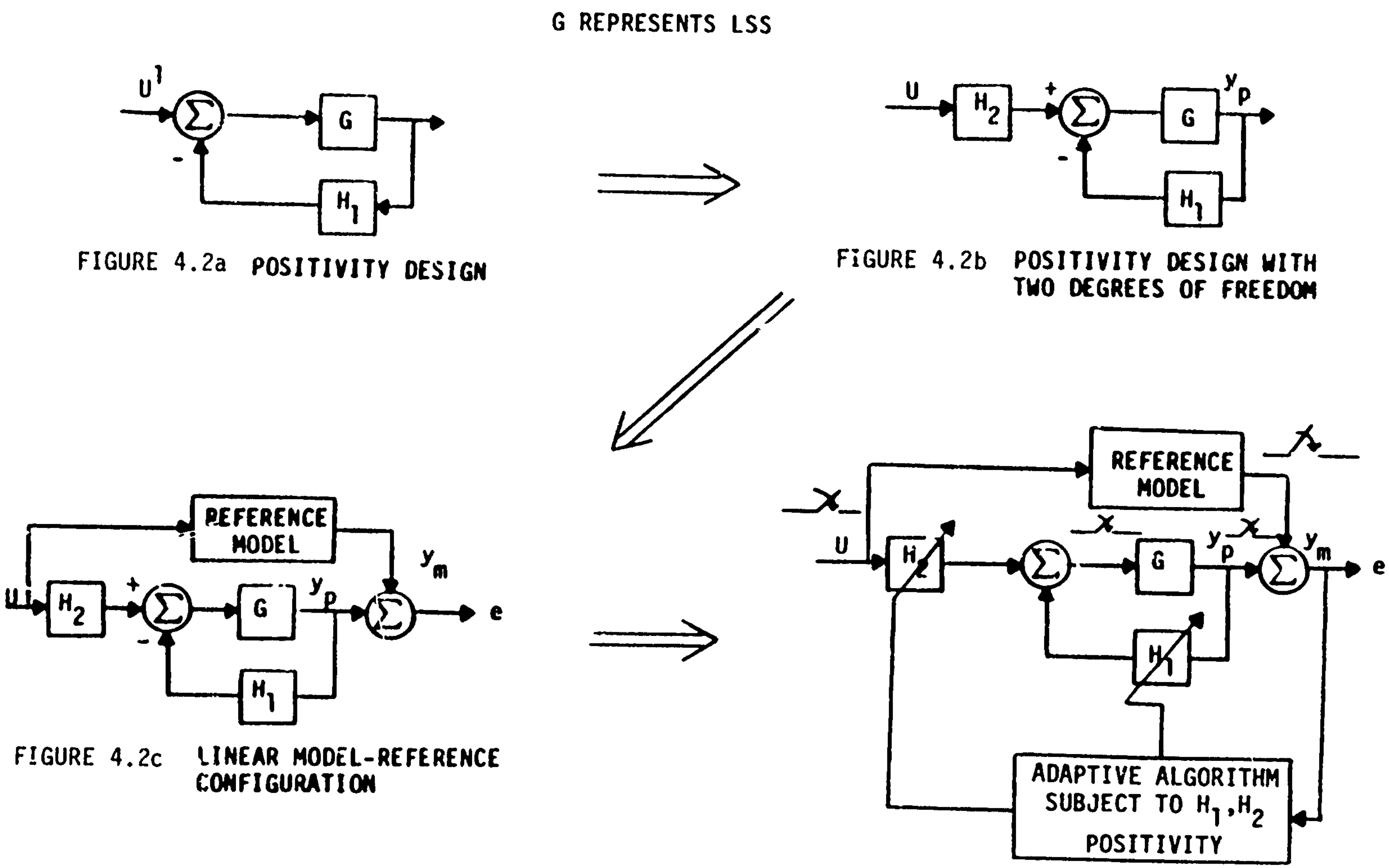

FIGURE 4.2a POSITIVITY DESIGN

FIGURE 4.2b POSITIVITY DESIGN WITH TWO DEGREES OF FREEDOM

FIGURE 4.2c LINEAR MODEL-REFERENCE CONFIGURATION

FIGURE 4.2d POSITIVITY CONSTRAINED MODEL REFERENCE ADAPTIVE CONTROL (MRAC)

Figure 4.2 Evolution of Positivity Design To Positivity Constrained Adaptive Control

observable and controllable.

4.1.3 Evolution of Positivity Design To Positivity Constrained Adaptive Control

The outgrowth of the adaptive design from the positive design is straightforward. Figures 2.2a-d show the evolution by using the positivity theorem and established linear model reference control principles.

Figure 4.2a shows the standard feedback connection of two s .s G and H_1. G is assumed to be the LSS and H_1 is assumed to be the oller. From positivity theory, we know that if G and H_1 are (strictly) positive, then the closed loop system is stable*.

In Figure 4.2b, an H_2 pre-filter is appended. It is well known that this so called "two-degree-of-freedom structure" is the most general feeback controls configuration available and that all other control configurations can be equivalenced to it with the proper choice of H_1 and H_2 [13]. Note, the stability of this system is guaranteed if H_2 is stable and G and H_1 satisfy the positivity theorem conditions.

Figure 4.2c adds a parallel reference model to the two-degree-of freedom structure. It is known that if G and the reference model are linear and pre-specified,** operators H_1 and H_2 exist which will make the error e identically zero [14]. Note that the reference model does not affect stability and in fact has no function other than to specify the desired behavior.

In practice, G is highly uncertain and of unknown order, so H_1 and H_2 cannot be pre-specified such that e is zero (or even at a minimum). Suppose H_1 and H_2 are continuously chosen to minimize e but subject to

* It is understood that if G is not positive, then embedding is used.

** G must be of known order and minimum phase

positivity conditions based on a priori knowledge (albeit, crudely) of G. In this case, performance could be improved on-line without sacrificing the GH_1 - loop stability.* The idea expressed is graphically shown in Figure 4.2d and will be called positivity constrained adaptive control. Note that because of the generality of the concepts used, the system can be continuous or digital.

4.1.4 Adaptive Controller Mechanization

The general structure for the positivity constrained controller has been shown in Figure 4-2d. The actual mechanization of the positivity constraints and the adaptive control algorithm will now be described and the implied computational requirements summarized.

Testing The Positivity Of The Compensators H_1 and H_2 One of the reasons for using adaptive control is that the LSS dynamics, G, is uncertain and possibly time-varying. Therefore, the compensators H_1 and H_2 (referring to Figure 4.2d) are subject to change on-orbit and the adaptive algorithm must include checking the positivity of H_1 and H_2 to assure stability. This, in general can be done using one of Anderson's positivity tests. However, it would be a very complex task and could hardly be performed on-line in real time, unless the configurations of H_1 and H_2 are somehow restricted. The idea here is to let the compensators be diagonal. The H^{ii} element can then be put in the form**

$$H^{ii}(D) = \sum_{j}^{\ell_c} \frac{a_{ij} D + b_{ij}}{D^2+2\zeta_{ij}\omega_{ij} D + \omega_{ij}^2} + \sum_{j}^{\ell_d} \frac{c_{ij}}{D+d_{ij}} + K_{ii}$$

That is, each diagonal element of the compensators consist of a parallel bank of filters and a frequency independent gain K_{ii}. Since the sum of positive operators is positive, then if each of the terms (parallel filters) in H^{ii} is strictly positive, then H^{ii} is strictly positive and so is H.

* Guarantee of a bounded parameter update sequence is required to establish adaptive loop stability.

** D is the derivative operator. For digital systems, replace D by the delay operator Z.

Checking the positivity of H^{ii} is now straightforward, requiring, in the continuous case, that each second order section

$$\frac{a_1 D + a_2}{D^2 + b_1 D + b_2}\ .$$

be constrained by

i) $a_1,\ a_2,\ b_1,\ b_2 > 0$

ii) $a_1 b_1 > a_2$

Analogously, in the discrete time case, each second order section

$$\frac{a_1 Z^2 + a_2 Z + a_3}{b_1 Z^2 + b_2 Z + b_3}$$

is constrained by

i) $C_1 Z^2 + C_2 Z + C_3$ has two roots inside the unit circle.

ii) $D_1 Z^4 + D_2 Z^3 + D_3 Z^2 + D_2 Z + D_1$ has two roots inside the unit circle

where

$$C_1 = a_1 + b_1$$

$$C_2 = a_2 + b_2$$

$$C_3 = a_3 + b_3$$

$$D_1 = (1/2)\,(a_3 b_1 + a_1 b_3)$$

$$D_2 = (1/2)(a_1 b_2 + a_2 b_3 + a_2 b_1 + a_3 b_2)$$

$$D_3 = a_1 b_1 + a_2 b_3 + a_3 b_3$$

<u>The Adaptive Control (Tuning) Mechanism</u> The objective of the tuning mechanism is to have the plant behave like the reference model. It is clear, however, because the positivity constraints preserve the GH_1 loop stability, that one is free to choose the tuning law as long as it generates bounded gains.

The general form of the tuning mechanism resembles the generalized-steepest descent rule:

Change in gain = $-\lambda \cdot S \cdot G_R$

where

$\lambda \overset{\Delta}{=}$ learning gain (possibly time-varying but always greater than zero)

$S \overset{\Delta}{=}$ positive definite normalization factor (possibly time varying).

$G_R \overset{\Delta}{=}$ gradient related direction

One may choose these variables, for example, based on least squares [15], gradient methods [16], or correlation/correlation-with-delay [17]. We prefer the cross correlation law because it has previously been shown to have some very desirable convergence [18] and stability properties [19]: it can be shown to generate a bounded sequence when a positive real reference model is used* [22]; and it is recursive and is easily computed on-line in real time.

The signal G_R in the cross-correlation law is computed as

$$\int_0^t [I_1 \otimes e^T] \frac{\partial \varepsilon}{\partial \alpha} [I_2 \otimes S] \, d\tau$$

where:

$\alpha = [\alpha_{ij}]$ is $m \times \ell$ matrix of adaptive gains.

e is the plant-model error vector, $r \times 1$

S is the vector of signals entering/controlled-by adaptive gains

* We can show this even for a mismatch between the order of the reference model and the plant and with insufficient control degrees of freedom. Also we conjecture that the requirement for a positive real reference model can be eliminated via embedding.

$\frac{\partial \mathcal{U}}{\partial \mathcal{A}}$ is the $m^2 \times \ell^2$ matrix of $m \times \ell$ partions $\left\{\frac{\partial \mathcal{A}}{\partial \alpha_{ij}}\right\}$

I_1 is the identity matrix of order r, the length of e

I_2 is the identity matrix of order m, the column dimension of $\mathcal{A}$.

$\otimes$ is the outer (or Kronecker) product.

The outer product of a ℓxm matrix M with a pxq matrix N is defined as the ℓp x mq matrix consisting of ℓxm partitions $m_{ij}N$.

e.g.,

$$\begin{bmatrix} 1 & 2 \\ 3 & 5 \end{bmatrix} \otimes [7 \ 11] = \left[\begin{array}{cc|cc} 1\cdot 7 & 1\cdot 11 & 2\cdot 7 & 2\cdot 11 \\ 3\cdot 7 & 3\cdot 11 & 5\cdot 7 & 5\cdot 11 \end{array}\right]$$

$$= \left[\begin{array}{cc|cc} 7 & 11 & 14 & 22 \\ 21 & 33 & 35 & 55 \end{array}\right]_{2\times 4}$$

Note that in general the outer product generates a matrix of matrices. This occurs because one is generally minimizing a vector of error signals and there is a matrix of parameters with which one could conceivably adapt (one parameter vector for each element of the transfer function matrix). Considerable simplification results, however, if one permits no coupling and a priori selects the order of the numerator and denominator dynamics of each element of the transfer matrix. The resulting G_R in this case, extremely sparse.

Parameterization Of The Adaptive Compensators Figure 4.3 has a more detailed block diagram of the adaptive design. The precompensator and feedback compensator are factored into two operators, the basis transfer matrix and the gain matrix. The first contains all the derivative/or delay dynamics. The latter contains only the adaptive gains. The realization is possible as any linear finite order differential (delay) operator H that is controllable can be put in the form [20]

$$H = N P^{-1}$$

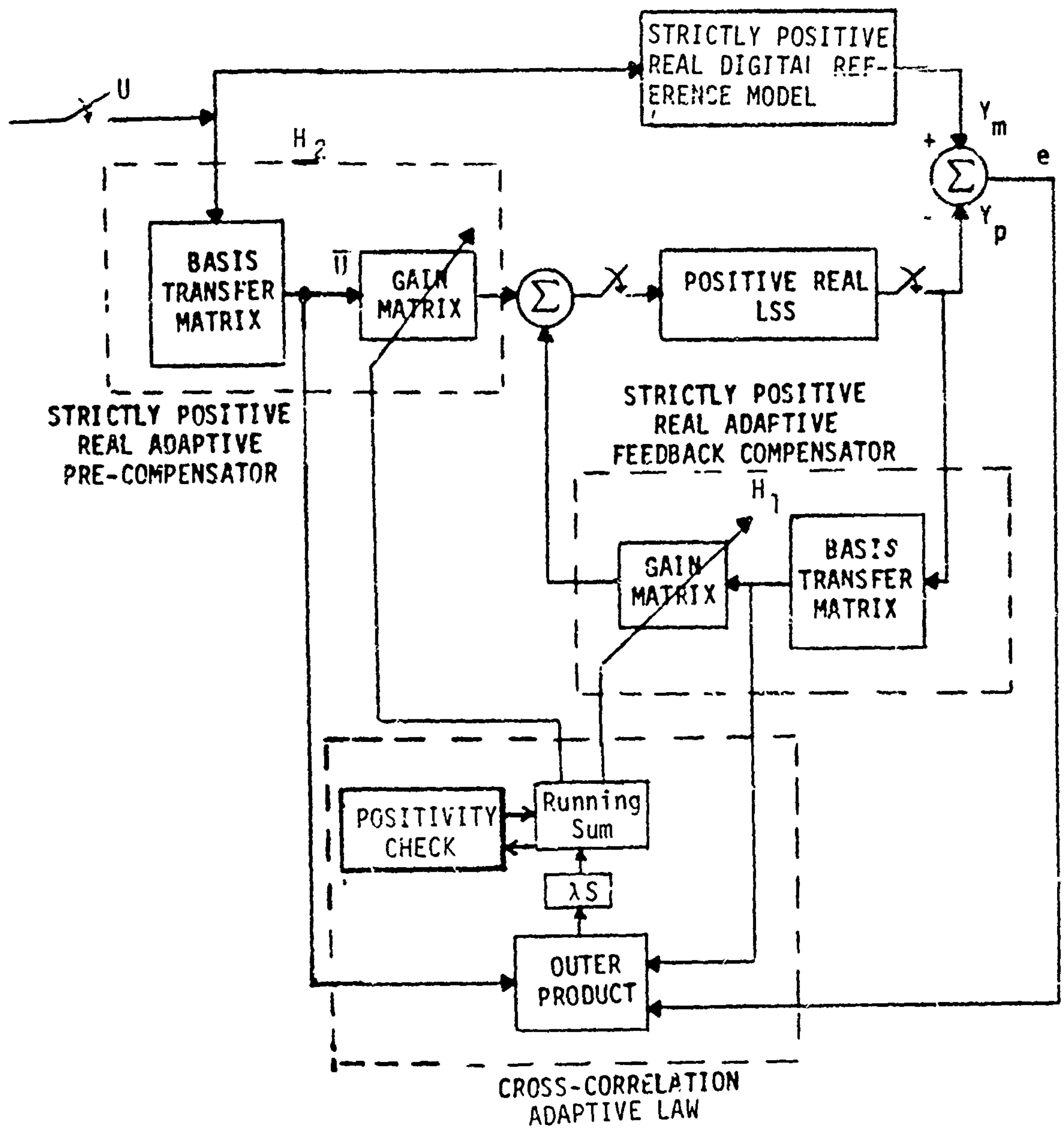

Figure 4.3. Positivity Constrained MRAC Configuration

Where N and P are matrices whose elements are polynomial functions of the derivative (delay) operator D. Our adaptive controller will vary only the compensator zeros; hence, N contains all the adaptive gains and P is fixed. N can be now factored into the form $\alpha \cdot \hat{N}$ where α contains only the adaptive gains and $\hat{N}$ contains only time invariant operators.

Example:

$$N = \begin{bmatrix} \alpha_1 D + \alpha_2 & 0 \\ \alpha_3 D^2 & \alpha_4 D + \alpha_5 \end{bmatrix} = \begin{bmatrix} 0 & \alpha_1 & \alpha_2 & 0 & 0 \\ \alpha_3 & 0 & 0 & \alpha_4 & \alpha_5 \end{bmatrix} \begin{bmatrix} D^2 & 0 \\ D & 0 \\ 1 & 0 \\ 0 & D \\ 0 & 1 \end{bmatrix}$$

Hence if $\hat{N}$ and P^{-1} are combined into one operator (what we call the basis transfer matrix) all the adaptive gains are left in one gain matrix. Note that if H is proper, derivative operations need not be performed.

On-Line Computational Requirements Despite the complex looking system topology shown in Figure 4-3, the computational requirements for digital LSS control applications are modest. Specifically, if one allocates one microprocessor to each physical control station, it can be shown that

1) The decentralized n^{th} order digital reference modes requires

2n	-	multiplies
2n	-	adds
4n+2	-	storage locations

2) The adaptive law with the basis in H_2 equal to the identity, adaptive diagonal forward gains, and adaptive diagonal rate output gains requires

9 - multiplies
1 - divide
25 - storage locations

3) The adaptive law for r 2^{nd}-order digital filters (either in H_1 or H_2) requires

1 + 11r - multiples
1 - divide

1 + 7r - adds

7 + 19r - storage locations

4) The positivity test for each 2^{nd} - order digital filter section requires

30 - multiplies
3 - divides
18 - adds
73 - storage locations

EXAMPLE: Assume the reference model is 6th order, the forward gains and rate feedback gains are adaptive, the dynamic feedback is an adaptive 6th order filter (three second order filter), and the maximum acceptable computational time delay is 3 msec. The computational requirements per control cycle are:

145 - Multiplies
11 - Divides
95 - Adds
664 - Storage locations (safety factor of two)

If one further assumes that (timewise)

1 multiply operation = 3 add operations

and

1 divide operation = 3 multiply operations, then the microprocessor must be capable of performing multiplication in about 14 μsec. This is well within the present state-of-the-art.

4.2 DESIGN COMPARISONS USING THE DRAPER TETRAHEDRON

This section will use the Draper Tetrahedral Truss to compare fixed gain controls with direct adaptive controls and with identification followed by fixed gain controls (indirect adaptive control). First the example structure will be described; then, design and simulation results for each approach will be summarized; finally, a comparison of computational and hardware requirements will be made.

4.2.1 Description of Draper Tetrahedron

The Tetrahedral Truss, shown in Figure 4-4, has been selected as a test example for comparing the various design approaches. This structure was devised by Draper Labs [21] as one of the simplest non-planar geometries capable of representing a large space structure. Despite its apparent simplicity, it models the feed-tower in a generic class of large antenna applications. The tetrahedral apex represents the antenna feed, members 1-6 are part of the feed support structure, and bi-peds 7-8, 9-10 and 11-12 are supports/controls attached to an inertially stabilized (assumed) antenna dish. Because of the nature of the real problem, the motion of the feed (apex) must be controlled through actuators and sensors placed at the bi-peds, none can be placed at the feed. The latter constitutes the control problem ; i.e., control the feed precisely despite large modeling uncertainty and without resorting to direct measurement or control of its motion.

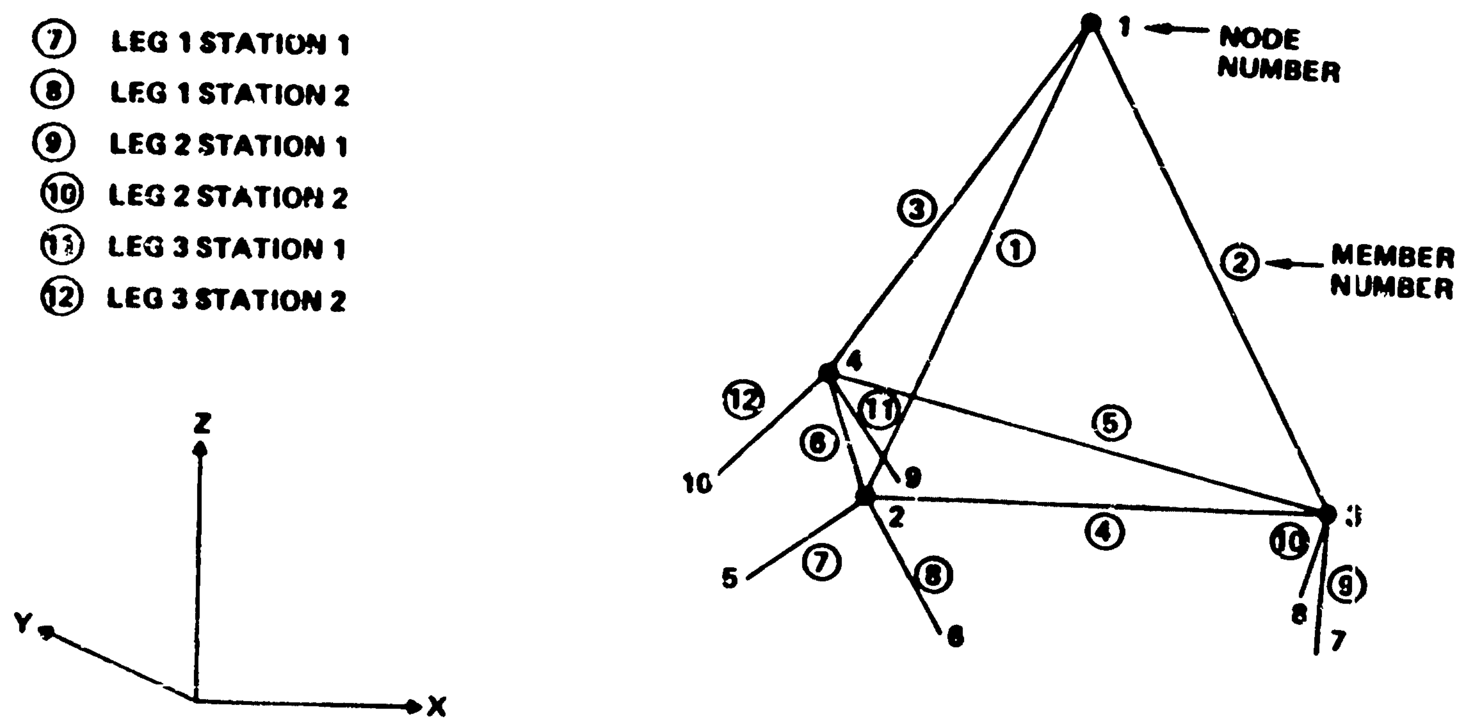

Figure 4.4 Draper Tetrahedral Truss

The finite element method was used to model the tetrahedron. Referring to Figure 4.4, the model contains ten nodes, each with three degrees of freedom, and twelve truss members. Node coordinates and element connectiveness for the "nominal" model are listed in Table 4.1. These elements are assumed to be capable of resisting axial forces only. The masses were assumed to be lumped at the nodes one through four.

Six co-located sensors/actuators were assumed to act as member dampers in parallel with members 7 through 12. The member dampers were assumed capable of sensing relative position and velocity and exerting force in the axial direction only.

The objective was to design a robust controller and evaluate the resulting controller on the full order nominal model. A second evaluation was then conducted using the true tetrahedral system parameters shown in Table 4.2. Both evaluations were based on the intial conditions given in Table 4.3. The goal was to damp the line-of-sight motion of Node 1 in the x and y directions to less than .0004 and .00025 units, respectively, in 20 seconds.

4.2.2 Digital Fixed Gain Control Of The Tetrahedron

A fixed gain control system for the tetrahedron will be designed first, to serve as representative of a standard control system design. The fixed gain control system design for the tetrahedron was conducted using the general frequency domain/positivity design procedure outlined in subsection 2.1.6. The exception was to use the digital controller design modification, outlined in subsection 4.1.2, so that comparisons with the digital adaptive design are fair.

The sampling rate was chosen to be .2 seconds. This rate is approximately three times faster than the rate required to reconstruct the highest controlled mode (.909 Hz). At this sample rate one can compute the positivity index of the plant, G_1 in either the Z-domain:

$$\nu(\cdot) = \lambda_{min}\left\{\frac{1}{2}\left[G(z) + G^*(z)\right]\right\}, \quad z=e^{j\omega T_{sample}}, \quad \omega\varepsilon[0,2\pi)$$

Table 4.1 Tetrahedron Structural Model Parameters (Nominal)

Node Point Locations

Node	X	Y	Z
1	0.0	0.0	10.165
2	-5.0	-2.887	2.0
3	5.0	-2.887	2.0
4	0.0	5.7735	2.0
5	-6.0	-1.1547	0.0
6	-4.0	-4.6188	0.0
7	4.0	-4.6188	0.0
8	6.0	-1.1547	0.0
9	2.0	5.7735	0.0
10	-2.0	5.7735	0.0

Restraints X,Y, & Z at nodes 5-10

Element Connectivities and Properties

Element	Node 1	Node 2	Area
1	1	2	1000.
2	1	3	100.
3	1	4	100.
4	2	3	1000.
5	3	4	1000.
6	2	4	1000.
7	2	5	100.
8	2	6	100.
9	3	7	100.
10	3	8	100.
11	4	9	100.
12	4	10	100.

Material E = 1.0

Lumped Masses

Node	Mass
1	2.0
2	2.0
3	2.0
4	2.0

Table 4.2 Tetrahedron Parameter Variation

Masses

Node	Mass
1	4.0

Element Property Changes

Element	Area
1	1200.0
2	150.0
3	150.0
4	1200.0
5	1200.0
6	1200.0
7	150.0
8	150.0
9	150.0
10	150.0
11	150.0
12	150.0

Table 4.3 Initial Conditions For Control Design Evaluations

Mode	Displacement (η)	Velocity ($\dot{\eta}$)
1	-.001	-.003
2	.006	.01
3	.001	.03
4	-.009	-.02
5	.008	.02
6	-.001	-.02
7	-.002	-.003
8	.002	.004
9	.0	.0
10	.0	.0
11	.0	.0
12	.0	.0

or in the W-domain*:

$$\delta(\omega) = \lambda_{min}\left\{ \frac{1}{2}[G(W) + G^*(W)] \right\}, \quad W\epsilon \; [0, j\infty)$$

The characteristic gains required in the frequency domain part of the design can similarly be computed in either the Z or W domain.

The decentralized controller resulting from a design in the W-domain was

$$H = I_{6x6} \cdot \left[11.492 + \frac{3.921162z - 3.9863812}{z^2 - 1.70921z + .846578} \right] \qquad \text{(CN)}$$

Figure 4.5a-f show the transient responses of the nominal and perturbed systems to the initial conditions given in Table 4.3 Figures 4.5a and d show that the residual modes are stable despite the use of the low order decentralized controller (CN). Figure 4.5b and e show that the nominal system meets design specification but that there is a small loss of performance using the perturbed model. Figures 4.5c and f show that actuator command forces are modest.

4.2.3 Digital Direct Adaptive Control Of The Tetrahedron. The next step is to design a direct adaptive controller so that one can compare this approach with the fixed-gain approach. The digital direct adaptive controller for the Tetrahedron was designed using the positivity constrained adaptive control theory outlined in Section 4.1. A design of this type is semi-automatic in the sense that once one chooses a reference model and controller configuration, the system seeks optimum** performance through self-adjustment. The design effort for the Tetrahedron was therefore spent on choosing a controller configuration which could be compared fairly with the fixed-gain

* $G(W) = G(z = \frac{1 + W}{1 - W})$

** If the plant were of finite order and the controller had sufficient degrees of freedom to make the model-plant error identically zero, the optimum reached is the same as in an absolutely cooperative game. Since our situation violates both these conditions, the game theoretic equilibrium the controller reaches must be investigated in future research.

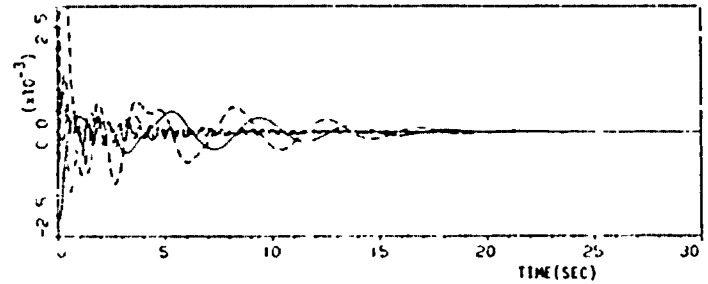

Figure 4.5a RESPONSE OF RESIDUAL MODES (NOMINAL SYSTEM)

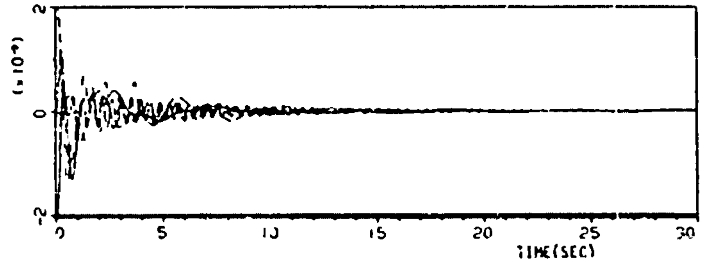

Figure 4.5d RESPONSE OF RESIDUAL MODES (PERTURBED SYSTEM)

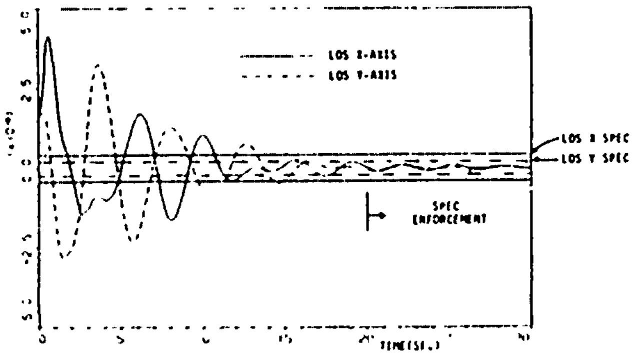

Figure 4.5b TRANSIENT RESPONSE OF NOMINAL SYSTEM TO INITIAL CONDITIONS

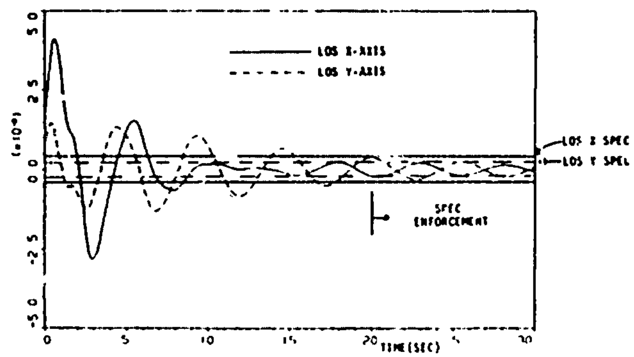

Figure 4.5e TRANSIENT RESPONSE OF PERTURBED SYSTEM TO INITIAL CONDITIONS

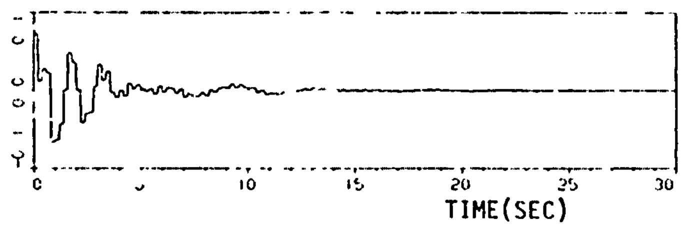

Figure 4.5c ACTUATOR FORCE AT LEG 1, STATION 1 (NOMINAL SYSTEM)

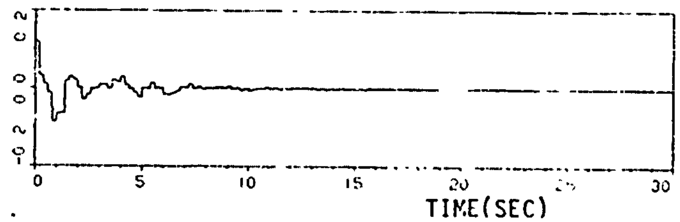

Figure 4.5f ACTUATOR FORCE AT LEG 1, STATION 1 (PERTURBED SYSTEM)

Figure 4.5 Transient Response Of Tetrahedron Using A Digital Fixed Gain Controller

Refering to Figure 4.6, the sample rate was chosen to be the same as was used in the fixed gain controller design, .2 seconds. The reference model picked uses the eight mode (number of controlled modes), nominal Tetrahedron model, but, with its damping augmented to reflect the effects of the nominal fixed-gain controller (NC) The adaptive decentralized feedback compensator was chosen to have exactly the same form as the controller (NC); i.e., has the same poles and only the numerator dynamics have been made adaptive. The adaptive precompensator consists of a diagonal gain matrix, to compensate for "averaged" mode shape uncertainty, and is only required during "servo" control.

Finally, the cross-correlation adaptive law used in the i^{TH} path (each of six control stations) is computed as

$$k_i(n+1) = k_i(n) - 10\, e^{-.02nT} \frac{e_i(n) \cdot [\text{Signal entering } k_i(n)]}{1 + NORM_i}$$

$$a_i(n+1) = a_i(n) - 10\, e^{-.02nT} \frac{e_i(n) \cdot [\text{Signal entering } a_i(n)]}{1 + NORM_i}$$

$$b_i(n+1) = b_i(n) - 10\, e^{-.02nT} \frac{e_i(n) \cdot [\text{Signal entering } b_i(n)]}{1 + NORM_i}$$

where

$$NORM_i(n) \triangleq [\text{Signal Entering } k_i(n)]^2 + [\text{Signal Entering } a_i(n)]^2 + [\text{Signal Entering } b_i(n)]^2$$

$$e_i(n) \triangleq \text{Plant output}_i(n) - \text{Desired output}_i(n)$$

Note, the exponentially decaying learning gains are used to reduce the effects of the non-matchable parts of the controlled plant and reference model.

Figure 4.6 shows a block diagram of the adaptive controller with the full order (12 mode) perturbed continuous dynamics of the Tetrahedron. The mode of operation is to have regularly scheduled "tuning" periods during which a training command is injected into the system and the adaptation loop is turned on. Normal operation follows with the adaptive loop turned off and the control gains remaining fixed at their last, converged value. This is

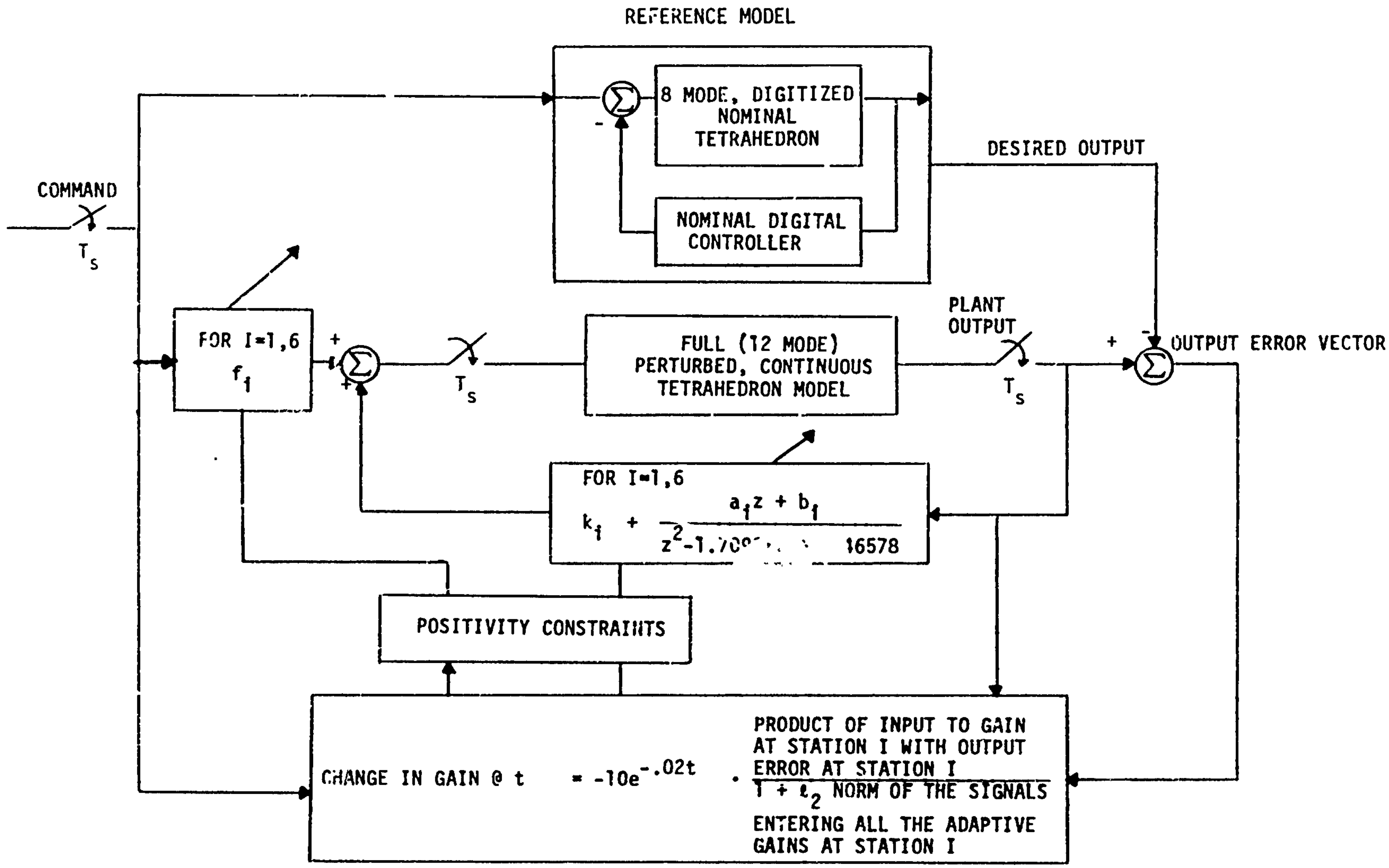

Figure 4.6 Block Diagram of the Direct Adaptive Controller With The Tetrahedral Truss

important from the viewpoint that the training signals required for adaptation can be annoying during a regulation mode. The proposed mode of operation would turn this signal on and off together with the adaptive loop.

Figures 4.7a-d show the time history of the various adaptive system signals during a "tuning" session, as simulated on a digital computer. Figure 4.7a shows the training signals input to stations 1 and 2 of leg 1. It is a periodic sequence consisting of 5 second pulses followed by a rest period of 17.5 seconds. The training system signals at the other legs were of similar periodicity but phased so that the apex was gyrated. Figure 4.7b shows the values/change in values* for the adaptive gains during this same period. The initial values for these gains were assumed to be at the nominal controller values (NC). Figures 4.7c and d compare the reference and "true" response of modes 1 and 5 during the training session. Mode 5 is shown to improve slightly but the effect on mode 1 is imperceptable. It can be shown that the reason for this poor state tracking of mode 1 is due to its poor observability/controllability from the tetrahedral legs. Indeed, analysis reveals that modes 1 and 2 contribute 25-50 db less power than other modes observable at the legs. Hence these modes remain "in-the-noise" with other unmodelled residual modes. This effect makes it difficult for the adaptation algorithm to extract any useful information from the output error signal. The net result presents a problem as the apex motion is dominated by these poorly observable modes.

Figure 4.8 shows the transient response of the perturbed system with the adaptive gain held fixed at the converged, post tunning session values. The adaptive control law performed well. But due to the fact that the modes that affect motion at the tetrahedron apex are poorly observable from the sensor measurements in the bi-ped legs, the adaptive law did not perform any better than the (very robust) fixed-gain law that it is being compared with. It should be noted, that the non-adaptive law, due to its robustness, was able to just about meet the 20 second settling specifications even when the perturbed structural model was used.

---

* Forward and rate feedback gains are measured relative to zero. Filter gains are measured relative to nominal filter gain values.

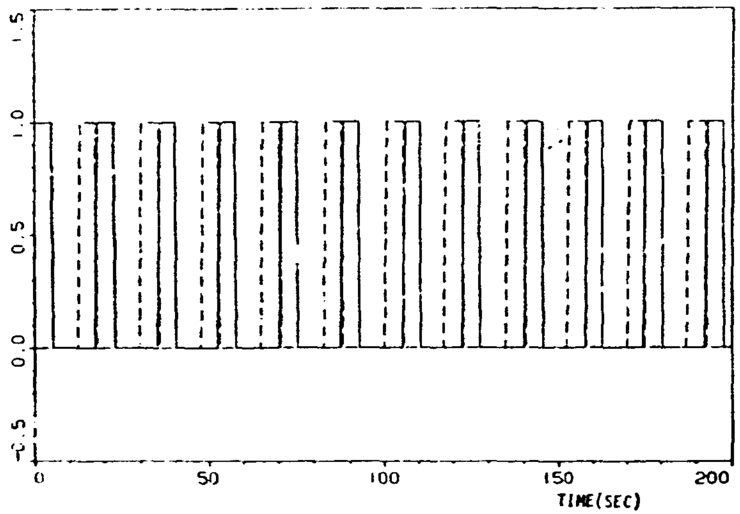

Figure 4.7a TUNING SIGNALS AT LEG 1

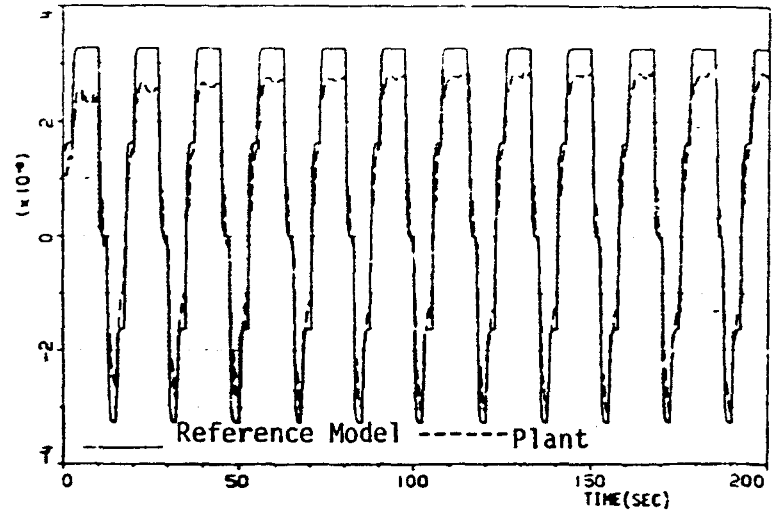

Figure 4.7c MODE 5 OF REFERENCE MODEL AND PLANT

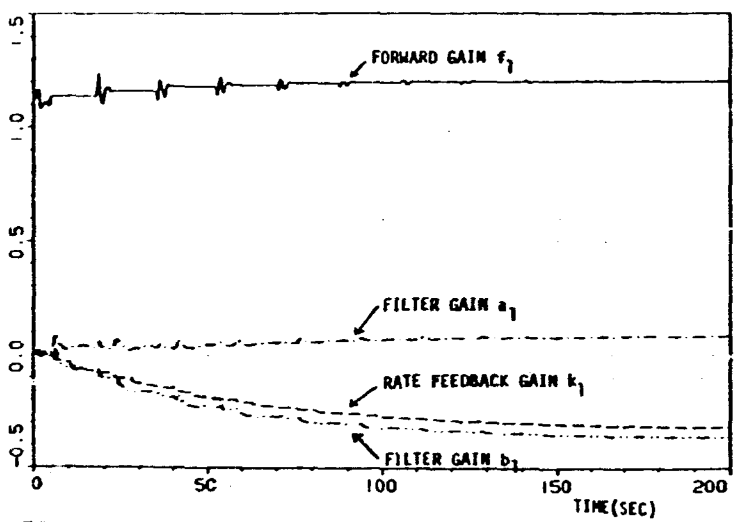

Figure 4.7b ADAPTIVE GAINS AT LEG 1 STATION 1

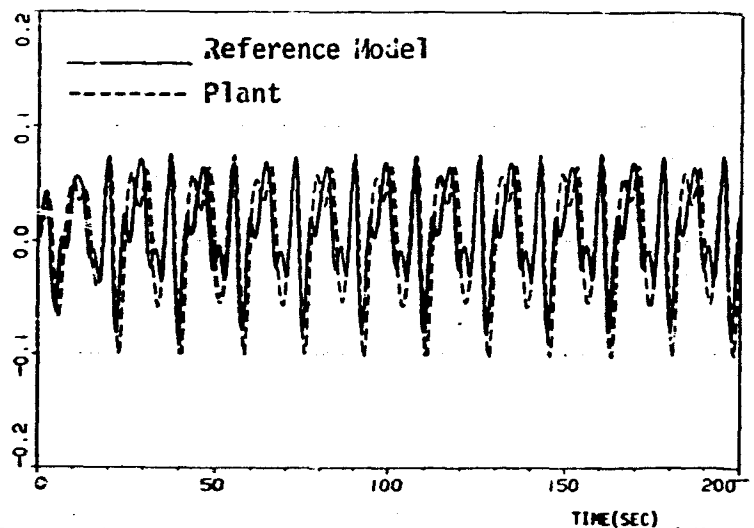

Figure 4.7d MODE 1 OF REFERENCE MODEL AND PLANT

Figure 4.7 Time History of Various Adaptive System Signals During "Tuning" Session

* Forward and rate feedback gains are measured relative to zero. Filter gains are measured relative to nominal filter gain values.

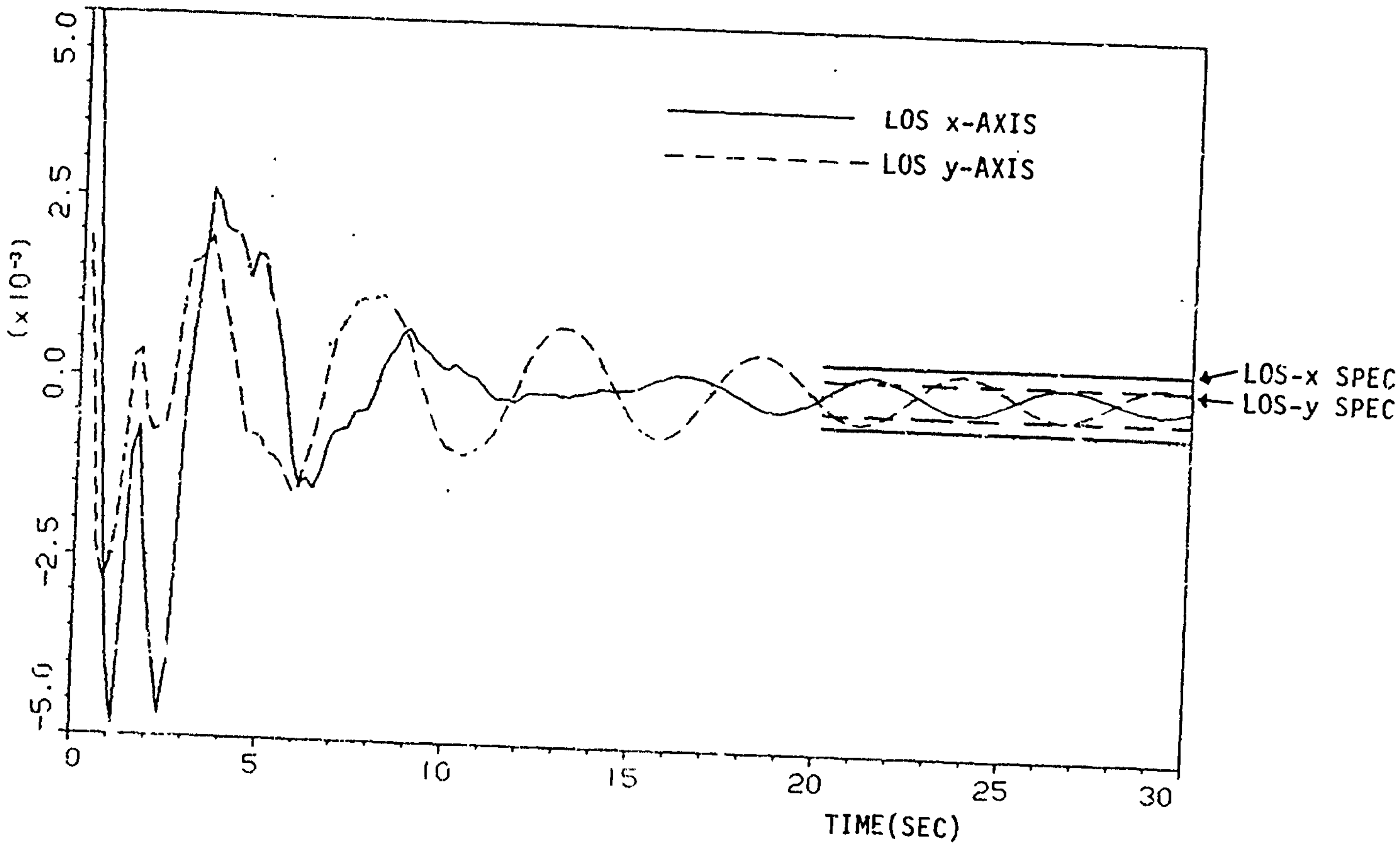

Figure 4.8 Transient Response of Perturbed Tetrahedron With Adaptive Gain Held Fixed at Final Post Tuning Session Values

Comparing these results with those from Section 4.2, it can be concluded that adaptive control is feasible and will work well for LSS, but that full advantage of its power can only be taken in situations where (i) the motion at the point(s) of interest on the structure is measurable (or can be estimated) in real time, and (ii) changes in the dynamic model of the structure are sufficiently drastic and occur in real time (e.g., on-orbit reorientation of articulated substructures), which would cause problems for fixed-gain controllers.

4.2.4 Identification of the Tetrahedron Followed By Fixed-Gain Digital Control [22].

After having designed and compared fixed-gain and adaptive controls, the third alternative, identification followed by fixed-gain control, will be designed and compared. The maximum likelihood identification approach described in Section 3 can be combined with the fixed-gain control technique outlined in Subsection 2.1.6 and 4.2.2 to design an indirect adaptive controller for the Tetrahedron. In the first part, system identification, a physically parameterized finite-dimensional state-space model is derived through the use of the finite element method. The parameters to be estimated are the cross-sectional area of all 12 tetrahedral truss members and the weight of the masses located at nodes 1 through 4. There are, therefore, 16 parameters to be estimated. Note that if modal frequencies and the corresponding mode shapes had been chosen to parameterize the system, the number of unknown parameters would be 56 for an 8 mode model, and 84 for a 12 mode model. Hence, by identifying physical parameters, one has, in fact, reduced the number of unknown parameters.

Figure 4.9 shows the input signals used to excite the structure and generate the data required by the maximum likelihood algorithm. The signals are pulses of magnitude 1 and last .25 seconds. Each pulse is staggered in time and is applied to the actuators located at the truss members identified in the figure. The rate sensor responses to these pulses, which are referred to as the Tetrahedral data, were simulated using the nominal model*, and, random noise was added (σ = .002). The perturbed" model parameters were then chosen as the initial parameter values used in the identification

* The role of the nominal and perturbed models were inadvertently reversed during the identification procedure. However, this does not impact the results to be presented.

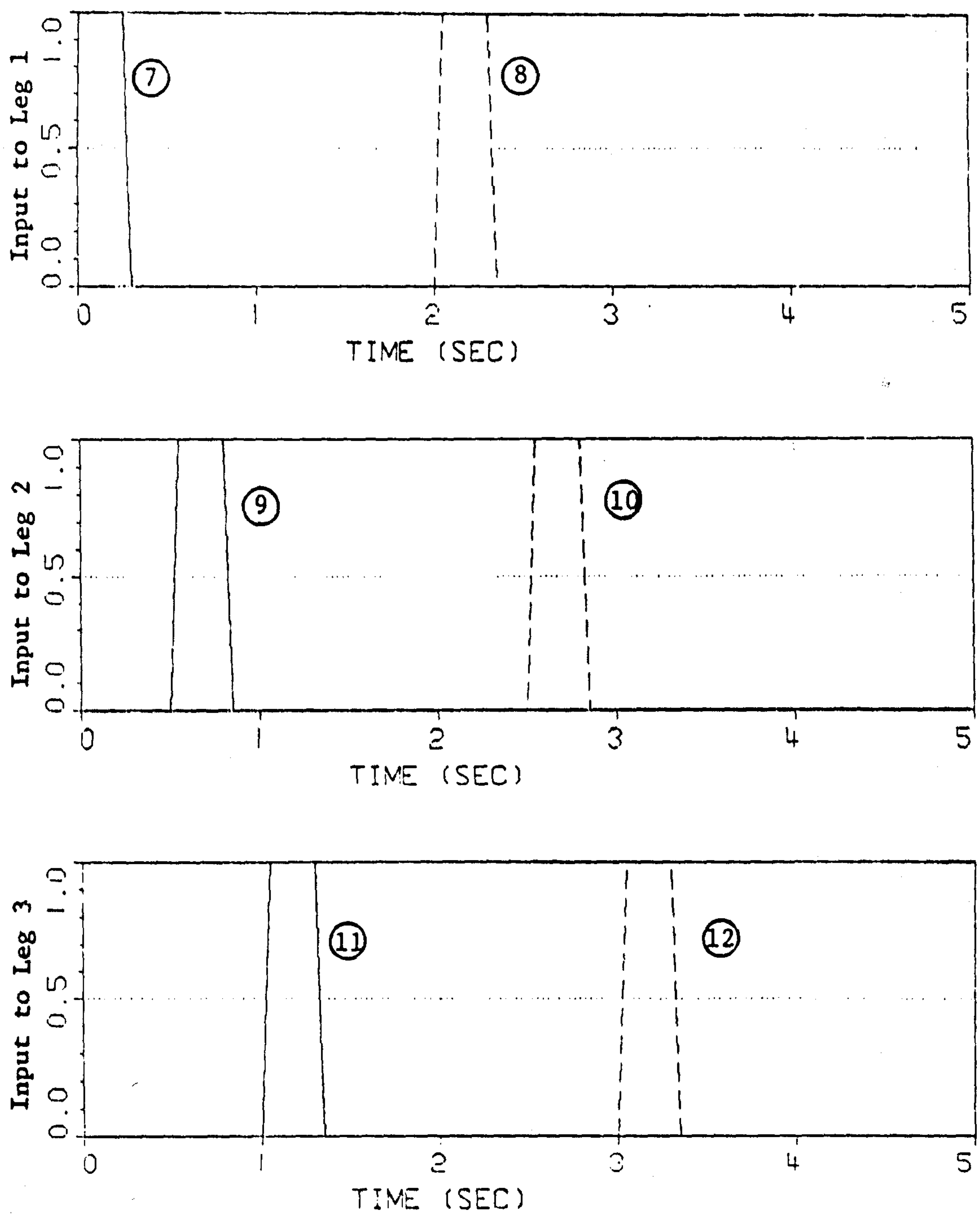

Figure 4.9 Input Signals Used To Exite Structure During Identification Procedure.

algorithm.

Table 4.4 shows the convergence of the parameter values in the Newton-Raphson iteration, using 5 seconds of data. All 16 parameters converged in 9 iterations and the final estimates are very close to the true parameter values.

Table 4.5 shows the equivalent modal quantities represented by the physical parameters in Table 4.4. These are obtained by finite element processing of each physical parameter set and demonstrate that indirect (i.e., via physical parameter estimation) modal parameter estimation is also excellent.

Figure 4.10 compares the time histories of the Tetrahedron data and the estimated data as obtained by using the final parameter estimates given in Table 4.4. It can be seen the fit is very good and it can be shown that the error consists primarily of measurement noise.

The second part of the indirect adaptive approach is control system design tune-ups. The feedback law tune-up was based on the W-domain fixed-gain design approach described earlier. In order to make comparisons with the direct adaptive design, however, the poles of the updated controller were fixed at the nominal controller values and only the numerator of the controller was updated (i.e., recomputed).*

The feedback law based on the final parameter estimates is:

$$H= I_{6x6} \cdot \left[14.3567 + \frac{6.96116z - 7.07695}{z^2-1.70921z+.846578}\right] \qquad \text{(NU)}$$

Note that only the numerator of (NC) was modified to create (NU).

Figure 4.17 shows the transient response of the perturbed Tetrahedron to the initial conditions given in Table 4.3. The traces show that all specifications are met by using the updated controller.

* Adaptive design theory permits adaptive "pole motion", but not simultaneously with "zero motion".

Table 4-4 Convergence of Physical Parameters In The Newton-Raphson Iteration.

Parameters			Initial Guess	Iterations				Final Estimate	True
			0	1	3	5	7	9	
1	Truss Member Cross-Section Area	a_1	1200	1177	1290	1230	1067	1005	1000
2		a_2	150	149	190	67	93	101	100
3		a_3	150	167	75	58	107	103	100
4		a_4	1200	1257	1103	1006	1017	1008	1000
5		a_5	1200	1056	1078	1135	1041	1030	1000
6		a_6	1200	1168	1138	1068	1061	999	1000
7		a_7	150	105	104	96	105	101	100
8		a_8	150	190	296	188	105	101	100
9		a_9	150	145	132	111	99	98	100
10		a_{10}	150	150	145	129	101	100	100
11		a_{11}	150	134	112	103	93	94	100
12		a_{12}	150	154	159	107	98	98	100
13	1/Mass	$1/m_1$	.250	.256	.293	.364	.441	.483	.500
14		$1/m_2$	.500	.476	.438	.453	.462	.483	.500
15		$1/m_3$	.500	.481	.420	.441	.508	.500	.500
16		$1/m_4$	.500	.474	.444	.485	.511	.515	.500

Table 4-5 Convergence of Equivalent Modal Parameters During The Newton-Raphson Iteration.

MODE FREQUENCIES* (Hz)	INITIAL	ITERATIONS				FINAL	True
	0	1	3	5	7	9	
ω_1	.186	.190	.168	.154	.201	.213	.214
ω_2	.233	.235	.241	.206	.251	.263	.265
ω_3	.471	.459	.460	.416	.447	.457	.460
ω_4	.566	.533	.495	.475	.473	.471	.471
ω_5	.612	.602	.598	.567	.530	.537	.541
ω_6	.819	.798	.784	.712	.666	.665	.669
ω_7	.903	.882	.818	.721	.743	.743	.742
ω_8	.908	.887	.839	.745	.755	.758	.757
ω_9	1.422	1.378	1.366	1.360	1.352	1.359	1.359
ω_{10}	1.639	1.609	1.510	1.458	1.472	1.472	1.472
ω_{11}	1.738	1.639	1.639	1.674	1.649	1.649	1.637
ω_{12}	2.222	2.155	2.039	2.044	2.050	2.054	2.054

* Mode frequencies were computed from estimated physical parameters.

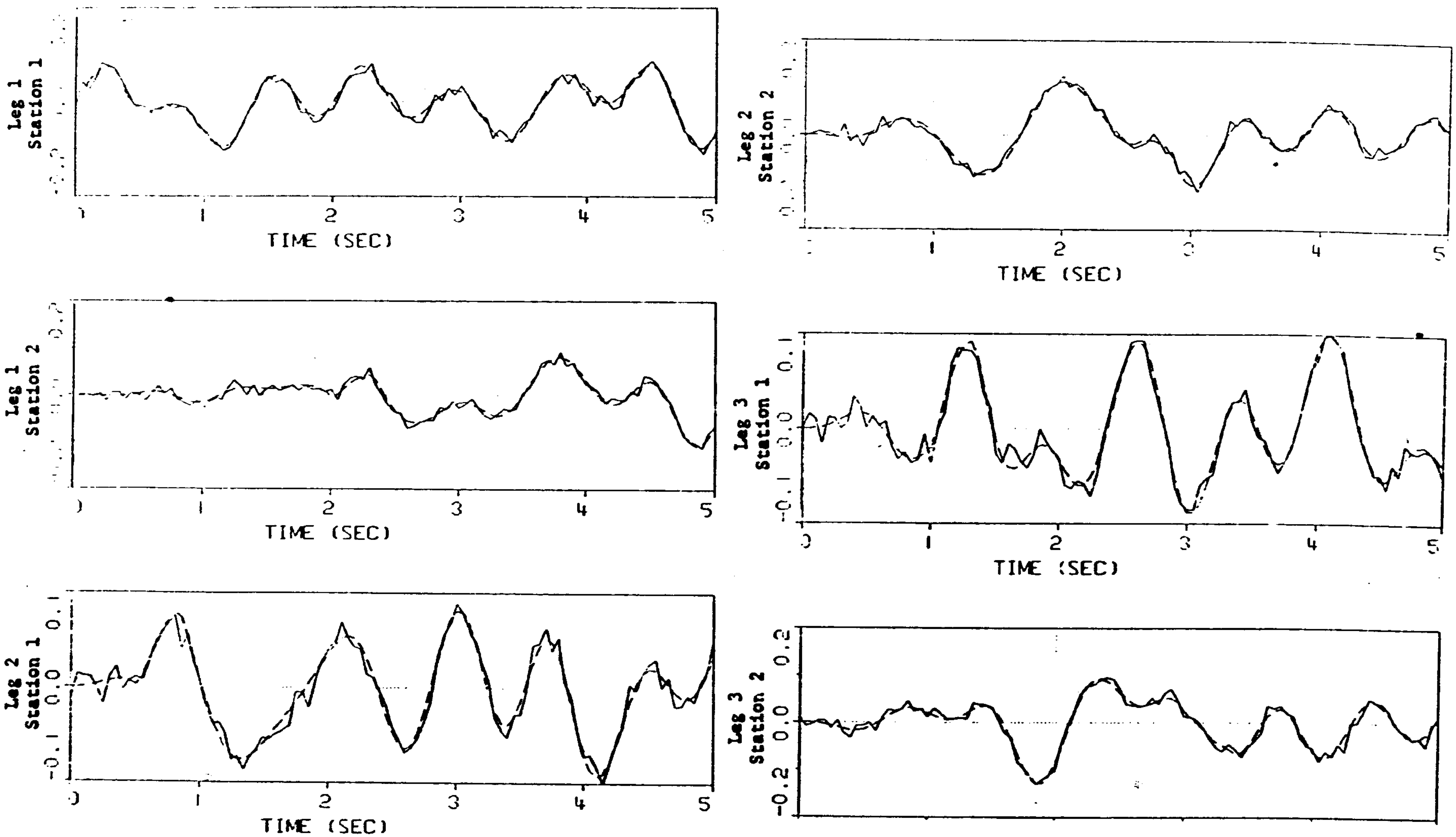

__________ Simulated Measurement Data

---------- Predicted Response Based On Updated Dynamic Model

Figure 4.10 Comparison of Time Histories Between Simulated Measurement Data and Predicted Dynamic Response.

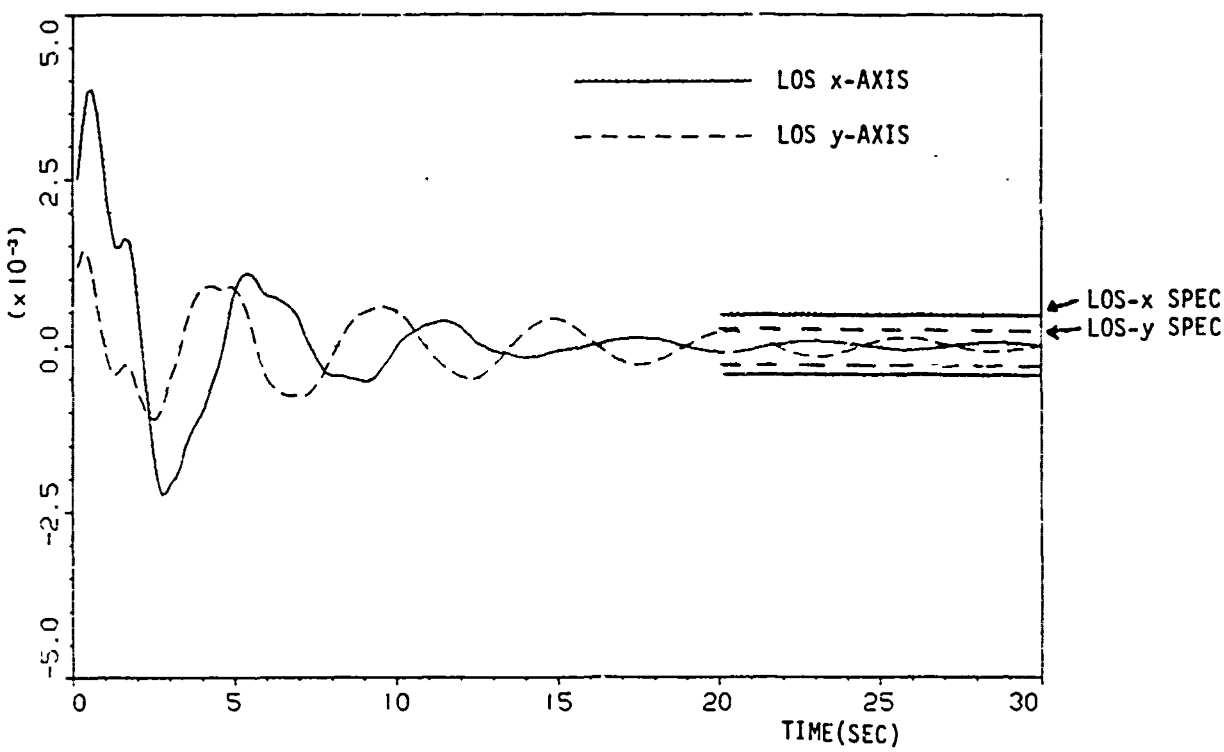

Figure 4.11 Transient Response of Perturbed Tetrahedron Using Post Identification Controller

4.2.5 Comparison Of Computational and Hardware Requirements For the Tetrahedron

Table 4.6 compares the computational and hardware requirements for the Tetrahedron. The table shows that the steady-state, on-orbit control computation requirements is the same for the three approaches studied. The difference occurs only during the training or learning session required when using the direct adaptive approach. During this period, the computational requirements increase to account for the adaptive control law and the on-line positivity tests that ensure stability. In terms of required on-orbit hardware, fixed-gain controllers are the simplest, and, depending on the acceptable computational delays, can be implemented using one microprocessor. Similarly, decentralized fixed-gain control may require only one microprocessor, but, a storage device must also be provided to store the input-output data required for the parameter identification processing to be done on the ground. The direct adaptive controller would require six microprocessors unless processors with 1-2 μsec multiply instruction cycles are used.

4.3 Conclusions and Recommendations

Chapter 4 has compared adaptive and non-adaptive controls. It has been shown that positivity theory can be used to ensure that either type is stable and that each type is realizable with current hardware. Fixed gain controllers were found to yield sub-optimal performance. It was uncovered, however, that direct adaptive controls do not significantly improve the fixed gain control performance if the controlled quantities are weakly observable/controllable from the "available" sensors and actuators. Indirect adaptive control, where one identifies physical parameters, can circumvent this difficulty if one accounts for the weak observability/controllability in the design phase and uses any other available information.

It is recommended that further studies be conducted in the following areas:

- Determine if the adaptive control reduced the bandwidths requirements over fixed-gain controllers.

Table 4-6 Comparison of Computational and Hardware Requirements For The Tetrahedron

	MEMORY* (SAFETY FACTOR OF 2)	ARITHMETIC OPERATIONS DURING CONTROL DELAY*			HARDWARE
		ADDS	MULTIPLIES	DIVIDES	
DECENTRALIZED FIXED GAIN CONTROLLER	36	3	5	-	1 MICROPROCESSOR WITH ON-BOARD LOCAL COMMUNICATION OR 6 MICROPROCESSORS
DECENTRALIZED ADAPTIVE CONTROLLER	WHILE LEARNING 316	42	58	5	6 MICROPROCESSORS
	AFTER LEARNING 36	3	5	-	
DECENTRALIZED FIXED GAIN CONTROLLER WITH PARAMETER I.D.	36	3	5	-	1) MICROPROCESSOR WITH ON-BOARD LOCAL COMMUNICATION OR 6 MICROPROCESSORS 2) STORAGE DEVICE (TAPE RECORDER) 3) COMMUNICATION LINK 4) ON-GROUND PROCESSING EQUIPMENT INCLUDING A HIGH CAPABILITY COMPUTER

* FOR EACH OF 6 CONTROL CHANNELS

- Explore control design tradeoffs when LSS dynamics are time-varying very rapidly with respect-to the time used for parameter estimation and controller updating.

- Determine if weakly observable modes that must be controlled can be identified using modal parameterizations rather than physical parameterizations.

- Design adaptation algorithms which "optimize" the basis-transfer-matrix elements on-line (see Figure 4.3).

REFERENCES

[1] Benhabib, Iwens, and Jackson, "Stability Of Distributed Control For Large Flexible Structures Using Positivity Concepts", Paper Number 79-1780, AIAA Guidance And Control Conference, Boulder, Colorado, August 1979.

[2] Anderson, B. D. O., "A System Theory Criterion For Positive Real Matrices, " SIAM J. Of Control, Vol. 5, No. 2, PP 171-182, May 1967.

[3] Iwens, Benhabib and Jackson, "A Unified Approach To The Design Of LSS Control Systems," JACC, 1980.

[4] "ACOSS ONE (Active Control of Space Structures) Phase I," General Dynamics, Sponsored by Defense Advanced Research Projects Agency, Report No. RADC-TR-80-79, March 1980.

[5] Balas, M., "Enhanced Control Of Flexible Structures Via Innovations Feedthrough", 2nd VPI Symposium on Dynamics and Control of Large Flexible Spacecraft, 1979.

[6] Mac Farlane, et. al., "Complex Variable Methods For Multivariable Feedback Systems Analysis and Design," in Alternatives For Linear Multivariable Control, NEC, Chicago, Ill., 1978.

[7] Shankar and Atherton, "Graphical Stability Analysis of Non-Linear Multivariable Control Systems," I.J.C., 1977, pp 375-388.

[8] Mees and Atherton, "The Popov Criterion For Multiple-Loop Feedback Systems," to be published IEEE A.C.

[9] Willems, J. C., "Dissipative Dynamical Systems, Parts I and II," Archive For Rational Mechanical Analysis, Vol. 45, 1972.

[10] Willems, J. C., "Mechanisms for the Stability and Instability of Feedback Systems," Proceedings of the IEEE, Vol. 64, No. 1, January 1976.

[11] Moylan and Hill, "Stability of Large-Scale Interconnected Systems," IEEE Transactions on Automatic Control, AC-23, April, 1978.

[12] Zames, G., "On The Input-Output Stability Of Time Varying Nonlinear Feedback Systems - Part I...", IEEE A.C., Vol. AC-11, No. 2, April 1966.

[13] Horowitz, I., "Synthesis of Feedback Systems", Academic Press, 1963.

[14] Horowitz, I., "The Superiority Of Transfer Function Over State-Variable Methods In Linear Time Invariant Feedback System Design", IEEE Vol. AC-20, No. 1, February 1975.

[15] Astrom, Wittenmark, "On Self Tuning Regulators", Automatica, Vol. 9, 1973.

[16] Kokotovic, P. V., "Method Of Sensitivity Points In The Investigation and Optimization Of Linear Control Systems," Automatic And Remote Control, No. 12, 1964.

[17] Narendra, et. al., "Adaptive Control Using Time Delay and Correlation", 3rd Annual Allerton Conference On Circuits and Systems Theory, October, 1965.

[18] Hang and Parks, "Comparative Studies of Model Reference Adaptive Control Systems", IEEE A.C., Vol. AC-18, October 1973.

[19] Morgan and Narendra, "On The Stability Of Non-Autonomous Differential Equations $\dot{X} = [A + B(t)]X$ with Skew Symmetric B(t)," SIAM J. of Control and Optimization, Vol. 15, No. 1, January 1977.

Wolovich, <u>Linear Multivariable Systems</u>, Springer, 1974.

[21] R. Strunce, "Description of Draper Example Structure Model", Charles Stark Draper Labs.

[22] Benhabib and Tung, "Large Space Structures Control: System Identification Versus Direct Adaptive Control", JACC, 1980.

[23] Benhabib, Iwens and Jackson, "Adaptive Control Of Large Space Structures", IEEE Conference on Decision and Control, 1979.

[24] Balakrishnan, A. V., "Stochastic Differential Systems I," Springer-Verlag, New York, 1973.

[25] Przemieniecki, J. S., "Theory of Matrix Structural Analysis," McGraw-Hill, 1968.

[26] Schweppe, F. C., "Evaluation of Likelihood Functions for Gaussian Signals," IEEE Trans. On Information Theory, January 1965.

APPENDIX A

APPENDIX A. Draper Example Structure Model #2

The Draper Model #2 shown in Figure A-1 is a large space structure model provided by R. Strunce and T. Henderson of Charles Stark Draper Laboratory (CSDL) for the purpose of testing and evaluating controller design methodologies and system identification algorithms. The structure consists of a flexible optical support structure ("clean structure") and an equipment section ("dirty box"), separated from the "clean structure" by passive isolators. The optical support consists of the primary and tertiary mirror support truss, and a lower support truss for the secondary mirror and focal plane sensor. The line-of-sight (LOS) path is also shown in Figure A-1. The isolated equipment section consists of a central rigid body containing the spacecraft attitude control system. The equipment section also supports two symmetric solar panels.

Draper has provided one nominal model and two perturbed models (nominal model with parameter variations), and an expression describing the LOS error, presented in Section A.3 of this Appendix.

A.1. Nominal Model

The finite element model is described in Figures A-2 through 5 and Table A-1. The modal frequencies and mode shapes are listed in Table A-2.

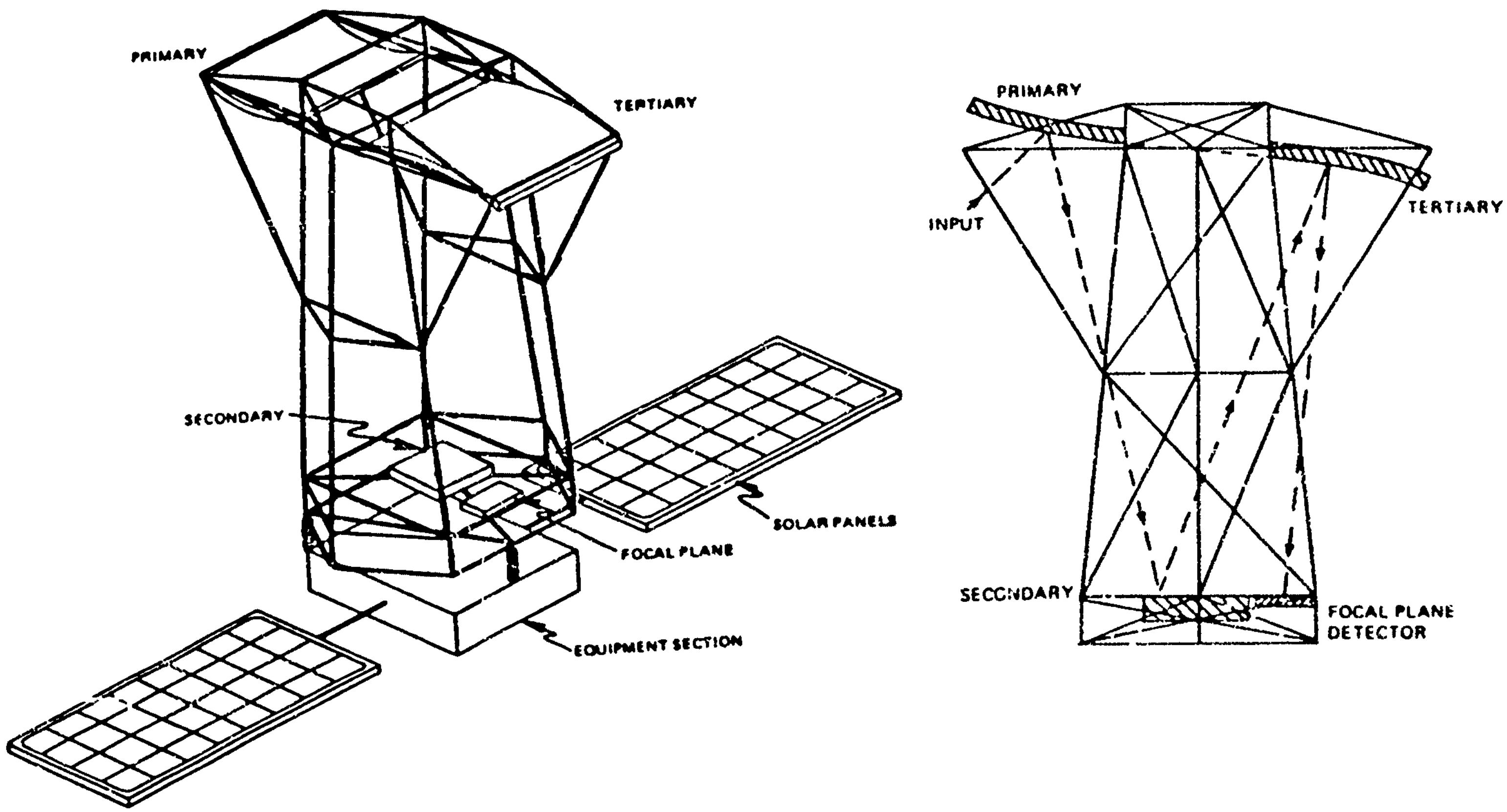

Figure A-1. Draper Example Structure Model #2

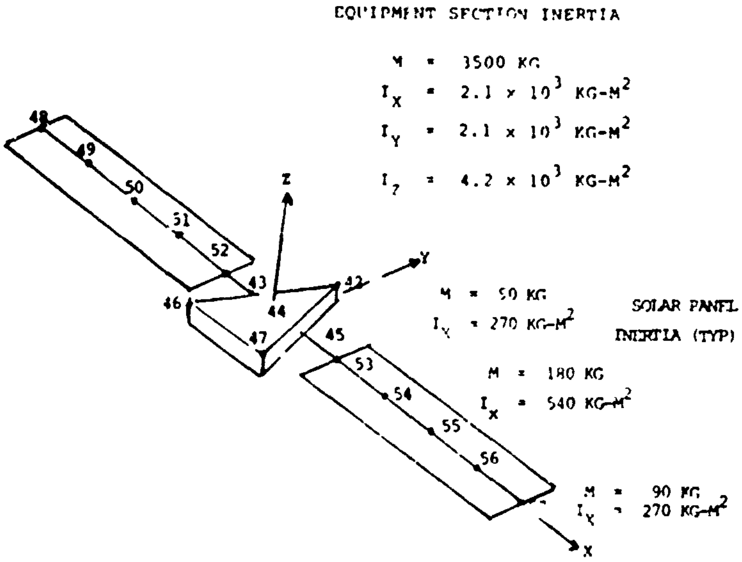

NODE	X	Y	Z
42	0.0	5.0	0.0
43	-2.0	0.0	0.0
44	0.0	0.0	0.0
45	2.0	0.0	0.0
46	-4.0	-5.0	0.0
47	4.0	-5.0	0.0
48	-26.0	0.0	0.0
49	-21.0	0.0	0.0
50	-16.0	0.0	0.0
51	-11.0	0.0	0.0
52	-6.0	0.0	0.0
53	6.0	0.0	0.0
54	11.0	0.0	0.0
55	16.0	0.0	0.0
56	21.0	0.0	0.0
57	26.0	0.0	0.0

NODES 42-47 RIGID PLATE

SOLAR PANELS - MEMBER CONNECTIVITIES

MEMBER #	NODE A	NODE B	PROP #
131	48	49	500
132	49	50	↓
133	50	51	↓
134	51	52	↓
[illegible]	52	43	↓
136	45	53	↓
137	53	54	↓
138	54	55	↓
139	55	56	↓
140	56	57	↓

Figure A-2 Nominal Model - Equipment Section and Solar Panels

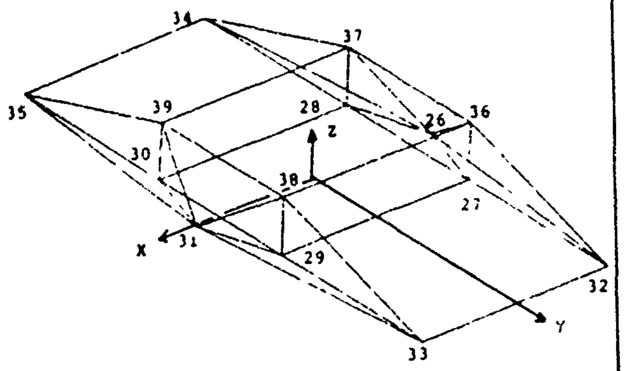

NODE	X	Y	Z	MASS (KG)
26	-5.0	0.0	22.0	
27	-4.0	3.0		375.0
28	-4.0	-3.0		375.0
29	4.0	3.0		375.0
30	4.0	-3.0		375.0
31	5.0	0.0		
32	-4.0	10.0		500.0
33	4.0	10.0		500.0
34	-4.0	-10.0		250.0
35	4.0	-10.0		250.0
36	-4.0	3.0	24.0	
37	-4.0	-3.0		
38	4.0	3.0		
39	4.0	-3.0		

DIAGONAL MEMBERS OMITTED FOR CLARITY

MEMBER #	NODE A	NODE B	PROP #	MEMBER #	NODE A	NODE B	PROP #
54	26	27	300	111	26	32	400
55	26	28		112	27	32	
56	27	28		113	27	33	
57	29	30		114	29	33	
58	29	31		115	31	33	
59	30	31		116	32	33	
60	27	29		117	26	34	
61	27	30		118	28	34	
62	29	30		119		34	
63	27	36		120		35	
64	28	37		121	31	35	
65	30	39		122	34	35	
66	29	38		123	32	36	
67	29	36		124	33	38	
68	27	37		125	34	37	
69	28	39		126	35	39	
70	30	38		127	26	37	300
71	36	37		128	26	36	
72	37	39		129	31	39	
73	39	38		130	31	[illegible]	
74	36	38					
75	37	38					

Figure A-2 Nominal Model - Upper Support Truss

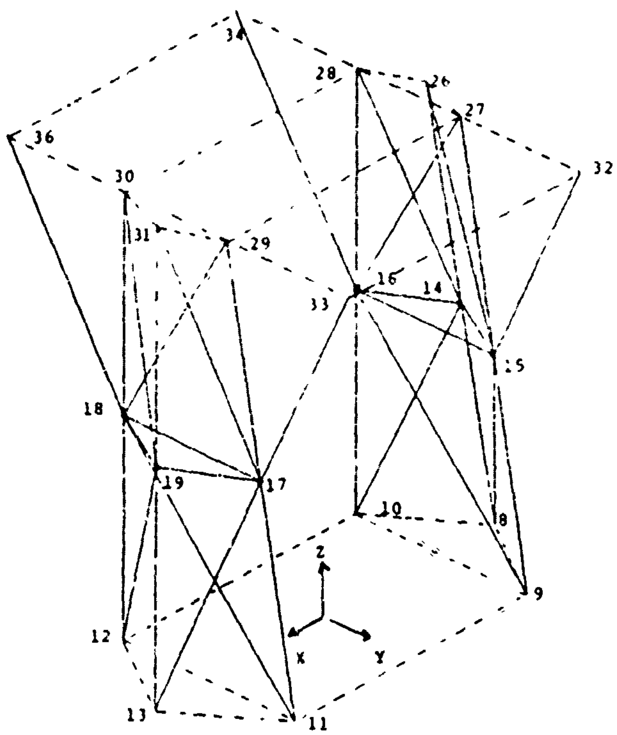

NODE	X	Y	Z	MASS(KG)
14	-6.0	0.0	12.0	8.0
15	-4.0	4.0		17.0
16	-4.0	-4.0		17.0
17	4.0	4.0		17.0
18	4.0	-4.0		17.0
19	6.0	0.0		8.0

MEMBER #	NODE A	NODE B	PROP #	MEMBER #	NODE A	NODE B	PROP #
42	14	15	300	86	13	17	400
43	14	16		87	14	26	
44	16	15		88	14	28	
45	17	18		89	16	28	
46	17	19		90	16	27	
47	18	19		91	15	27	
76	9	14	400	92	15	26	
77	10	14		93	17	29	
78	10	16		94	18	29	
79	16	9		95	18	30	
80	9	15		96	19	30	
81	11	17		97	19	31	
181	8	15		98	17	31	
82	11	18		99	15	32	
83	12	18		100	16	34	
84	12	19		101	17	33	
85	13	19		102	18	35	

Figure A-4 Nominal Model - Metering Truss

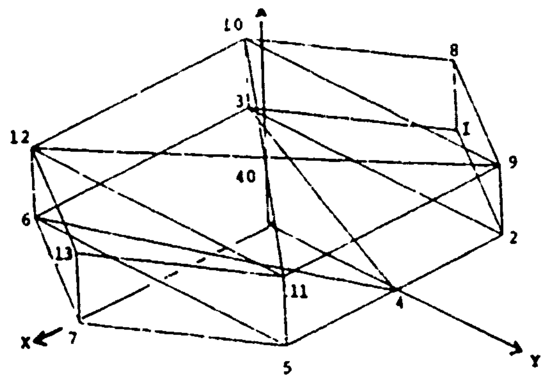

NODE	X	Y	Z	MASS (KG)
1	-7.0	0.0	0.0	
2	-4.0	5.0	0.0	
3	-4.0	-5.0	0.0	
4	0.0	5.0	0.0	
5	4.0	5.0	0.0	
6	4.0	-5.0	0.0	
7	7.0	0.0	0.0	
8	-7.0	0.0	2.0	
9	-4.0	5.0	2.0	500.0
10	-4.0	-5.0	2.0	500.0
11	4.0	5.0	2.0	500.0
12	4.0	-5.0	2.0	500.0
13	7.0	0.0	2.0	
40	0.0	0.0	2.0	
41	0.0	-5.0	1.0	

DIAGONAL MEMBERS OMITTED FOR CLARITY

MEMBER #	NODE A	NODE B	PROP #	MEMBER #	NODE A	NODE B	PROP #
1	1	2	200	21	4	9	200
2	1	3		22	4	11	
3	2	3		23	5	12	
4	2	4		24	5	13	
5	3	4		25	6	13	
6	4	5		26	12	41	
7	4	6		27	6	41	
8	3	6		28	10	41	
9	5	6		29	3	41	
10	5	7		30	8	9	
11	6	7		21	8	10	
12	1	8		32	9	10	
13	2	9		33	9	40	
14	3	10		34	10	40	
15	5	11		35	11	40	
16	6	12		36	12	40	
17	7	13		37	9	11	
18	1	8		38	10	12	
19	2	8		39	11	12	
20	3	9		40	11	13	
				41	12	13	

Figure A-5 Nominal Model - Lower Support Truss

Table A-1. Nominal Model Member Properties

TYPE 200

20 cm dia. x .1 cm Round Tube

$A = 6.250 \times 10^{-4}\ m^2$

$I = 3.075 \times 10^{-6}\ m^4$

$J = 6.189 \times 10^{-6}\ m^4$

TYPE 300

20 cm dia x .05 cm Round Tube

$A = 3.133 \times 10^{-4}\ m^2$

$I = 1.559 \times 10^{-6}\ m^4$

$J = 3.118 \times 10^{-6}\ m^4$

TYPE 400

25 cm dia x .05 cm Round Tube

$A = 3.919 \times 10^{-4}\ m^2$

$I = 3.0496 \times 10^{-6}\ m^4$

$J = 6.099 \times 10^{-6}\ m^4$

TYPE 500

40 cm dia x .075 cm Round Tube

$A = 9.407 \times 10^{-4}\ m^2$

$I = 1.874 \times 10^{-5}\ m^4$

$J = 3.749 \times 10^{-5}\ m^4$

Table A-2. Nominal Model Modal Frequencies and Mode Shapes

	Freq. (Hz)	Description		Freq. (Hz)	Description
1-6	0.0	rigid body	17	1.72	torsion
7	.145	Isolator Y-rotation	18	1.82	2nd S.P. X-Z plane
8	.263	Isolator Z-rotation	19	1.82	2nd S.P. X-Y plane
9	.317	1st S.P. X-Z plane	20	1.89	1st S.P. torsion asym
10	.333	1st S.P. X-Y plane	21	2.36	1st bending
11	.443	Isolator Z-trans	22	2.99	1st S.P. torsion sym
12	.577	Isolator Y-trans	23	3.18	3rd S.P. X-Y plane
13	.581	Isolator X-trans	24	3.39	3rd S.P. X-Z plane
14	1.22	2nd S.P. X-Z plane	25	5.16	2nd S.P. torsion
15	1.30	2nd S.P. X-Y plane	26	5.26	2nd S.P. torsion
16	1.35	Isolator X-rotation	27	7.87	3rd S.P. torsion

Table A-2. Nominal Model Modal Frequencies and Mode Shapes (continued)

	FREQ(HZ)	DESCRIPTION		FREQ(HZ)	DESCRIPTION
28	8.11	LEG TORSION	39	15.65	LEG & LOWER TRUSS BENDING
29	8.36	3rd S.P. TORSION	40	16.07	LEG BENDING
30	8.57	LEG TORSION	41	16.52	UPPER TRUSS BENDING
31	8.81	3rd S.P. X-Y PLANE	42	16.75	UPPER TRUSS BENDING
32	8.81	3rd S.P. X-Z PLANE	43	17.16	UPPER AND LOWER BENDING
33	11.35	4th S.P. X-Y PLANE	44	17.83	STRUCTURAL BENDING X-Y
34	11.50	LEG BENDING	45	19.07	LOWER TRUSS BENDING
35	12.73	LEG BENDING	46	23.77	UPPER TRUSS BENDING
36	13.58	4th S.P. X-Z PLANE	47	24.41	UPPER & LOWER BENDING
37	13.71	LEG BENDING	48	25.91	UPPER TRUSS AXIAL
38	14.16	LEG & LOWER TRUSS BENDING	49	26.36	UPPER TRUSS BENDING
			50	26.43	S.P. AXIAL

A.2. Perturbed Models

Two perturbed models are given - Case #2 and Case #4. The changes in masses and stiffnesses are listed in Table A-3 and A-4. All other parameters are unchanged.

Table A-3. Changes in Masses for Perturbed Models

Node	Original Mass	Case #2	Case #4
27	375.0	350.0	375.0
28	375.0	350.0	375.0
29	375.0	350.0	375.0
30	375.0	350.0	375.0
32	500.0	500.0	550.0
33	500.0	550.0	450.0
34	250.0	300.0	300.0
35	250.0	250.0	200.0

Table A-4. Changes in Stiffnesses for Perturbed Models

Memb.	NA	NB	Section Property†	
			Case #2	Case #4
76	8	14	1	1
80	9	15	1	2
81	11	17	1	1
85	13	19	1	2
99	15	32	1	2
101	17	33	1	2

† Section Properties

#1 - 25cm DIA. x .10 cm round tube

$A = 7.823 \times 10^{-4}\ m^2$

$I = 6.063 \times 10^{-6}\ m^4$

$J = 1.213 \times 10^{-5}\ m^4$

#2 - 25 cm DIA. x .025 cm round tube

$A = 1.962 \times 10^{-4}\ m^2$

$I = 1.529 \times 10^{-6}\ m^4$

$J = 3.059 \times 10^{-6}\ m^4$

A.3. LOS Error Algorithm

Equations (A-2), (A-3), and (A-4), relate optical surface motion and the resultant LOS rotations about the X and Y axes. The notation and orientation is consistent with the structural analysis. The movement of each mirror is defined to be the displacements and rotations in the global X, Y, Z directions at a point on the sphere (primary, tertiary) or plane (focal plane) which intersects the optical (global Z) axis. The LOS rotation and defocus are given by

$$LOSX = Y/F \qquad LOSY = X/F \qquad \text{Defocus} = Z \tag{A-1}$$

where

$$F = 8.051$$

$$X = A_1 \, [-X_p + X_t - R\cdot\theta Y_p + A_2\cdot\theta Y_s - 2T\cdot\theta Y_t] + X_t - X_f \tag{A-2}$$

$$Y = A_1 \, [-Y_p + Y_t + R\cdot\theta X_p - A_2\cdot\theta X_s + 2T\cdot\theta X_t] + Y_t - Y_f \tag{A-3}$$

$$Z = A_3 \, [Z_p - 2Z_s + Z_t] + Z_t - Z_f \tag{A-4}$$

where

$$A_1 = 0.2987$$

$$A_2 = 93.90$$

$$A_3 = 0.0892$$

$$R = 53.9$$

$$T = 66.95$$

The terms X_i, Y_i, Z_i θX_i, θY_i, θZ_i refer to the translations and rotations in the global X, Y, and Z directions of the primary (p) and secondary (s), tertiary (t), and focal plane (f).

The expresssions for the translation and rotation of each mirror in global coordinates are a function of the support point displacements.

Primary:

$$X_p = X_{34} + 1.25 \, Y_{34} - 1.25 \, Y_{35}$$

$$Y_p = 0.50 \, Y_{34} + 0.50 \, Y_{35}$$

$$Z_p = -0.2143 \, Z_{34} + -0.2143 \, Z_{35} + 0.7143 \, Z_{28} + 0.7143 \, Z_{30}$$

$$\theta X_p = -0.0714\ Z_{34} - 0.0714\ Z_{35} + 0.0714\ Z_{28} + 0.0714\ Z_{30}$$

$$\theta Y_p = 0.0125\ Z_{34} - 0.125\ Z_{35}$$

$$\theta Z_p = -0.125\ Y_{34} + 0.125\ Z_{35}$$

Secondary:

$$X_s = X_{40} \qquad \theta X_s = \theta X_{40}$$

$$Y_s = Y_{40} \qquad \theta Y_s = \theta Y_{40}$$

$$Z_s = Z_{40} \qquad \theta Z_s = \theta Z_{40}$$

Tertiary:

$$X_t = X_{27} + -0.3750\ Y_{27} + 0.3750\ Y_{29}$$

$$Y_t = 0.50\ Y_{27} + 0.50\ Y_{29}$$

$$Z_t = 0.0714\ Z_{27} + 0.7143\ Z_{29} - 0.2143\ Z_{32} - 0.2143\ Z_{33}$$

$$\theta X_t = -0.0714\ Z_{27} - 0.0714\ Z_{29} + 0.0714\ Z_{32} + 0.0714\ Z_{33}$$

$$\theta Y_t = 0.125\ Z_{27} - 0.125\ Z_{29}$$

$$\theta Z_t = -0.125\ Y_{27} + 0.125\ Y_{29}$$

Focal Plane:

$$X_f = X_{11} + 0.6250\ Y_{11} - -0.6250\ Y_9$$

$$Y_f = 0.50\ Y_{11} + 0.50\ Y_9$$

$$Z_f = Z_{40}$$

$$\theta X_f = 0.10\ Z_{11} + 0.10\ Z_9 - 0.20\ Z_{40}$$

$$\theta Y_f = -0.125\ Z_{11} + 0.125\ Z_9$$

$$\theta Z_f = 0.125\ Y_{11} - 0.125\ Y_9$$

addresses	number of copies	line number
Richard Carman RADC/OCSE	5	
RADC/ISLD GRIFFISS AFB NY 13441	1	2
RADC/DAP GRIFFISS AFB NY 13441	2	3
ADMINISTRATOR DEF TECH INF CTR ATTN: DTIC-DDA CAMERON STA BG 5 ALEXANDRIA VA 22314	12	5
General Dynamics Convair Division P.O. Box 80847 San Diego, CA 92138	5	3
Charles Stark Draper Labs 555 Technology Square Cambridge, MA 02139	5	4
Charles Stark Draper Lab Attn: Dr. Keto Soosar 555 Technology Square M.S. -95 Cambridge, MA 02139	1	5
Charles Stark Draper Lab Attn: Dr. J.B. Linn 555 Technology Square Cambridge, MA 02139	1	6
Charles Stark Draper Lab Attn: Mr. R. Strunce 555 Technology Square M.S.-60 Cambridge, MA 02139	1	7

Charles Stark Draper Lab Attn: Dr. Daniel R. Hegg 555 Technology Square M.S. 60 Cambridge, MA 02139	1	8
ARPA/MIS 1400 Wilson Bl Arlington, VA 22209	1	9
ARPA/STO Attn: Lt Col A. Herzberg 1400 Wilson Blvd Arlington, VA 22209	1	10
ARPA/STO Attn: Mr. J. Larson 1400 Wilson Blvd Arlington, VA 22209	1	11
ARPA/STO Attn: Maj E. Dietz 1400 Wilson Blvd Arlington, VA 22209	1	12
Riverside Research Institute Attn: Dr. R. Kappesser Attn: Mr. A. DeVilliers 1701 N. Ft. Myer Drive Suite 711 Arlington, VA 22209	3	13
Riverside Research Attn: HALO Library, Mr. Bob Passut 1701 N.Ft. Myer Drive Arlington, VA 22209	1	14
Itek Corp Optical Systems Division 10 Maguire Rd. Lexington, MA 02173	1	15
Perkin Elmer Corp Attn: Mr. H. Levenstein Electro Optical Division Main Avenue Norwalk, CT 06856	1	16
Hughes Aircraft Company Attn: Mr. George Speak M.S. B_150 Culver City, CA 90230	1	17

Hughes Aircraft Company Attn: Mr. Ken Beale Centinela & Teale Sts Culver City, CA 90230	1	18
Air Force Flight Dynamics Lab Attn: Dr. Lynn Rogers Wright Patterson AFB, OH 45433	1	19
AFWAL/FIBG Attn: Mr. Jerome Pearson Wright Patterson AFB, OH 45433	1	20
Air Force Wright Aero Lab. FIEE Attn: Capt Paul Wren Wright Patterson AFB, OH 45433	1	21
Air Force Institute of Technology Attn: Prof. R. Calico/ENY Wright Patterson AFB, OH 45433	1	22
Aerospace Corp. Attn: Dr. G.T. Tseng 2350 E. El Segundo Blvd El Segundo, CA 90245	2	23
Aerospace Corp. Attn: Mr. J. Mosich 2350 E. El Segundo Blvd El Segundo, CA 90245	1	24
Aerospace Corp/Bldg 125/1054 Attn: Mr. Steve Burrin Advanced Systems Tech Div. 2400 E El Segundo Blvd El Segundo, CA 90245	1	25
SD/YCD Attn: Lt Col T. May P.O. Box 92960 Worldway Postal Center Los Angeles CA 90009	1	26
SD/YCD Attn: YCPT/Capt Gajewski P.O. Box 92960 Worldway Postal Center Los Angeles, CA [illegible]	1	27

Grumman Aerospace Corp Attn: Dr. A. Mendelson South Oyster Bay Road Bethpage, NY 11714	1	28
Grumman Aerospace Corp Attn: Mr. Art Bertapelle Plant 25 Bethpage, NY 11714	1	29
Jet Propulsion Laboratory Attn: Mr. D.B. Schaechter 4800 Oak Grove Drive Pasadena, CA 91103	2	30
MIT/Lincoln Laboratory Attn: S. Wright P.O. Box 73 Lexington, MA 02173	1	31
MIT/Lincoln Laboratory Attn: Dr. D. Hyland P.O. Box 73 Lexington, MA 02173	11	32
MIT/Lincoln Laboratory Attn: Dr. J. Smith P.O. Box 73 Lexington, MA 02173	11	33
Control Dynamics Co. Attn: Dr. Sherman Seltzer 221 East Side Square, Suite 1B Huntsville, Al 35801	1	34
Lockheed Space Missile Corp. Attn: A. Woods, Bldg 130 Organ 62-E6 3400 Hillview Ave Palo Alto, CA 94304	2	35
Lockheed Mis[illegible]les Space Co. Attn: Mr. P[illegible] Williamson 3251 Hanover [illegible] Palo Alto, [illegible] 94304	1	36

General Dynamics Attn: Ray Halstenberg Convair Division 5001 Keary Villa Rd San Diego, CA 92123	1	37
STI Attn: Mr. R.C. Stroud 20065 Stevens Creek Blvd. Cupertiono, CA 95014	1	38
NASA Langley Research Ctr Attn: Dr. G. Horner Attn: Dr. Card Langley Station Bldg 1293B M/S 230 Hampton, VA 23665	2	39
NASA Johnson Space Center Attn: Robert Piland Ms. EA Houston, TX 77058	1	40
McDonald Douglas Corp Attn: Mr. Read Johnson Douglas Missile Space Systems Div 5301 Bolsa Ave Huntington Beach, CA 92607	1	41
Integrated Systems Inc. Attn: Dr. Narendra Gupta 151 University Ave. Suite 400 Palo Alto, CA 94301	1	42
Boeing Aerospace Company Attn: Mr. Leo Cline P.O. Box 3999 Seattle, WA 98124 MS 8 W-23		43
TRW Defense Space Sys Group Inc. Attn: Ralph Iwens Bldg 82/2054 One Space Park Redondo Beach, CA 90278	1	44
TRW Attn: Mr. Len Pincus Bldg R-5, Room 2031 Redondo Beach, CA 90278	1	45
Department of the Navy Attn: Dr. K.T. Alfriend Naval Research Laboratory Code [illegible] Washington, DC 203[illegible]	1	46

AiResearch Manuf. Co. of Calif. Attn: Mr. Oscar Buchmann 2525 West 190th St. Torrance, CA 90507	1	47
Analytic Decisions, Inc. Attn: Mr. Gary Glaser 1401 Wilson Blv. Arlington, VA 22209	1	48
Analytic Decisions, Inc. Attn: Mr. Richard Mollicone 5350 West Rosecrans Ave Suite 203 Lawndale, CA 22209	1	49
Center for Analysis Attn: Mr. Jim Justice 13 Corporate Plaza Newport Beach, CA 92660	1	50
General Research Crop. Attn: Mr. G. R. Curry P.O. Box 3587 Santa Barbara, CA 93105	1	51
General Research Corp Attn: Mr. Thomas Zakrzewski 7655 Old Springhouse Road McLean, VA 22101	1	52
Institute of Defense Analysis Attn: Dr. Hans Wolfhard 400 Army Navy Drive Arlington, VA 22202	1	53
Karman Sciences Corp. Attn: Dr. Walter E. Ware 1500 Garden of the Gods Road P.O. Box 7463 Colorado Springs, CO 80933	1	54
MRJ Inc. 10400 Eaton Place Suite 300 Fairfax, VA 22030	1	55

Photon Research Associates Attn: Mr. Jim Myer P.O. Box 1318 La Jolla, CA 92038	1	56
Rockwell International Attn: Russell Loftman (Space Systems Group) (Mail Code - SL56) 12214 Lakewood Blvd. Downey, CA 90241	1	57
Science Applications, Inc. Attn: Mr. Richard Ryan 3 Preston Court Bedford, MA 01730	1	58
U.S. Army Missile Command Attn: DRSMI-RAS/Mr. Fred Haak Redstone Arsenal, AL	1	59
Naval Electronic Systems Command Attn: Mr. Charles Good PME_106-4 National Center I Washington, DC 20360	1	60
Naval Research Laboraбtory Attn: Dr. John McCallum EOTPO 4555 Overlook Ave., SW Washington, DC 20375	1	61
U.S. Army/DARCOM Attn: Mr. Bernie Chasnov AMC Bldg 5001 Eisenhower Ave Alexandria, VA 22333	1	62
Honeywell Inc. Attn: Dr. Thomas B. Cunningham Attn: Dr. Michael F. Barrett 2600 Ridgway Parkway MN 17-2375 Minneapolis, MN 55413	2	65